

20831 -FR

N 69 19 07 1
NASA CR 86125

RESEARCH IN ELECTRICALLY SUPPORTED VACUUM GYROSCOPE

VOLUME IV- ESGV READOUT
ACCURACY IMPROVEMENT RESEARCH

**CASE FILE
COPY**

Distribution of this report is provided in the interest of
information exchange. Responsibility for the contents
resides in the author or organization that prepared it.

November 1968

Prepared Under Contract NAS-12-542

HONEYWELL INC.
Systems & Research Division
Minneapolis, Minnesota
for

NATIONAL AERONAUTICS AND SPACE ADMINISTRATION

NASA CR

RESEARCH IN ELECTRICALLY
SUPPORTED VACUUM GYROSCOPE

VOLUME IV - ESGV READOUT
ACCURACY IMPROVEMENT RESEARCH

Prepared by: J. C. Wacker

Distribution of this report is provided in the interest of
information exchange. Responsibility for the contents
resides in the author or organization that prepared it.

November 1968

Prepared Under Contract NAS-12-542

HONEYWELL INC.
Systems & Research Division
Minneapolis, Minnesota
for

NATIONAL AERONAUTICS AND SPACE ADMINISTRATION

CONTENTS

	Page	
SECTION I	INTRODUCTION	1
SECTION II	READOUT ERRORS OF EXISTING ESVM'S	5
	Errors in the Rotor Pattern	5
	Errors Contributed by the Rotor	8
	Optical Sources of Error	10
	Electronic Sources of Error	11
	Other Sources of Error	12
	Observational Effects of Readout Errors	14
	Approach to Error Compensation	16
	Critical Areas of Required Improvement	20
SECTION III	PATTERN DESIGN STUDY	25
	Pattern Parameters	25
	Nominal Pattern Characteristics	26
	Calculation of Direction Cosine from Phase-Angle Data	27
	Mechanization Equations for the Pattern Types	30
	Error Minimization Criteria	34
	Calculation of Error Sensitivities	42
	Comparison of Pattern Types	52
SECTION IV	PICKOFF ARRANGEMENT STUDY	71
	Solutions to the Third Direction Cosine Sensitivity Problem	71
	General Direction Cosine Calculations From Pickoff Cosines	72
	Arrangement of Three Pickoffs	75
	Arrangement of a Four-Pickoff System	81
	Optimum Parameter Study	94
SECTION V	PATTERN EDGE IMPROVEMENT	99
	Sources of Pattern Edge Uncertainties	99
	Results of Previous Improvement Studies	100
	ARC Marks and Triggering Errors	102
	Recommendations for Future Study	103

CONTENTS -- Concluded

	Page	
SECTION VI	PHASE-ANGLE MEASUREMENT TECHNIQUES	105
	All-Digital Clock System	105
	Hybrid Phaselock System	107
	Conclusions	112
SECTION VII	DYNAMIC ENVIRONMENTS	115
	Static Acceleration	115
	Vibration	119
	Angular Rotation	121
	Conclusions	124

ILLUSTRATIONS

Figure		Page
1	Typical ESVG Rotor Optical Calibration	6
2	Amplification of Line Edge Uncertainty by Pattern Slope	8
3	Error From Fixed Trigger Level	16
4	Height - Insensitive Trigger Block Diagram	18
5	Height - Insensitive Trigger Wave Forms	18
6	Pair of Pattern Lines on the Rotor	28
7	Geometry of Line Edge Error	35
8	Pattern Edge in Field of View	38
9	Normalized Expected rms Error from Phase Angle Timing Errors, Great Circle Patterns for Various Pattern Ranges	45
10	Normalized rms Expected Error from Line Edge Dispersion, Great Circle Patterns for Various Pattern Ranges	46
11	Normalized Expected rms Error from Phase Angle Timing Error, Cosine Patterns for Various Pattern Ranges	48
12	Normalized Expected rms Error from Line Edge Dispersion, Cosine Patterns for Various Pattern Ranges	49
13	Normalized Expected rms Error from Phase Angle Timing Error, Colatitude Patterns for Various Pattern Ranges	50
14	Normalized rms Expected Error from Line Edge Dispersion, Colatitude Patterns for Various Pattern Ranges	51
15	Comparison of Direction Cosine Errors from Pattern Edge Dispersion for Three Pattern Types	53
16	Third Direction Cosine Error from Pattern Edge Dispersion for Three Pattern Types	54

ILLUSTRATIONS -- Concluded

Figure		Page
17	A Great Circle Pattern Applicator	56
18	Patterning Jig	57
19	A Colatitude Pattern Applicator	58
20	A Cosine Pattern Applicator	59
21	Plane of Two ESG Pickoffs	73
22	Geometry of Direction Cosine Calculation	73
23	Arrangement of a System of Four Pickoffs	82
24	Determination of Minimum Pattern Ranges for Two- and Three-Pickoff Modes	83
25	Measurement of a Phase Angle for the Sign of the Third Direction Cosine	88
26	(No Title)	97
27	A possible Setup for Defining Cosine Pattern with Laser	104
28	Block Diagram of Present Phase-Angle Measurement System	106
29	Diagram of Basic Phaselock Loop	108
30	Phase-Angle Amplification by Doubling the Frequency	110
31	A Phaselock System for ESG	113
32	A Phaselock System with Phase Amplification	114
33	Geometry of Rotor Response to Acceleration	116
34	Observed Colatitude Sensitivity to Rotor Translation	117
35	Curvilinear Shift Geometry	118

TABLES

Table		Page
I	Present ESVG Readout Error Characteristics	21
II	Command Sequence for Calculating μ	61
III	Command Sequence for Nominal Cosine Mechanization	62
IV	Command Sequence for Polynomial	63
V	Instruction Sequence for Nominal Colatitude Mechanization	65
VI	Command Sequence of Great Circle Mechanization Given "SIN μ "	67
VII	Comparison of Computer Memory Requirements for Three Pattern Mechanizations	69

SECTION I

INTRODUCTION

The concept of supporting a rapidly spinning body by means of electric fields to obtain an inertial reference is motivated by the desire to avoid a common problem among all conventional inertial devices - mechanical friction that occurs among the linkages that support the spinning body (or bodies). Fluid-bearing devices have been used as a partial answer to the problem and serve well in short-term applications in such severe environments that the use of conventional sensors is impractical, if not impossible. Viscous forces associated with these devices generally render them unsuitable for long-term applications.

By supporting a spherical body (the rotor) by electric fields in an evacuated housing, mechanical and viscous forces on the rotor are removed. Long-term stability of the momentum vector, or compensated momentum vector, becomes adequate for many long-term inertial reference and navigation applications. However, mere establishment of such a stable inertial reference is not adequate; to gainfully utilize this reference, one must be able to measure exactly where that vector is, relative to a convenient set of coordinates.

The ideal mechanism for measuring the momentum vector of the rotor (reading out the gyro) is one which does not degrade the stability and predictability of the device. In a strict sense, this mechanism does not exist; therefore, the best alternate is one which minimizes the disturbance. An optical device is one such mechanism in that the minimum disturbance is the impulse of photons that strike the rotor; this disturbance is of the order of the ratio of the photon momenta to the rotor momentum, which is much smaller than the disturbance offered by the torque produced by electric supporting fields.

To employ an optical system, the rotor must possess some means of codifying the optical signals received by the device; the information can then be processed to determine the direction of the momentum vector. A spinning rotor automatically "codes" the signal by a doppler shift of frequency of the incident signal by the moving surface. Measurement of this shift determines the location of the spin vector; if it coincides with the momentum vector, readout is accomplished. However, the technology of measuring the doppler shift to the required accuracy has not advanced to the point of feasibility for the ESGV. Therefore, another method of codifying the signal is needed - at least for the present time.

The present method of codifying the optical signal is to manufacture the rotor so that its surface is highly reflective in some areas and diffuse and/or absorptive in other areas. Electric torque and electric field breakdown considerations dictate that the diffuse and absorptive areas (where the surface finish is rough and jagged in a microscopic sense or where material is deposited that exhibits different electrical properties) be kept to a minimum. The diffuse areas define a pattern in such a manner that the code generated by it can be related uniquely to a specific colatitude of the surface with respect to the pattern axis. This pattern axis is aligned as closely as possible to the momentum axis first by fabricating a preferred axis (axis of maximum moment) into the rotor, then by aligning the pattern axis to be coincident with the preferred axis, and finally by damping out the initial rotor nutation in the startup process.

Two approaches of signal codification have been employed on strapdown ESVG readout systems. One approach uses coded latitude lines; a specific sequence of pulses on a parallel of latitude is used as a coarse estimate of the region of the rotor on which the optical signal is focused. A series of alternating lines provides a fine measurement by measuring the amplitude of the signal. This type of pattern occupies a considerable area of rotor surface and fails to minimize the diffuse areas of the surface.

Another approach utilizes fine pattern lines in which the pattern edge precisely defines a specific function of the colatitude. The colatitude is uniquely determined by the longitude angle that separates the points of two pattern lines viewed by the optical system and the functions which the pattern lines define.

It is the latter type that is presently employed on a number of strapdown ESVG's. There is no evidence in recent test data from these units that this type of pattern line, as presently applied, degrades the ESVG drift performance. However, the same test data indicate that the accuracy of the readout system needs to be improved to be commensurate with the predictability of the ESVG momentum vector and to match accuracies of readouts on other inertial devices. The need for improvement, plus the need to streamline the information processing functions so that it may be implemented on a vehicle, is the motivation for this study program on the strapdown ESVG readout system.

The program was based on the premise that the approach presently employed (optical system, longitude measurement between pattern lines) has the capability of reading out the ESVG momentum vector direction to an accuracy of the one-second range. It was first necessary to identify the dominant sources of error, which if reduced would significantly improve system error. An error analysis of the present system was therefore

conducted; this analysis is reported in Section II. Sources of error which limit the accuracy of the readout system are identified; three sources wherein improvements are needed are sources which produce uncertainties in pattern line edge definition.

With pattern line edge uncertainty identified as the primary limitation of ESVG readout accuracy, consideration is given to steps which can reduce the observed uncertainty. These steps fall into two categories: steps which reduce the effect or amplification of the error through the train of readout logic and the necessary calculations; and steps which reduce the uncertainty of the pattern line edge itself.

Sections III and IV consider means of reducing the amplification of error. With a modest increase in the region of the rotor which is patterned and a change of readout strategy to one which utilizes three pickoffs when they view the pattern, a significant reduction of overall error amplification can be expected. Section V deals with prospective methods of defining the pattern edge more precisely. Some methods appear to be encouraging and should be pursued with laboratory experimentation.

To accurately define the colatitude angle with the presently used approach, the longitude angle separating the points of the pattern lines viewed by the pickoff must be precisely defined. Section VI compares the advantages of two methods of measuring that angle -- an all-digital clock system which is the method presently employed and a hybrid phaselock system. If the phase discrimination can be made sufficiently sensitive, the hybrid system can be compatible with projected system requirements and offers an attractive bonus -- the prospect of obtaining rate information from the ESVG.

Section VII describes the effects of dynamic environments on the ESVG readout. With consideration for their effects in readout system logic design and computer compensation, the effects of static acceleration, vibration, and angular rotation can be reduced to tolerable levels.

SECTION II

READOUT ERRORS OF EXISTING ESGV'S

To accomplish an improvement in the readout accuracy of an ESGV, one must ascertain which of the individual error sources will significantly improve overall accuracy when the magnitude of these errors is reduced. Subsequent effort can then be concentrated on the sources so defined. An error analysis of existing gyro readout systems was therefore conducted to delineate the potentially fertile areas of improvement.

The analysis begins by defining the physical sources at the fabrication, piece part, or subsystem level and describing its effect on readout accuracy. Methods of controlling and/or compensating these errors are discussed. Foreseeable improvements are indicated, and a breakdown of what the errors must be to achieve a one-second readout accuracy is provided. The areas where improvements are required or are of greatest benefit are then defined.

ERRORS IN THE ROTOR PATTERN

Pattern Application Error

This is the low-frequency deviation of the application tool from the desired position of the pattern caused by an error in the master pattern (if a master is used) and by play in the tool driving linkage. Generally, a master is required for nonplanar patterns such as the cosine pattern. The deviation of the solid line from the null ordinate in Figure 1 illustrates the effect of this error when the nominal mechanization is used for calculating the direction cosine.

This error is compensated in large part by altering the mechanization equation. In the case of the cosine pattern, the nominal mechanization equation is

$$\cos \theta = A_0 + B_0 \phi$$

To compensate for application error, the altered equation could take the polynomial form

$$\cos \theta = \sum_{k=0}^n P_k \phi^k$$

with P_0 and P_1 deviating slightly from A_0 and B_0 , respectively. All coefficients are determined by a least-squares curve fit to calibration data.

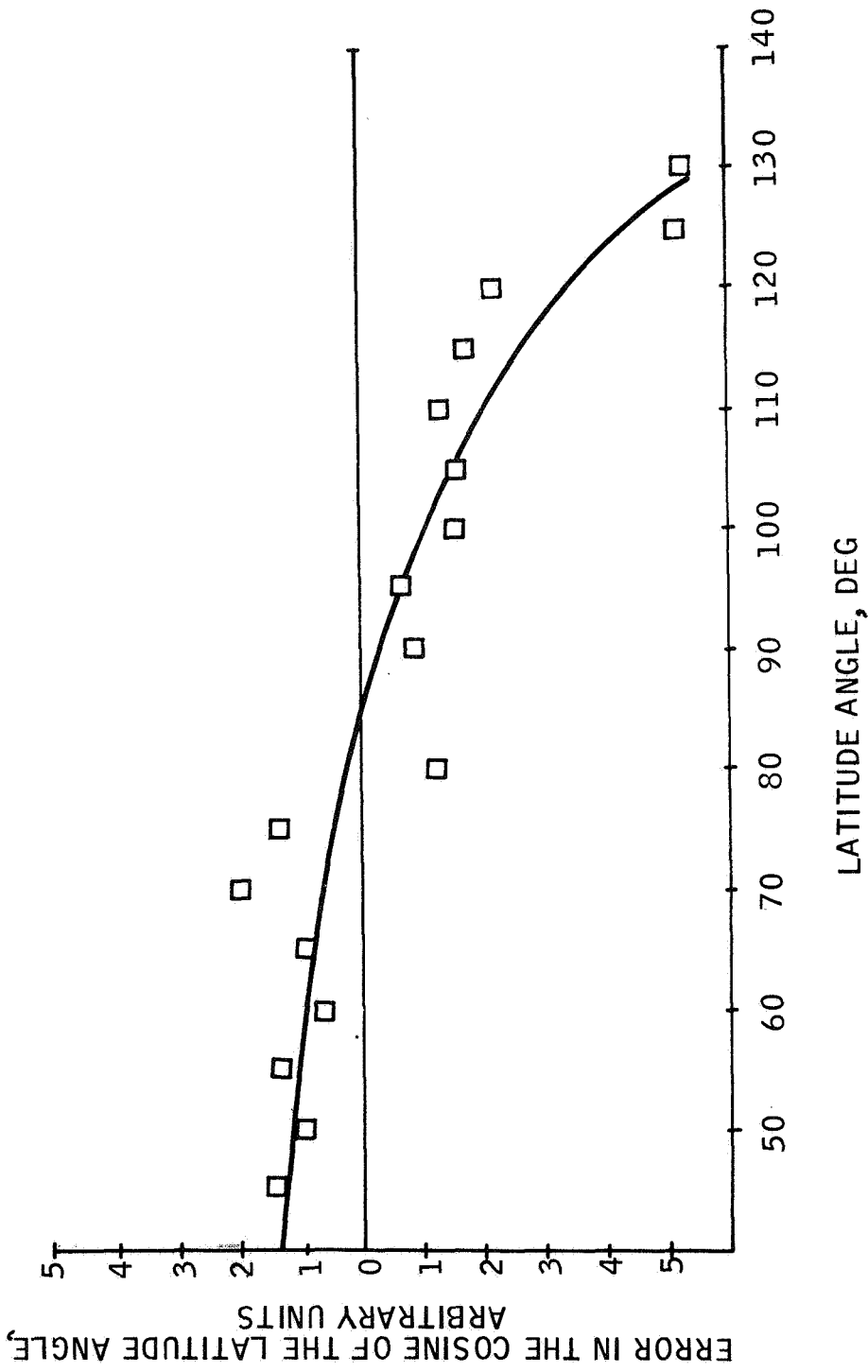


Figure 1. Typical ESGV Rotor Optical Calibration

Spin Axis - Pattern Axis Misalignment

Associated with ESVG rotor patterns is an axis which should be aligned parallel to the spin axis. For several reasons, these axes may not be parallel; consequently, a readout error can arise if coincidence is assumed. The error is a low-frequency error and can be compensated in large part by altering the nominal mechanization coefficients A_o and B_o .

The misalignment of the pattern axis can be precisely determined in the present system by ascertaining that meridional angle which is simultaneously read on all three pickoff outputs (denoting that the spin axis angles with all three pickoff axes are equal). Geometrical considerations and knowledge of the location of the pickoff axes enable a calculation of the direction cosine associated with that angle. Two such angles can be determined, which are located symmetrically about the equator. Correlation of these results with the calibration data from which Figure 1 is plotted yields a calculation of the pattern axis misalignment.

Line Edge Uncertainty

A severe problem in any pattern application process is line edge control. In a masking technique, for instance, the mask which defines the line edge can be torn when the pattern line is defined on the surface or when the mask is stripped from the rotor. A grit-blast technique causes uncertainties because of the dispersion of the blast. Since the grit-blast method offers a distinct advantage of fewer steps, this method has been employed in patterning most rotors. Rotor noise, which is discussed later, produces an effect identical to edge dispersion; these contributions cannot be separated. The resulting error is a random function from rotor to rotor with characteristic frequencies ranging up to the 100th harmonic of the colatitude angle.

Higher-frequency uncertainties can occur in the case of a nonplanar pattern cosine in which the application tool drive is servoed to a quantized master pattern line. This contributor produces smaller error than the lower-frequency contributors but can remain a significant factor by itself. The high-frequency characteristic of this error renders it impractical for compensation; but, if readout occurs while the direction cosines are changing slightly, this error can be reduced to a certain extent by averaging.

The scatter of the data points about the solid line in Figure 1 shows the effect of line edge uncertainties. Let ψ denote the scatter observed in the meridional angle measurement between pattern lines. From a statistical standpoint, an accumulated scatter of ψ would be produced by $\psi/\sqrt{2}$ of scatter in each line. Since it is a measurement projected along a constant latitude line, it is an oblique projection of the line uncertainty (see Figure 2). The normal projection, ϵ , can be calculated by

$$\epsilon = \frac{\psi}{\sqrt{2}} \sin \left| \tan^{-1} \frac{d\theta}{d\phi} \right|$$

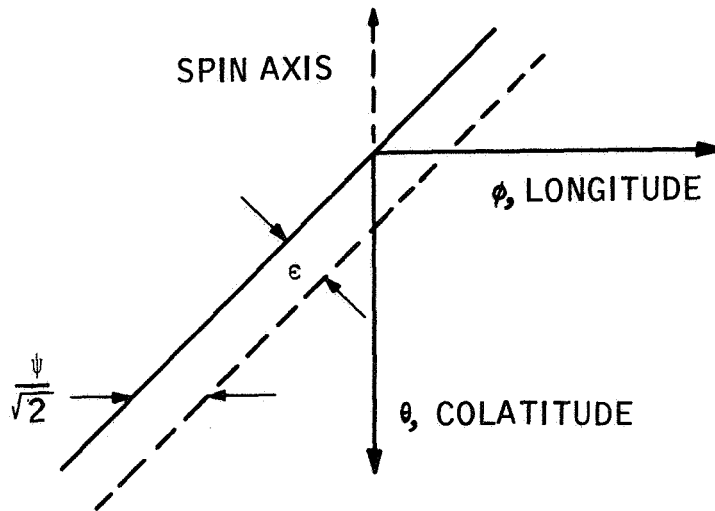


Figure 2. Amplification of Line Edge Uncertainty by Pattern Slope

For the present gyro,

$$\frac{d\theta}{d\phi} = \frac{0.522}{\sin \theta}$$

Figure 2 shows how small slopes can amplify line edge errors in the longitude measurement. At a sacrifice in resolution afforded by small slopes, this amplification can be reduced by increasing the slope.

ERRORS CONTRIBUTED BY THE ROTOR

Reflectivity Variations

The signal level received by the optical sensor is a function of the rotor reflectivity. If triggering occurs at a fixed signal level, the fraction of the pickoff field of view that must be exposed to the pattern line would depend on the reflectivity of the unpatterned surface. The quality of the surface finish is a determining factor of reflectivity. Low-frequency variations can occur as a result of polishing variations on the sintered surface.

Variations in reflectivity have not been measured on recently built gyros. It has been estimated that such variations are less than 10 percent of the nominal signal. With the triggering voltage set at 50 percent of the nominal signal, a 10-percent variation would cause up to 15 seconds of colatitude angle error. Compensation is provided by triggering at a point in proportion to the peak-to-peak signal, which reduces the error to that caused by nonlinearities in the sensor curve and the triggering electronics.

Rotor Noise

Local variations in reflectivity occur as a result of surface perturbations and arcing between the rotor and the electrodes, giving rise to a noise component in the pickoff signal. Most of the noise pulses are electronically filtered by establishing a triggering threshold and pulse width discrimination. Very large pulses cannot be distinguished from pattern pulses and cause false triggering. Equally serious from an accuracy standpoint are marks and perturbations on or adjacent to the pattern line. Their contribution of noise cannot be separated from the pattern signal and is not distinguished from pattern line edge uncertainties by the optics.

An estimate of the error caused by rotor noise can be obtained by comparing the scatter in calibration data taken under gyro operating conditions with the scatter in the microscope calibration data. Such a comparison indicates that the rotor noise in one gyro contributed 22 seconds of error in the latitude angle. Like line edge uncertainties, this error source causes deviations about the solid line of Figure 1.

Centrifugal Distortion

Stress analyses of thin spherical shells¹ have predicted that the beryllium rotor radial contraction at the pole is approximately the same as the radial expansion at the equator as the rotor speed increases. One can look upon the strain as a migration of the rotor surface toward the equator; such a migration causes an error in the readout.

If the migration that occurs in the rotor can be reduced from a three-dimension problem to a two-dimension problem, a quantitative calculation of the angular distortion can be calculated quite simply by utilizing the results of the stress analysis and tables of the elliptic functions and their integrals. For a two-inch rotor at a speed of 700 rps, the maximum migration predicted by this method is three seconds at colatitudes of 45° and 135°.

Compensation can be implemented for centrifugal distortion by altering the mechanization equation appropriately. However, if the original calibration data is collected at operating speed and regressed for coefficients, the distortion will automatically be taken into account.

Nutation

Readout errors can occur if the rotor nutation is not completely damped out during the starting process. In Honeywell ESG history, nutation has not been a limiting factor in readout accuracy, either in the gimbaled or strap-down mode. If nutation does become a problem, the error can be reduced by averaging successive revolutions over the period of the nutation.

¹Refer to the Appendix of Volume II of this report.

OPTICAL SOURCES OF ERROR

Illumination Variations

If the field of view is not uniformly illuminated, the portion of the field occupied by the pattern line to cause triggering is a function of the pattern angle in the field. To reduce this effect, great care has been taken in designing and manufacturing pickoff lamps having uniform luminosity. Despite this effort, small variations have been known to remain.

Field-of-View Irregularities

If the field of view is not circular, the triggering point is dependent on field-of-view geometry and the angle of the pattern line in the field. At the assembly level, this source of error cannot be distinguished from illumination variations. Their combined effect can be observed by rotating the case of an operating gyro about the pickoff axis and noting changes in the phase angle as it rotates.

Theoretically, a center of illumination can be defined, the location of which depends on the combined effect of illumination variations and field-of-view irregularities. If this axis is coincident with the desired location of the pickoff axis, readout error can be reduced to zero by triggering at 50 percent of the peak-to-peak signal. Other factors may render one or more of these conditions unattainable. If this is the case, compensation can be implemented by introducing a correction to the calculated direction cosine that is a function of the pattern line angle of approach.

The pickoff alignment procedure used on recently built gyros is one in which angle-of-approach sensitive errors can be a significant source of uncertainty in the alignment data. When effects which can be attributed to pickoff misalignment and spin axis drift are taken out of the data, a peak-to-peak variation of 10 seconds in the colatitude angle has been noted. Since other sources of error contribute to the noise, it is difficult to discern how much of the noise is caused by illumination variations and field-of-view uncertainties.

Lamp Luminosity Variations

The luminosity of the lamp changes if the power supply fluctuates. Lamp efficiency can be expected to change as the lamp ages. Such changes produce changes in the signal level. If triggering occurs at a fixed level, an error in the readout angle from lamp power variations can occur. Power supply transients can be controlled to some extent with regulation equipment. Lamp life is prolonged by extending the turn-on time and operating them at prudently selected color temperature levels. Extensive life tests have been conducted on pickoff lamps to determine how life changes with color temperature, to select the optimum operating temperature.

Electronic compensation is provided for any changes in power that do occur by the height-insensitive trigger in recent gyros. The triggering point is regulated to occur at a specified proportion of the peak-to-peak signal level.

ELECTRONIC SOURCES OF ERROR

Rise Time Variations

Random variations in rise times of the signal-processing electronic components is a source of noise in the readout data. The vendor literature claims a rise time of 0.2 microsecond for the photosensor used in one of the present gyros, and the rise time of the preamp is 0.4 microsecond. The rise time of the sensor-preamp combination is taken to be the rss of the component rise times, or 0.45 microsecond. The input pulse at a rotor speed of 700 rps is 0.9 microsecond, with a peak-to-peak variation of 10 percent occurring due to the change of pattern slope with latitude. An electronic variation of five percent would produce a 0.01 microsecond error in the time interval measurement between pulses, which produces an error in the colatitude angle measurement of approximately three seconds.

This error can be reduced by cutting down the rotor speed, averaging over several revolutions, and using higher-speed electronics components. Higher-speed components are available at a sacrifice in gain; however, one may take advantage of recent advancements to increase electronic speed without sacrificing gain and noise. It is believed that this error can be reduced to less than one second with present-day technology. In addition, the expected error from these variations can be reduced by averaging.

Amplifier Noise

Amplifier noise, like rotor noise, produces uncertainties in the readout measurement. A dominant source of noise is electromagnetic pickup of the suspension bridge frequencies by the electronics and the transmission lines.

Triggering Level Error

If triggering does not occur at 50 percent of the peak-to-peak signal, the pulse defining the crossing of a line edge occurs at some point other than the center of illumination. In addition to failing to null errors caused by illumination variations and field-of-view irregularities, a predictable pulse-timing bias that is a function of pattern slope occurs. It will be shown in Section III that the pattern can be designed to minimize the effects of this bias.

Triggering Uncertainty

In addition to the uncertainties already present in the input signal, intrinsic uncertainties can be developed by the pulse-shaping electronics of the height-insensitive trigger. For example, the output rise time of the present circuit is of the order of 0.1 microsecond. At the rotor speed for which it is

designed (200 rps), a gating error of 0.1 microsecond would produce an error of about six seconds. At an operating speed of 700 rps, the same gating error causes an error of 21 seconds.

Like the rise time uncertainties, triggering uncertainty can be reduced by the use of faster electronics, by averaging, and by operating at a lower rotor speed. Present electronic technologies would permit a higher-speed trigger circuit so that errors can be reduced to less than one second at a speed of 200 rps.

Phase Angle Measurement Error

A digital method of phase angle measurement is employed in testing the present system. Clock pulses are counted, with the counter gated by the pulses from the readout system. In this system, three potential sources of error are considered.

- Clock instability - No data is available concerning the clock stability. Test experience supports the belief that clock instabilities produce insignificant error compared to other sources.
- Counter uncertainty - The quantized nature of a digital measurement is no more accurate than the least count of the counter. In the 100 mc counters now used, the least count represents an error of 0.01 microsecond per revolution, or two seconds of latitude angle error at 700 rps.
- Gating circuits - It is important that the gating circuits be sufficiently fast and uniform in their characteristics to be commensurate with the accuracy requirements of the gyro. The circuits presently used have been shown to introduce no more error than that introduced by the quantization error of the counter.

All of the electronic sources of error are random and have high characteristic frequencies. The expected errors of all can be reduced by averaging over several revolutions. If the same approach is used in measuring phase angles in future systems, the use of the present electronic techniques, but with faster components and circuits, appears to be adequate for future accuracy requirements.

OTHER SOURCES OF ERROR

Pickoff Alignment

To utilize the readout information, the location of the pickoff axis must be known to an accuracy commensurate with the system requirements. Pickoff

alignment errors are presently determined with pickoff output data as the case of an operating gyro is rotated about that axis along which each pickoff axis is to coincide. The accuracy of the determination, therefore, depends on the accuracy of the readout system.

In recently built gyros, the alignment of pickoffs can be adjusted so that the pickoff axis can nominally be aligned coincident with the desired axis. The accuracy of the determination depends on the range of the pattern used. The range decreases in proportion to the pickoff axis-desired axis angle; as the range becomes more restricted, the accuracy of the determination is improved. The present accuracy limit is five seconds, the noise attributed to pickoff electronics and to illumination variations and field-of-view irregularities.

Pickoff Alignment Stability

The stability of the alignment generally is a function of temperature, acceleration environment, and environment history. One can introduce compensation if a repeatable sensitivity to temperature is discovered. In other respects, the alignment stability depends on construction materials and mechanical design of the pickoffs and their mounting. No data have been collected to evaluate the alignment stability or its sensitivity to temperature.

Computational

System computational accuracy depends on the accuracy of the direction cosines. In the present system, two direction cosines are determined directly from the pickoff signals and the pattern mechanization equation. A third cosine is calculated from pickoff alignment information and the identity which direction cosines of a unit vector satisfy in an orthogonal coordinate system:

$$\cos^2 \theta_1 + \cos^2 \theta_2 + \cos^2 \theta_3 = 1$$

The error generated in the third direction cosine from readout errors in the first two direction cosines can be estimated from the implicit differential of the identity.

$$\epsilon_3 = - \frac{\cos \theta_1 \epsilon_1 + \cos \theta_2 \epsilon_2}{\cos \theta_3}$$

where

$$\epsilon_i = \Delta(\cos \theta_i) = - \sin \theta_i \Delta \theta_i$$

Not only is the error in the third direction cosine a function of the error in the other two cosines, but also of the cosines themselves. The range of the cosines from pickoff information is governed by the patterned region of the rotor. In the present system,

$$|\cos \theta| \leq \sqrt{\frac{2}{2}}$$

From the orthogonality identity, it follows that the the magnitude of the third direction cosine can range from 0 to 1. Although it is ordinarily avoided in gyro operations, the possibility of a very small value for a third direction cosine and its effect on computational errors cannot be overlooked.

The computational error here is a compounding of other readout errors that is reduced by reducing the other errors. The compounding effect can be reduced by taking it into account in planning the operation of the readout system. This is considered in greater detail in Section IV.

OBSERVATIONAL EFFECTS OF READOUT ERRORS

The sources of error produce effects in the readout which follow distinctive patterns. The error sources may be classified according to the patterns observed in their effects. Often these patterns indicate how the effects of these errors may be compensated or reduced.

Nonrandom Changes in Pickoff Signal and Signal-to-Noise Ratio

Error sources which produce these effects are

- Rotor reflectivity variations
- Lamp luminosity variations
- Rotor noise isolated from the pattern
- Illumination variations
- Field-of-view irregularities

The effects of the first two sources are nulled by the height-insensitive trigger (HIT). The operation of the HIT is discussed later. Most of the rotor noise is filtered out by establishing a triggering threshold and using a pulse width discriminator. The last two sources produce an irregular pulse shape that can be nulled in principle by aligning the center of illumination to the desired readout axis and triggering at the 50-percent point of the pulse.

Errors Which Correlate With Spin Axis-Pickoff Axis Angle

Error sources whose effects can be correlated with pickoff axis colatitude are

- Pattern application error
- Pattern axis-spin axis misalignment

- Centrifugal distortion
- Line edge uncertainties
- Rotor noise at or adjacent to the pattern edge

Compensation for these errors can be implemented by modifying the mechanization equation for the direction cosine. Most of the error produced by the first three sources can be compensated by the addition of a few terms to the nominal mechanization. Many more terms must be added to handle line edge uncertainties and rotor noise effects. While these effects are random in the spatial domain, they are bounded; a potentially feasible method of compensation would be a Fourier expansion with the measured phase angle employed as the independent variable. The limit to which such an expansion can be carried would be defined by the resolution of the calibration data, the allotted computer capacity for the mechanization, or the point at which the benefits gained with the step wise addition of terms that correlate with the data no longer outweigh the inconvenience of carrying that additional term.

Errors Sensitive to Pattern Line Angle of Approach

Error sources whose effects are sensitive to angle of approach are

- Illumination variations
- Field-of-view irregularities
- Pickoff misalignment

Compensation for these effects can be introduced by subsequent mathematical operations on the direction cosines obtained from the mechanization equation. Pickoff misalignment is included here because the technique of compensation is similar. Moreover, the most significant effects of illumination variations and field-of-view irregularities cannot be separated from misalignment effects in an assembled gyro.

Cyclic and Random Effects

Error sources producing these effects are

- Rotor nutation
- Rise time variations
- Amplifier noise
- Triggering uncertainty
- Phase-angle measurement error

The effect of rotor nutation can be nulled by averaging over the number of revolutions required for the spin vector to precess one revolution about the maximum moment axis. The expected error of the other effects is reduced by averaging (summing) over several revolutions of the rotor.

Except for nutation, these error sources are electronic, the effect of which is a random error in the time axis. The effects of these errors can be reduced by other means as well as by averaging. The error itself can be reduced with the use of faster electronics. Such a reduction is within the scope of present technology. Another way to reduce it is to increase the measured time intervals which can be accomplished by running the gyro at a lower speed.

APPROACH TO ERROR COMPENSATION

Four approaches to compensation are thus suggested as means to reduce the effects of errors without reducing the errors themselves. The historical development of these approaches is discussed in the order by which they would be employed.

Height-Insensitive Trigger (HIT)

Reflectivity variations and changes in lamp output appear as short-term and long-term changes in pulse height. If the trigger occurs at a fixed voltage, a time interval error (ΔT) results, as shown in Figure 3.

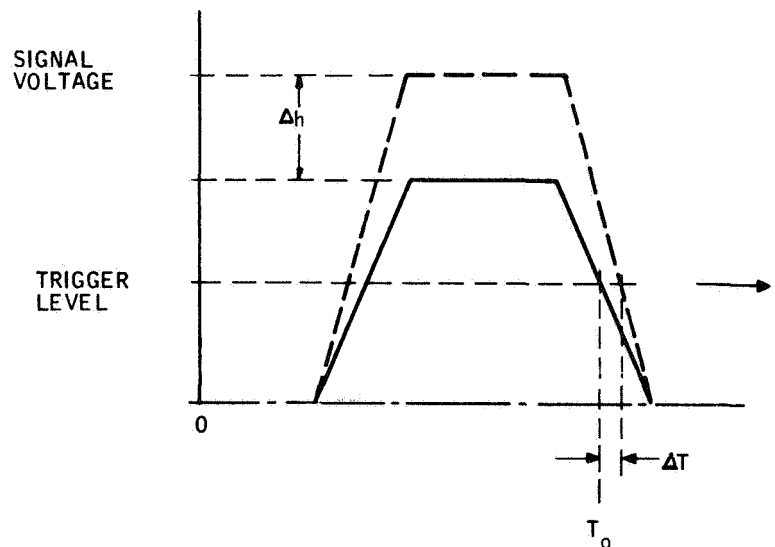


Figure 3. Error From Fixed Trigger Level

Since the basic electronic trigger circuits are voltage-sensitive, some method of compensation is desired to remove this error source. One method is by compensating the trigger device to render it sensitive to a fixed proportion of height rather than a fixed voltage. This is the purpose of the HIT. The block diagram of the HIT is shown in Figure 4, and the waveforms are shown in Figure 5. The basic operation is as follows.

The input pulse is amplified; the amplified pulse is sent to a peak level sensor that samples the peak voltage (flat top) of the input pulse and holds it. The amplified input pulse is then subtracted from one-half of the output of the peak level sensor. The zero-volt crossing of the resultant signal is a fixed percentage (nominally 50 percent) of the incoming pulse height. The zero-crossing signal is amplified to increase the slope of the zero crossing, and the zero crossing is then sensed by a tunnel diode threshold detector circuit. The trailing edge of the output pulse is the time mark used to control the time interval counters. The input pulse is differentiated and clipped, amplified, and used to discharge the voltage level sensor so it can accurately sample the peak voltage of the next input pulse.

Time Interval Measurement Averaging

The meridional angle of the pattern is determined by calculating the ratio of the time interval measurement between the pattern lines and the time interval measurement of the rotor period. To obtain an average value of the meridional angle, both time interval measurements are summed over the desired number of revolutions. The logic necessary to perform the summing is built into digital data processing circuits that gate the high-frequency pulse counters used in measuring the time intervals and record the counter data on punched paper tape. A selector control enables an operator to average over 1, 2, 4, 8, or 10 revolutions, the number chosen depending generally on the nature of the test to be conducted and the rotor speed for the test.

Compensation in the Direction Cosine Equation

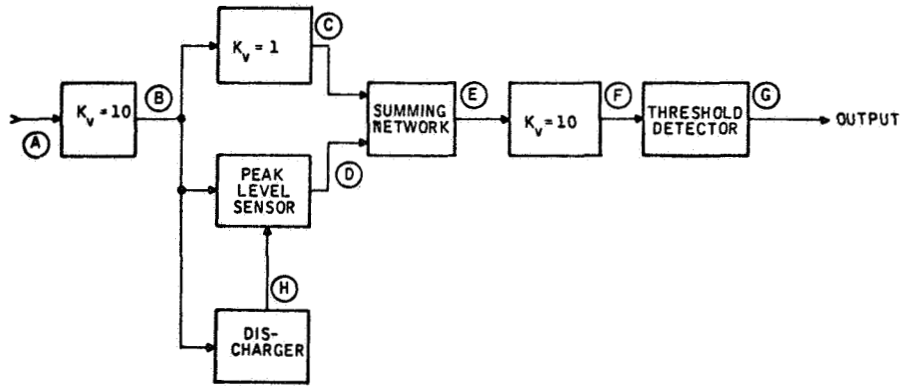
When a great circle pattern is used, the nominal mechanization equation takes the form:

$$\cos \theta = \cos \left[\cot^{-1} (K \cos \phi) \right]$$

or

$$\cos \theta = \frac{K \cos \phi}{\sqrt{1 + K^2 \cos^2 \phi}}$$

where ϕ is the measured meridional angle, and K is a constant determined by the slope of the pattern line with respect to the spin axis. It is apparent that to mechanize this equation to the required accuracy in a vehicle-mounted



NOTE: CIRCLED LETTERS REFER TO WAVEFORMS SHOWN IN FIGURE 5

Figure 4. Height - Insensitive Trigger Block Diagram

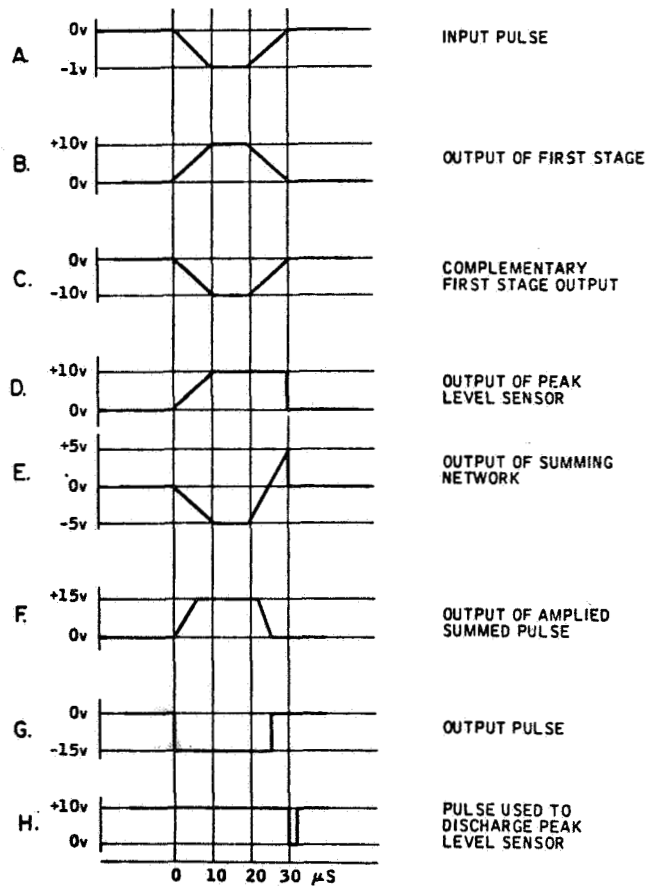


Figure 5. Height - Insensitive Trigger Wave Forms

computer would require more arithmetic steps and memory bits than that required for the cosine pattern. The memory requirements of these patterns are compared in Section III.

Computer compensation for cosine pattern application error and pattern axis-spin axis misalignment has been implemented by the addition of a few terms to the mechanization equation and regressing for all coefficients. Compensation for the higher-frequency errors (line edge uncertainties and rotor noise) has not yet been attempted. Experience in gathering calibration data from an operating gyro indicates that great care must be paid to procedural details and data gathering techniques in order to obtain calibration data in which uncertainties produced by spin vector drift does not exceed the accuracy requirements of the calibration.

Once the data collection procedure is perfected, the problem of characterizing the higher-frequency errors remains. These effects are random (in the sense that they cannot be predicted a priori) but repeatable as a function of spin axis-pickoff axis angle. In addition, these errors are expected to be bounded; a potentially feasible method of compensation is a Fourier expansion which employs the meridional angle as the independent variable. While a Fourier form of this characterization is in principle not difficult to find, the implementation of such a mechanization in a vehicle computer would require a considerable amount of memory.

Compensation for Angle of Approach

Compensation for pickoff misalignment has been implemented in a system of computer programs which reduces and analyzes drift data from the present strapdown ESGV. The location of the pickoffs in case axis coordinates is determined from the alignment calibration data. For each readout mode (combination of pickoffs read), an intermediate system is defined. One axis of the coordinate system, \hat{X}_1 , is coincident with one pickoff axis; a second axis, \hat{X}_2 , is normal to the first but in the plane defined by the two pickoff axes. The angle between this axis and the second pickoff is equal to the non-orthogonality between the two pickoff axes. The third coordinate axis, \hat{X}_3 , is normal to the other two. Spin vector components in these coordinates are calculated as follows:

$$\begin{aligned}\hat{S} \cdot \hat{X}_1 &= \cos \theta_1 \\ \hat{S} \cdot \hat{X}_2 &= \frac{\cos \theta_2 - \cos \theta_1 \cos \tau}{\sin \tau} \\ \hat{S} \cdot \hat{X}_3 &= \pm \sqrt{1 - (\hat{S} \cdot \hat{X}_1)^2 - (\hat{S} \cdot \hat{X}_2)^2}\end{aligned}$$

where θ_i is the spin vector colatitude angle with the i th pickoff axis and τ is the angle between the pickoff axes. The sign of $\hat{S} \cdot \hat{X}_3$ is determined from continuity criteria. Spin vector components in case axis coordinates are then calculated from the transformation matrix of the intermediate set. Second and higher harmonics of the angle of approach have been noted in alignment calibration data collected from present gyros. The causes of these harmonics have not been fully investigated; in principle, there are three possibilities: field-of-view irregularities, illumination variations, and spin vector drift. Drift can be separated from the other causes by collecting calibration data with the gyro case rotating in each direction about the reference axis and reducing the data from each simultaneously.

If field-of-view irregularities and illumination variations are shown to produce errors which correlate with higher harmonics of the angle of approach and which must be compensated, the method of compensation would likely take a different form from that described above for pickoff alignment. The direction of the spin vector projection on the plane normal to the pickoff axis would be determined from information provided by the other pickoffs. The angle of approach would be determined from this result and from the pattern slope at the observed colatitude. The correction, a function of the angle of approach, can then be calculated.

CRITICAL AREAS OF REQUIRED IMPROVEMENT

With the aid of Table I, the critical areas where improvements must be made can now be defined. Estimates of the error in present systems without compensation are given where data is not available. The data which is on hand is, however, classified; this data is furnished in Volume V of this report. Characteristic dependencies are listed, so that the error frequencies for a given system application may be calculated. Where compensation has been provided, the estimated error after compensation in the present system is indicated.

Error estimates of an improved readout system are also listed. In all cases, the applicable form of compensation is assumed. The only source not considered capable of compensation is the master quantization error of a cosine pattern. Improvements in pattern, rotor, and optic sources of error are credited to the use of faster electronics which yield greater resolution in the calibration data on which compensation is based. No limits were assumed on the number of terms in the mechanization equation. System error estimates are 7.5 seconds for a system employing a cosine pattern and 4.5 seconds for one using a great circle pattern. The difference between them is the absence of the master quantization error when using a great circle pattern.

An error budget which provides a system error of one second is presented in the last column of the table. The comparison of this error budget with the estimates of the improved system is the basis for defining those areas where

TABLE I. - PRESENT ESVM READOUT ERROR CHARACTERISTICS

Error Source	Error in "Direction Cosine"		Observed (sec)	Characteristic Dependencies		Other
	Theoretical (sec)	Rotor Size (r) Rotor Speed (ω_s)		Direction Angle (θ) Angle of Approach (ϕ)		
I. Pattern A. Application Error B. Line Edge Uncertainty Master Quantization C. Spin-Pattern Axis Align		r^{-1} ω_s^{-1} r^{-1} r^{-1}	(Classified)*	$\sin(\cos)n\theta, 0 \leq n \leq 5$ $\sin(\cos)n\theta, 10 \leq n \leq 100$ $\sin(\cos)n\theta, n > 100$ $\sin\theta, \cos\theta$	(Field Stop) ⁻¹ (Field Stop) ⁻¹	
II. Rotor A. Reflectivity Variations B. Surface Noise C. Centrifugal Distortion D. Nutation	12-20 3	r^{-1} r^{-1} $\omega_s^2 r^2$ ω_s		$\sin(\cos)n\theta, 0 \leq n \leq 10$ $\sin(\cos)n\theta, 10 \leq n \leq 100$ $\sin 2\theta$	(Field Stop) ⁻¹ Damping Time	
III. Optic A. Illumination Variations B. Field of View Irregularities C. Lamp Lum. Variations	60 12-20			$\sin(\cos)n\theta, 0 \leq n \leq 5$	(Field Stop) Power, Sup. Freq.	
IV. Electronic A. Rise Time Variations B. Amplifier Noise C. Trig. Level D. Trig. Uncertainty E. Phase Angle Error	7 3 0.5	ω_s ω_s^{-1} r^{-1} ω_s ω_s		$\sin\theta$	Pattern slope, Field Stop	
V. Other A. Pickoff Misalignment B. Alignment Stability C. Computational	2-10 1 X ∞	r^{-1} r^{-1}		$\sin\phi, \cos\phi$ $\sin\phi, \cos\phi$ $\sin 2\phi, \cos 2\phi$	Temperature Acceleration Other Errors	

* Refer to Volume V of this report.

TABLE I. PRESENT ESGV READOUT ERROR CHARACTERISTICS -- Concluded

Error Source	Error Compensation History		Estimated Improved Accuracy	
	Method of Compensation	Residual Error (sec)	With Present Technology (sec)	Maximum Budget in sec/sec of System Error
I. Pattern		(Classified)*	(Classified)*	
A. Application Error	Mechanization Eq.			0.3
B. Line Edge Uncertainty Master Quantization	None (Mech. Eq.) None			0.4 0.3
C. Spin-Pattern Axis Align	Mechanization Eq.			0.1
II. Rotor				
A. Reflectivity Variations	HIT	2.0	0.5	0.2
B. Surface Noise	None (Mech. Eq.)			0.4
C. Centrifugal Distortion	None (Mech. Eq.)	3.0	0.5	0.3
D. Nutation	Averaging			0.1
III. Optic				
A. Illumination Variations	HIT, Alignment	6.0	2.0	--
B. Field of View Irregularities	Computer (Not Used)	2.0	0.5	0.2
C. Lamp Lum. Variations	HIT	2.0	0.5	0.2
IV. Electronic				
A. Rise Time Variations	Averaging	2.0	0.3	0.3
B. Amplifier Noise	Averaging			0.3
C. Trig. Level	Pattern Design	--	--	--
D. Trig. Uncertainty	Averaging	1.0	0.2	0.2
E. Phase Angle Error	Averaging	0.2	0.1	0.1
V. Other				
A. Pickoff Misalignment	Alignment, Computer	1.0	0.5	0.2
B. Alignment Stability	Computer (Not Used)			0.2
C. Computational	Placement (Not Used) Operational Strategy	0 - 3X	0 - 3X	0 - 1X

*Blank spaces indicate classified material. Refer to Volume V of this report.

improvement is needed. The greatest improvement is needed in the reduction of error from pattern edge uncertainties. Methods of reducing its effect are considered in Section IV, while methods of reducing the error itself are discussed in Section V. All contributing sources of edge uncertainties -- which includes dispersion encountered in applying the pattern, arc marks, and surface finish imperfections -- are considered.

Optical sources of error are presently not serious contributors. Electronic sources and centrifugal distortion are serious contributors at present; however, they can be reduced to tolerable levels by using faster circuits and operating the gyro at a lower speed. Recent drift performance data from a 700 rps unit and a 200 rps unit indicate that both have about the same performance potential. From a readout accuracy standpoint, the lower speed is desirable; from the performance data one may conclude that an intermediate operating speed would provide better drift performance. In either case, faster electronics and centrifugal distortion are not expected to produce errors which exceed the accuracy requirements of future ESG units.

The electronic equipment used to measure phase angles of present units is too bulky to accompany vehicle-mounted ESG's. Section VI considers a system which may prove to be feasible for use with such units.

Improvement is needed in the control and compensation of pickoff alignments. Also, some assessment is needed of the alignment stability and how it is affected by environments. Laboratory effort is needed to provide improvements and knowledge in this area. Such an effort was not pursued in this study because it was beyond the scope of the study.

Computational compounding of errors has been shown to be a problem worthy of further attention. This compounding is a major point in the study of readout modes in Section IV.

In this error analysis, no assessment was made of the environmental effects on readout. The effects of three environmental factors - steady acceleration, vibration, and vehicle angular motion - are considered in Section VII.

SECTION III PATTERN DESIGN STUDY

An example was given in Section II which illustrates how the magnitude of one source of readout error is affected by the slope of the pattern line on the rotor. In this section we shall examine whereby several sources of error produce effects sensitive to pattern slope and other parameters such as rotor speed and the rotor colatitude observed by the pickoff axis; it will be seen to what extent error considerations have influenced the present pattern design concept.

Error sensitivity equations in terms of selected pattern parameters are derived and compared for three pattern types -- great circle, cosine, and colatitude. Optimum parameters are then selected which minimize the effects of the error sources. From the error amplification standpoint, the colatitude pattern is favored because its direction cosine error sensitivity is uniform and it has the smallest rms value. However, other factors can influence the choice of pattern type; two such factors are the ease of application and the mechanization equation computer memory size requirements. The great circle pattern is the easiest to apply to the rotor, while the cosine pattern requires the smallest memory size.

PATTERN PARAMETERS

The patterns considered here are defined by three parameters; pattern type, pattern range, and number of pattern lines. For any specific application, pattern range is likely to be determined by other considerations. However, a given pattern range may influence the choice of pattern type and the number of lines.

Types of Pattern

Patterns which have been applied to ESG rotors to date are of two types: great circle and cosine. These two pattern types probably represent the extremes in difficulty of application to the rotor and in computer requirements for mechanizing the direction cosine. The great circle pattern is an easily applied pattern because it is a planar pattern. The cosine pattern is desirable because it has a point-slope mechanization for the direction cosine. A third pattern type which may be desirable is one in which the colatitude angle is provided by a point-slope mechanization. This pattern shall be called the colatitude pattern.

For a readout system in which a phase angle is measured and used to calculate the direction of the momentum vector, these three pattern types provide a reasonable diversification of features associated with many types of patterns compatible with this system. An error analysis of these features may then point out a desirable pattern or the desirable features of each pattern.

Pattern Range

The pattern range is determined by whether or not all-attitude readout is required and the number and arrangement of the pickoffs. In most applications, all-attitude readout capability is required; in certain applications, a limited-attitude capability may be sufficient, or all-attitude capability may be sacrificed for greater readout accuracy in the region of interest. For this study, it is worthwhile to consider the pattern range as a variable.

Quantity of Pattern Lines

In gyros which have been patterned to date, three lines have been employed--two pattern lines from which phase-angle information is derived and one logic line for separating pulse trains in the pickoff signal. The use of more than three lines has the advantage of reducing the effect of random errors by an averaging process. Other advantages may become apparent as the pattern study is pursued.

NOMINAL PATTERN CHARACTERISTICS

The direction cosine function has odd symmetry about the equator. Since good accuracy for all attitudes is of primary concern, there is no reason to consider error requirements which are not symmetric about the equator. The patterns to be considered in this study will, therefore, have the symmetry required to produce odd symmetry in the mechanization equation. The great circle and the cosine pattern which have been employed on gyros exhibit this symmetry, and the colatitude pattern to be considered in this study will also satisfy this symmetry criterion.

The number of pattern lines is defined by the variable, n , which denotes the number of pairs of lines. At present, no consideration will be given to the logic line. A pair will consist of two adjacent lines, each of which covers the entire colatitude range of the patterned region of the rotor. Each line of a pair is a mirror image of the other with respect to a meridional line; i. e., they have equal but opposite slopes at each colatitude point. It will be shown later that this condition minimizes the effect of a potentially significant source of error.

Suppose that the lines of the first pair respectively satisfy the equations

$$\theta = F_{11}(\phi)$$

$$\theta = F_{12}(\phi)$$

The equational statement of this symmetry is

$$\frac{d F_{12}}{d \phi} = - \frac{d F_{11}}{d \phi}$$

Each pair of pattern lines differs from another pair only in its meridional placement on the rotor. The pairs are equally distributed about the rotor in the longitudinal angle; no two lines overlap. Suppose that corresponding lines of the first two pairs, respectively, are segments of the following equations

$$\theta = F_{11}(\phi)$$

$$\theta = F_{21}(\phi)$$

The criterion of equal distribution requires that

$$F_{21}(\phi) = F_{11}\left(\phi + \frac{2\pi}{n}\right)$$

It is desirable to utilize as much meridional range for the pattern as possible. This desire, plus the criteria of slope symmetry and equal distribution of nonoverlapping lines, leads to the specification of two important mechanization parameters:

- Each line is confined to a region having a meridional range of $\frac{\pi}{n}$. The colatitude range of the line in the region will be defined by the lower bound θ_0 and upper bound $\pi - \theta_0$.
- The equatorial intercepts of the pattern lines are equally distributed. The angle between intercepts of adjacent lines is, therefore, $\nu_0 = \frac{\pi}{n}$.

CALCULATION OF DIRECTION COSINE FROM PHASE-ANGLE DATA

With the aid of the pair of pattern lines illustrated in Figure 6, the steps required to calculate the direction cosine may be outlined:

- Determine the phase-angle ν with the signal processing electronics
- Calculate the meridional-angle μ from the pattern symmetry characteristics
- Obtain the direction cosine from the equation of the pattern line

The details of the first step are treated in Section VI ; it is assumed here that ν is known. The last step demands that the pattern equation be known explicitly; this will be derived later for each pattern type under consideration. The derivation of the angle μ can be completed with the pattern characteristics that so far have been specified.

From Figure 6, the angle $(\phi_2 - \phi_1)$ can be expressed as a sum of three angles:

$$\nu_0 = \phi_2 - \phi_1 = (\phi_2 - \phi_2') + (\phi_2' - \phi_1') + (\phi_1' - \phi_1)$$

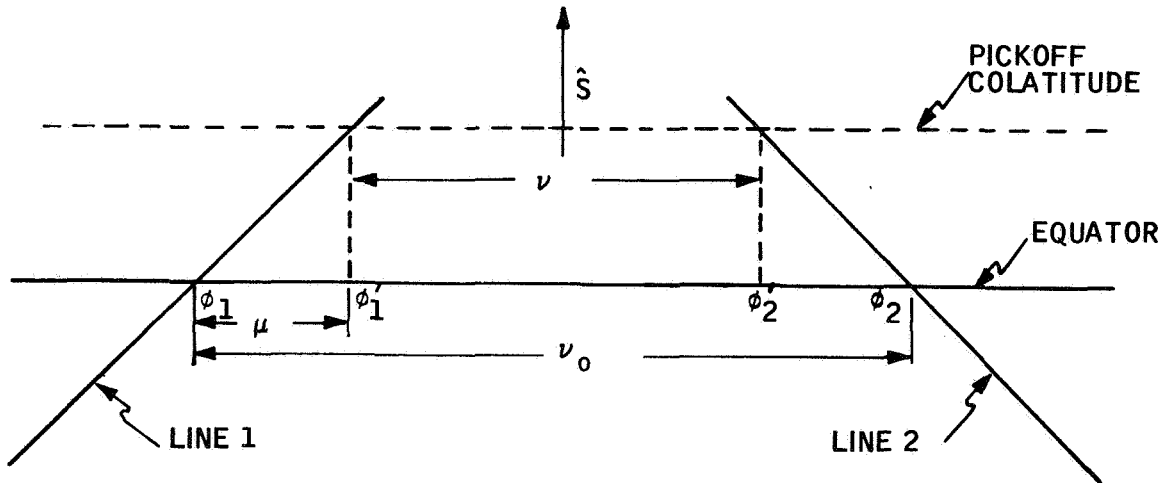


Figure 6. Pair of Pattern Lines on the Rotor

Now,

$$\nu = \phi_2' - \phi_1'$$

which is known from phase-angle data. From the pattern line symmetry,

$$\phi_2 - \phi_2' = \phi_1' - \phi_1 = \mu$$

Therefore,

$$\nu_o = \nu + 2\mu$$

If there are n pairs of pattern lines, the phase angle provided is the average value of the set ν_k :

$$\nu = \frac{1}{n} \sum_{k=1}^n \nu_k$$

Since

$$\nu_o = \frac{\pi}{n}$$

$$\mu = \frac{1}{2n} \left(\pi - \sum_{k=1}^n \nu_k \right) \quad (1)$$

This equation for μ can then be substituted into the pattern equation to determine the colatitude or the direction cosine.

The upper bound of μ is useful for determining the parameters for the pattern slopes. Nominally,

$$0 \leq \sum_{k=1}^n \nu_k \leq 2\pi$$

The lower bound of this sum defines the upper bound of μ . Therefore,

$$\mu_{\max} = \frac{\pi}{2n}$$

The equational representations of the errors will define errors in terms of deviations, or expected deviations, of the meridional coordinate ϕ_i of each pattern line as sensed by the phase-angle measurement electronics. The sensitivity of the direction cosine to the errors is determined by tracing their effect through the chain of calculations which determine the direction cosine. Given that the pattern-mechanization equation can be written

$$\lambda = \cos \theta = F(\mu)$$

the sensitivity of λ to an error in μ is

$$\Delta\lambda = \frac{dF}{d\mu} \Delta\mu$$

The standard deviations of $\Delta\lambda$ and $\Delta\mu$ are similarly related (with precautions taken to assure that standard deviations do not become negative):

$$\sigma(\Delta\lambda) = \left| \frac{dF}{d\mu} \right| \sigma(\Delta\mu)$$

The sensitivity of μ to an error in ϕ_i' can be similarly related. Let the standard deviation of the meridional-angle error be denoted by $\sigma(\Delta\phi_i)$. Since all of the pattern lines are alike or symmetric, these standard deviations are the same. Since two pattern lines define each angle ν_k , and since there are n pairs of lines,

$$\sigma\left(\Delta \sum_{k=1}^n \nu_k\right) = \sqrt{2n} \sigma(\Delta\phi_i)$$

Thus,

$$\sigma(\Delta\mu) = \frac{1}{2n} \sigma\left(\sum_{k=1}^n \nu_k\right) = \frac{1}{\sqrt{2n}} \sigma(\Delta\phi) \quad (2)$$

MECHANIZATION EQUATIONS FOR THE PATTERN TYPES

Great Circle Pattern

The general equation for a great circle on a spherical surface is

$$a \sin \theta \cos \phi + b \sin \theta \sin \phi + c \cos \theta = 0$$

where θ is the colatitude angle; ϕ is the longitudinal angle of the spherical polar coordinates; and a , b , c are the direction cosines of the axis normal to the plane of the great circle with respect to the X , Y , Z cartesian coordinates, respectively.

The great circle pattern lines which would be applied to an ESGV rotor are segments of lines satisfying this equation. The parameter of these segments can be determined by combinations of a , b , c and the coordinates of the end points of the segments.

For this design study, only one pattern line needs to be considered (which corresponds to Line 1 of Figure 6). The direction cosine solution from this great circle segment can be written

$$\lambda = \cos \theta = - \frac{a_1 \cos \mu + b_1 \sin \mu}{\sqrt{c_1^2 + (a_1 \cos \mu + b_1 \sin \mu)^2}}$$

From the fact that $\mu = 0$ at $\theta = \frac{\pi}{2}$,

$$a_1 = 0$$

Let K_1 be the slope of the pattern line at the equator:

$$K_1 = \left. \frac{d\lambda}{d\mu} \right|_{\mu=0} = -\frac{b_1}{c_1}$$

The direction cosine mechanization equation is, therefore,

$$\lambda = \frac{K_1 \sin \mu}{\sqrt{1 + K_1^2 \sin^2 \mu}} \quad (3)$$

The parameter K_1 can be more tangibly defined in terms of the pattern bounds with the following equivalent form:

$$\cot \theta = K_1 \sin \mu \quad (4)$$

At the lower bound of the pattern region,

$$\begin{aligned} \mu &= \frac{\pi}{2n} \\ \theta &= \theta_o \end{aligned}$$

Therefore,

$$K_1 = \frac{\cot \theta_o}{\sin \frac{\pi}{2n}} \quad (5)$$

For the error analysis, the equation for the direction cosine derivative is needed:

$$\frac{d\lambda}{d\phi} = \frac{d\lambda}{d\mu} = \frac{K_1 \cos \mu}{[1 + K_1^2 \sin^2 \mu]^{3/2}}$$

Equation (4) can be used for writing this derivative in terms of the colatitude angle.

$$\frac{d\lambda}{d\phi} = \sin^3 \theta \sqrt{K_1^2 - \cot^2 \theta} \quad (6)$$

From Equation (4), it is seen that K_1 and $-K_1$ define the upper and lower bounds of $\cot \theta$; thus, $\frac{d\lambda}{d\theta}$ is real for all values of θ intercepted by the great circle. Combining Equations (2), (5), and (6) provides the equation relating the error sensitivity of the direction cosine to $\sigma(\Delta \phi)$:

$$\sigma(\Delta \lambda) = \frac{\sin^3 \theta}{\sqrt{2n}} \sqrt{\frac{\cot^2 \theta_o}{\sin^2 \frac{\pi}{2n}} - \cot^2 \theta} \sigma(\Delta \phi) \quad (7)$$

Cosine Pattern

The general equation of the cosine pattern line is

$$\cos \theta = A \phi + B$$

As it was developed for the great circle pattern, it is desirable to formulate parameters for the pattern characteristics by the equatorial intercept and its slope at the intercept. Again, only one line is considered:

$$\lambda = \cos \theta = A_1 \mu + B_1$$

for

$$\mu = 0, \quad \theta = \frac{\pi}{2};$$

therefore,

$$B_1 = 0$$

The mechanization simplicity is demonstrated by the derivative of the cosine:

$$\frac{d\lambda}{d\phi} = \frac{d\lambda}{d\mu} = A_1 \quad (8)$$

As can be expected, this derivative is independent of the colatitude angle. The parameter A_1 is determined by the coordinates of the pattern line at the colatitude lower bound of the pattern region:

$$A_1 = \frac{2n \cos \theta_o}{\pi} \quad (9)$$

The pattern mechanization equation is, therefore,

$$\cos \theta = \frac{2n \cos \theta_o}{\pi} \mu \quad (10)$$

Combining (2), (8), and (9) yields the error sensitivity to $\sigma(\Delta \phi)$ for the cosine pattern:

$$\sigma(\Delta \lambda) = \frac{\sqrt{2n} \cos \theta_o}{\pi} \sigma(\Delta \phi) \quad (11)$$

Colatitude Pattern

The general equation of the colatitude pattern line is

$$\theta = M \phi + N \quad (12)$$

Again, following the same procedure, the equation for the line of interest is

$$\theta = M_1 \mu + N_1$$

For

$$\mu = 0, \theta = \frac{\pi}{2}$$

therefore,

$$N_1 = \frac{\pi}{2}$$

Therefore,

$$\lambda = \cos \theta = \cos \left(M_1 \mu + \frac{\pi}{2} \right) = -\sin M_1 \mu \quad (13)$$

is the general pattern mechanization equation. Using the value of μ at the pattern lower bound ($\mu = \frac{\pi}{2n}$ at $\theta = \theta_o$) on the general form Equation (12) produces the result

$$M_1 = 2n \left(\frac{\theta_o}{\pi} - \frac{1}{2} \right)$$

It should be noted that since $\theta_o < \frac{\pi}{2}$, M_1 is always negative.

The derivative of the direction cosine function is

$$\frac{d\lambda}{d\mu} = - M_1 \cos M_1 \mu$$

With Equation (13) and a series of trigonometric manipulations, one can show that

$$\frac{d\lambda}{d\mu} = - M_1 \sin \theta \quad (14)$$

Let

$$T = \frac{1}{2} - \frac{\theta_o}{\pi}$$

The error sensitivity equation can now be written.

$$\sigma(\Delta\lambda) = T \sin \theta \sqrt{2n} \sigma(\Delta\phi) \quad (15)$$

ERROR MINIMIZATION CRITERIA

There are a number of error sources in which the system uncertainty from these errors is sensitive to certain rotor pattern characteristics. Four such characteristics are discussed and derived here.

Sensitivity to a Phase-Angle Measurement Error

Since the phase angle is the angle which is calculated directly from the pick-off signals, it is desirable to ascertain the sensitivity of the readout variables (direction cosines, or direction angles) to a phase-angle error. A generalized error equation can be derived in function notation.

Let the direction cosine be the variable of interest for the moment. Given that

$$\theta = F_1(\phi)$$

the inverse function can be written

$$\phi = F_1^{-1}(\theta)$$

Now let

$$\lambda = \cos \theta = \cos [F_1(\phi)] = G_1(\phi)$$

An error in the phase angle produces an error defined by

$$\Delta \lambda = \frac{d G_1(\phi)}{d \phi} \Delta \phi = G'_1(\phi) \Delta \phi$$

It is desirable to state the error equation as a function of the colatitude angle θ .

$$\Delta \lambda = G'_1 [F_1^{-1}(\theta)] \Delta \phi$$

An expected value for the magnitude of $\Delta \phi$ is the standard deviation of $\Delta \phi$, which shall be denoted by $\sigma(\Delta \phi)$. If $\Delta \phi$ is replaced by $\sigma(\Delta \phi)$, an expectation of the magnitude of $\Delta \lambda$ is the result. This entity shall be similarly expressed as

$$\sigma(\Delta \lambda) = |G' [F^{-1}(\theta)]| \sigma(\Delta \phi) \quad (16)$$

To assure a positive result for $\sigma(\Delta \lambda)$, the absolute value of the function is taken. In the case of a phase-angle measurement error, from electronic sources, $\sigma(\Delta \phi)$ is independent of θ .

Sensitivity to Line Edge Error

Line edge error is a function of the patterning process; as such, the line edge deviation is measured normal to the line itself. Its projection in any other direction is amplified; therefore, the projection of line edge deviation along a parallel of latitude is a function of the slope of the line at that point (Figure 7).

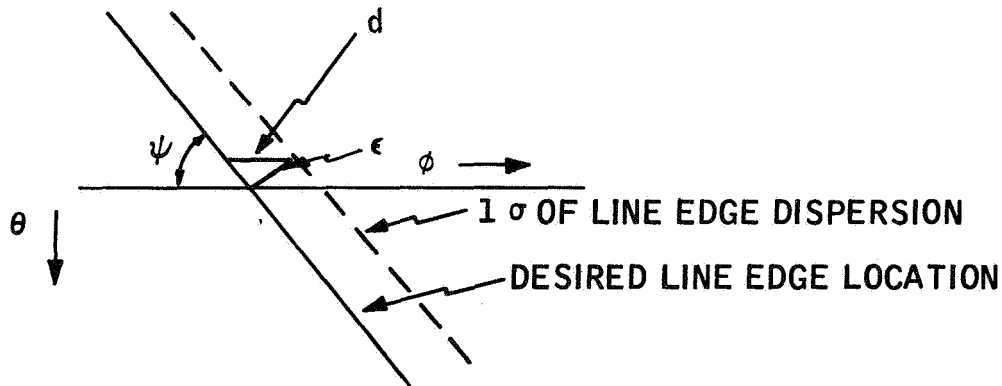


Figure 7. Geometry of Line Edge Error

The general equation for line edge error sensitivity can also be derived in terms of function notation.

Referring to Figure 7, let ϵ denote the expected value of the normal projection of the line edge dispersion and d the resulting longitudinal dispersion, so that

$$\sigma(d) = \epsilon \csc \psi$$

where

$$\tan \psi = \frac{d \theta}{d \phi} \quad (17)$$

Since

$$\csc \psi = \pm \sqrt{1 + \frac{1}{\tan^2 \psi}}$$

the longitudinal dispersion can be expressed in terms of the derivative

$$\sigma(d) = \epsilon \frac{1}{\frac{d \theta}{d \phi}} \sqrt{1 + \left(\frac{d \theta}{d \phi}\right)^2}$$

The longitudinal error is related to α as follows:

$$d = r \sin \theta \Delta \phi$$

so that

$$\sigma(\Delta \phi) = \frac{d}{r \sin \theta} = \frac{\epsilon}{r \sin \theta} \frac{1}{\frac{d \theta}{d \phi}} \sqrt{1 + \left(\frac{d \theta}{d \phi}\right)^2} \quad (18)$$

Later, it will be convenient to have $\sigma(\Delta \phi)$ expressed in terms of the direction cosine derivative:

$$\sigma(\Delta \phi) = \frac{\epsilon}{r} \sqrt{\csc^2 \theta + \frac{1}{\left(\frac{d \lambda}{d \phi}\right)^2}} \quad (19)$$

To determine the error in direction cosine, this equation is substituted into the equation for the phase angle error:

$$\Delta \lambda = \frac{\epsilon}{r} G_1' [F_1^{-1}(\theta)] \frac{\sqrt{1 + \left(\frac{d\theta}{d\phi}\right)^2}}{\sin \theta \frac{d\theta}{d\phi}}$$

Now the derivative can be denoted by

$$\frac{d\theta}{d\phi} = F_1'(\phi)$$

so that

$$\sin \theta \frac{d\theta}{d\phi} = \frac{d}{d\phi} (-\lambda) = -G_1'(\phi)$$

The final generalized equation for the direction cosine error is

$$\Delta \lambda = \frac{\epsilon}{r} \sqrt{1 + \{F_1' [F_1^{-1}(\theta)]\}^2} \quad (20)$$

(Since the absolute value of $\Delta \lambda$ is of primary interest, signs have been disregarded.)

Sensitivity to Triggering Level Error

The pickoff signal is used to produce pulses for the phase-angle measurement electronics. This signal is changing as long as the pattern edge traverses the pickoff field of view, which represents an angle of the order of several minutes. Consequently, the triggering level of the signal must be precisely defined. The ideal triggering point is the instant at which the line crosses the center of the field of view.

It is worth-while to evaluate the dependence of errors caused by triggering level deviations on the pattern parameters. Let A denote the unpatterned surface area viewed by the pickoff (Figure 8).

$$A = \pi \rho^2 - (\rho^2 \sigma - \rho^2 \sin \sigma \cos \sigma)$$

The signal output is proportional to the complement of this area. An expression for the normalized complement of this area is

$$S = 1 - \frac{1}{\pi \rho^2} = \frac{1}{\pi} \left[\cos^{-1} \left(\frac{h}{\rho} \right) - \frac{h}{\rho} \sqrt{1 - \left(\frac{h}{\rho} \right)^2} \right] \quad (21)$$

since

$$\sigma = \cos^{-1} \frac{h}{\rho}$$

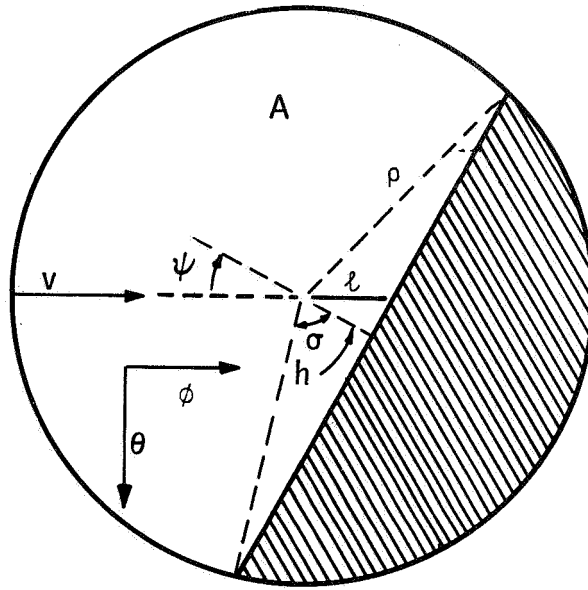


Figure 8. Pattern Edge in Field of View

Let t_i be defined as the time at which the edge of the i th pattern line crosses the center of the field of view. Then

$$h = \frac{\rho(t - t_i)}{T_i}, \quad -T_i \leq (t - t_i) \leq T_i \quad (22)$$

where T_i is the time required for the line edge to travel from the edge to the center of the field. If v is the linear speed of the line edge,

$$T_i = \frac{\rho}{v \cos \psi_i} = \frac{\rho}{\omega_s r \sin \theta \cos \psi_i} \quad (23)$$

Let the triggering point be defined as t_i' , the instant when the normalized signal S is equal to η . Therefore,

$$\eta = \frac{1}{\pi} \left[\cos^{-1} \left(\frac{t_i' - t_i}{T_i} \right) - \left(\frac{t_i' - t_i}{T_i} \right) \sqrt{1 - \left(\frac{t_i' - t_i}{T_i} \right)^2} \right]$$

or

$$\pi (0.5 - \eta) = \sin^{-1} \left(\frac{t_i' - t_i}{T_i} \right) - \left(\frac{t_i' - t_i}{T_i} \right) \sqrt{1 - \left(\frac{t_i' - t_i}{T_i} \right)^2} \quad (24)$$

If the region of interest is restricted to

$$0.4 \leq \eta \leq 0.6$$

a good approximation to Equation (24) is

$$\pi (0.5 - \eta) = 2 \left(\frac{t_i' - t_i}{T_i} \right) \quad (25)$$

The time interval between pulses generated by two pattern lines (call them lines 1 and 2) would be

$$\Delta t(\eta) = t_2' - t_1' = \frac{\pi}{2} (0.5 - \eta) (T_2 - T_1) + t_2 - t_1$$

If the trigger level is perfectly set at

$$\eta = 0.5$$

the desired time interval would be obtained; i. e.,

$$\Delta t(0.5) = t_2 - t_1$$

The error in the time interval caused by an error in the trigger level setting is, therefore,

$$\begin{aligned} e(\Delta t) &= \frac{\pi}{2} (0.5 - \eta) (T_2 - T_1) \\ &= \frac{\pi(0.5 - \eta)\rho}{2 \omega_s r \sin \theta} \left(\frac{1}{\cos \psi_2} - \frac{1}{\cos \psi_1} \right) \end{aligned} \quad (26)$$

in view of Equation (23).

Now, if pattern lines with complementary slope functions [i. e., $\psi_2(\theta) = -\psi_1(\theta)$] are used, then $\cos \psi_2 = \cos \psi_1$, and triggering level errors are eliminated. The correct time interval between pulses would be generated regardless of where the triggering level is set. Some distinct advantages develop as a result of eliminating this error.

- Triggering levels may be adjusted to eliminate false triggering from arc marks, if necessary.
- No compensation is necessary for the possibility that levels may vary among the pickoffs. Measures such as a separate mechanization equation for each pickoff are eliminated.

For these reasons, pattern designs which are considered in this study will exhibit this slope symmetry between pattern line pairs.

Sensitivity to Signal Rise Time

The accuracy of the electronics which produces a pulse at the trigger level depends on the signal rate of rise at the triggering point. Differentiating the equation for the normalized pickoff signal Equation (21) with respect to time yields

$$\frac{dS}{dt} = \frac{dS}{dh} \frac{dh}{dt} = - \frac{2}{\pi\rho} \sqrt{1 - \left(\frac{h}{\rho}\right)^2} \frac{dh}{dt} = - \frac{2}{\pi\rho} \sin \sigma \frac{dh}{dt}$$

From Equations (22) and (23)

$$\frac{dh}{dt} = \frac{\rho}{T_i} = \omega_s r \sin \theta \cos \psi_i$$

Therefore,

$$\left| \frac{dS}{dt} \right| = \frac{2}{\pi\rho} \sin \sigma \omega_s r \sin \theta \cos \psi_i \tag{27}$$

For the pattern analysis, only the pattern-sensitive parameters need to be carried explicitly - namely, θ and ψ . Assuming that the readout error is inversely proportional to the rate of rise, the longitudinal error generated by rate of rise attributed to pattern factors is proportional to e , where

$$e = \frac{1}{\sin \theta \cos \psi}$$

(It is no longer necessary to carry the subscript to ψ for this analysis.)

By using Equation (17) and trigonometric relationships,

$$\cos \psi = \frac{\frac{d\theta}{d\phi}}{\sqrt{1 + \left(\frac{d\theta}{d\phi}\right)^2}}$$

Consequently,

$$e = \frac{1}{\sin \theta \frac{d\theta}{d\phi}} \sqrt{1 + \frac{d\theta}{d\phi}^2}$$

A comparison of this Equation with Equation (18), in view of the fact that $\Delta \phi \propto e$, shows that the cosine error function from rate of rise takes the same form as that from line edge dispersion. Since a pattern which reduces one of these errors reduces the other in the same way, Equation (19) will be considered to represent both factors in this study.

Sensitivity of Readout Variables to Error Sources

There are, therefore, two error-sensitivity equations from which pattern characteristics can be evaluated. The direction cosine error has already been derived. It is also desirable to know the colatitude angle error sensitivity to these effects as well as some idea as to how sensitive the third direction cosine is to these errors. Both of these can be obtained from the basic direction cosine sensitivities. Since

$$\Delta \lambda = \Delta (\cos \theta) = -\sin \theta \Delta \theta$$

the colatitude sensitivity (disregarding signs) is

$$\sigma (\Delta \theta) = \frac{1}{\sin \theta} \sigma (\Delta \lambda) = \csc \theta \sigma (\Delta \lambda) \quad (28)$$

From the orthogonality identity,

$$\lambda_1^2 + \lambda_2^2 + \lambda_3^2 = 1 \quad (29)$$

therefore,

$$\lambda_1 \Delta \lambda_1 + \lambda_2 \Delta \lambda_2 + \lambda_3 \Delta \lambda_3 = 0$$

It is convenient in showing the third direction cosine sensitivity that only two direction cosines be considered. To accomplish this, it shall be assumed that λ_2 is zero.

Then,

$$\Delta\lambda_3 = -\frac{\lambda_1}{\lambda_3} \Delta\lambda_1$$

and

$$\lambda_3 = \pm\sqrt{1 - \lambda_1^2}$$

therefore,

$$\Delta\lambda_3 = \pm \frac{\lambda_1}{\sqrt{1 - \lambda_1^2}} \Delta\lambda_1$$

By putting $\lambda_1 = \lambda$ and disregarding the signs, we find that

$$\sigma(\Delta\lambda_3) = \cot \theta \sigma(\Delta\lambda) \quad (30)$$

Once the direction cosine sensitivity is derived, the colatitude sensitivity and third direction cosine sensitivities can be expressed directly through Equations (28) and (30).

CALCULATION OF ERROR SENSITIVITIES

The sensitivity of the direction cosine equations for each pattern type can now be evaluated for two types of error. To evaluate the sensitivity to a phase-angle measurement error, let the standard deviation of the meridional angle error be given by

$$\sigma(\Delta\phi) = \omega\tau$$

where τ is the intrinsic timing error of the phase-angle electronics, and ω is the rotor speed. To determine the sensitivity to line edge dispersion, Equation (19) and the direction cosine derivative for the pattern type under consideration are used. Each of these expressions for $\sigma(\Delta\phi)$ is substituted into the error sensitivity equation derived for each pattern type.

To determine optimum values of the number of pattern line pairs for given pattern ranges, an expression for $\sigma(\Delta\lambda)$, which represents the error for

the entire pattern range, is desired, rather than the error at a given colatitude. A convenient representation is the rms value of $\sigma(\Delta\lambda)$ over the nominal range:

$$\bar{\sigma} = \sigma_{\text{rms}} = \left\{ \frac{\int_{\theta_0}^{\pi-\theta_0} [\sigma(\Delta\lambda)]^2 d\theta}{\int_{\theta_0}^{\pi-\theta_0} d\theta} \right\}^{1/2}$$

Great Circle Pattern

For the great circle pattern, the sensitivity of the direction cosine to a timing error is

$$\sigma(\Delta\lambda) = \frac{\omega\tau}{\sqrt{2n}} \sin^3 \theta \sqrt{\frac{\cot^2 \theta_0}{\sin^2 \frac{\pi}{2n}} - \cot^2 \theta}$$

The rms value of the expected timing error is

$$\frac{\bar{\sigma}_{\tau}}{\omega\tau} = \frac{1}{\sqrt{2n}} \left\{ \frac{1}{\sin^2 \frac{\pi}{2n}} \left[\frac{5}{16} \cot^2 \theta_0 + \frac{\cot \theta_0 \cos^2 \theta_0}{\pi - 2\theta_0} \left(\frac{5}{8} + \frac{3}{4} \sin^2 \theta_0 - \frac{\sin^2 \theta_0 \cos^2 \theta_0}{3} \right) \right] - \left[\frac{1}{16} + \frac{\sin \theta_0 \cos \theta_0}{\pi - 2\theta_0} \left(\frac{1}{8} - \frac{\sin^2 \theta_0}{4} + \frac{\sin^2 \theta_0 \cos^2 \theta_0}{3} \right) \right] \right\}^{1/2}$$

The expected line edge dispersion equation is written in terms of a direction cosine derivative; the equation for the derivative is substituted before the final equation is obtained. Using Equations (5) and (6) in Equation (19), one obtains

$$\sigma(\Delta\phi) = \frac{\epsilon}{r} \sqrt{\csc^2 \theta + \frac{1}{\sin^6 \theta \left(\frac{\cot^2 \theta_0}{\sin^2 \frac{\pi}{2n}} - \cot^2 \theta \right)}} \quad (31)$$

The rms over the pattern range is

$$\bar{\sigma}_{\epsilon} \left(\frac{r}{\epsilon} \right) = \frac{1}{2\sqrt{n}} \left\{ \frac{1}{\sin^2 \frac{\pi}{2n}} \left[\frac{3}{4} \cot^2 \theta_o + \frac{\cos^2 \theta_o}{\pi - 2\theta_o} \left(\frac{3}{2} \cot \theta_o + \sin \theta_o \cos \theta_o \right) \right] + \frac{1}{4} \left[7 - \frac{\sin 2\theta_o \cos 2\theta_o}{\pi - 2\theta_o} \right] \right\}^{1/2} \quad (32)$$

A graph of each rms function is shown in Figures 9 and 10 for various values of θ_o . The normalized timing error curves (Figure 9) show that the number of pattern line pairs should be kept to a minimum, while the normalized line edge error curves establish optimum values for n . In the ESVG, pattern line edge errors are expected to be greater than timing errors; the choice of n is, therefore, likely to be dictated by the optimum values for pattern line edge errors. The timing error contribution motivates a choice of one of the lower values of n which optimizes the pattern line edge errors.

Cosine Pattern

For the cosine pattern, the expected deviation from a phase-angle measurement is

$$\sigma(\Delta\lambda) = \omega \tau \frac{\sqrt{2n} \cos \theta_o}{\pi} \quad (33)$$

Since Equation (33) is independent of the colatitude, it is equal to the rms value of that error.

From Equations (8), (9), and (19), the expected error from the line edge dispersion is obtained.

$$\sigma(\Delta\phi) = \frac{\epsilon}{r} \sqrt{\csc^2 \theta + \frac{1}{A_1^2}} = \frac{\epsilon}{r} \sqrt{\csc^2 \theta + \frac{\pi^2}{4n^2 \cos^2 \theta_o}}$$

Substitution of this expression into Equation (11) yields

$$\sigma(\Delta\lambda) = \frac{\epsilon}{r} \sqrt{\frac{2n \cos^2 \theta_o \csc^2 \theta}{\pi^2}} + \frac{1}{2n} \quad (34)$$

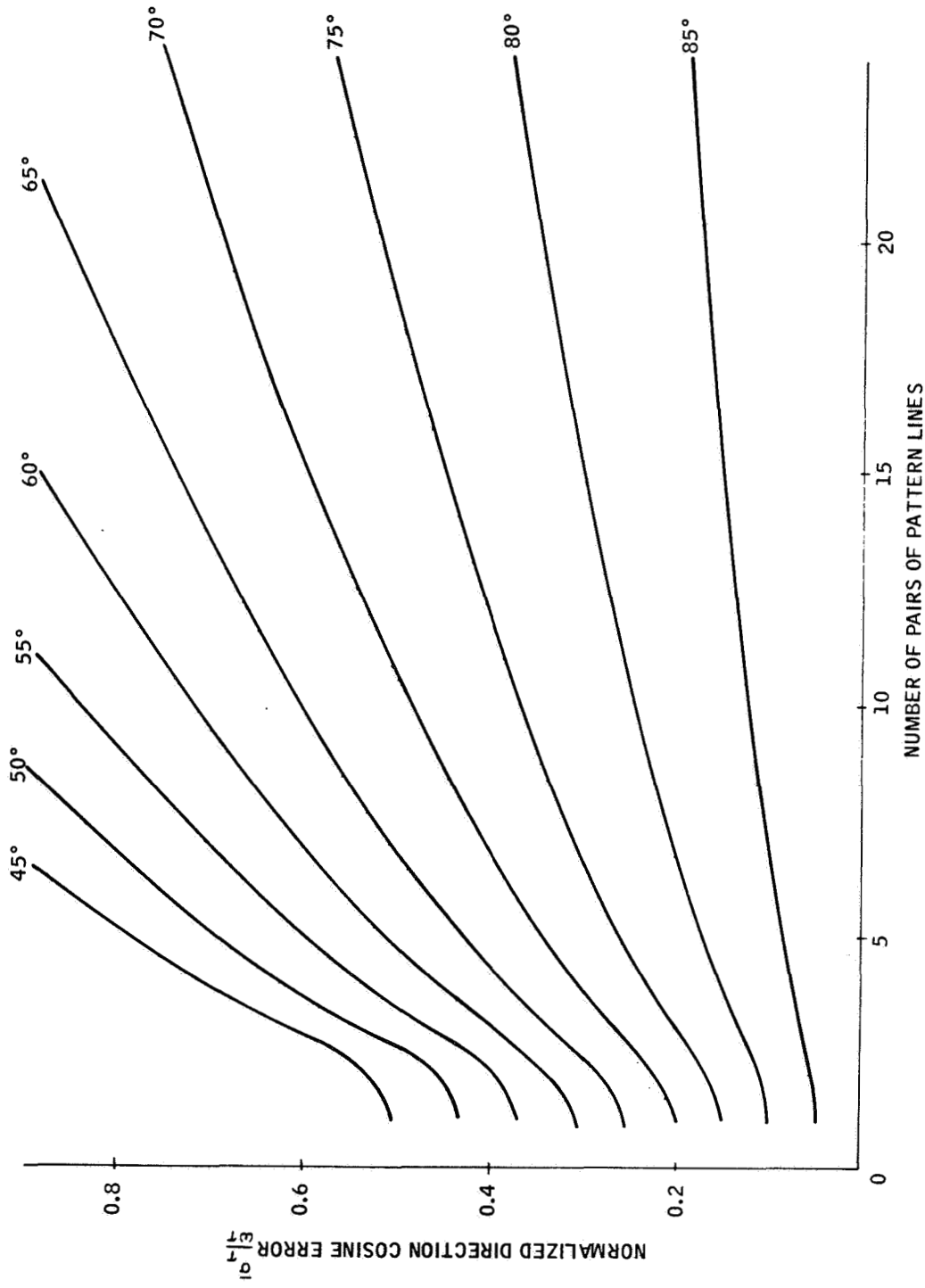


Figure 9. Normalized Expected rms Error from Phase Angle Timing Errors, Great Circle Patterns for Various Pattern Ranges

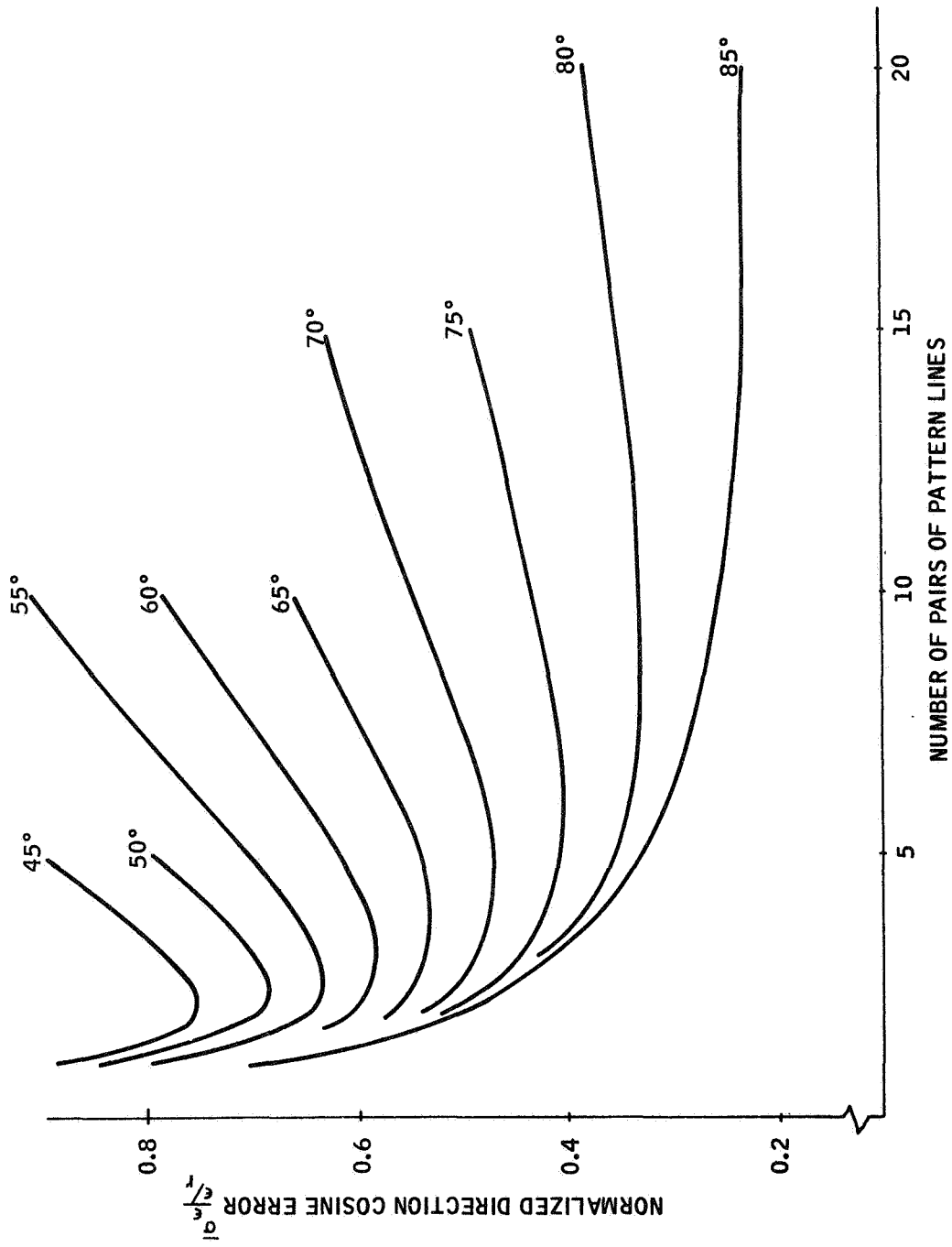


Figure 10. Normalized rms Expected Error from Line Edge Dispersion, Great Circle Patterns for Various Pattern Ranges

The normalized rms representation of this error is

$$\bar{\sigma}_\epsilon \frac{r}{\epsilon} = \left[\frac{1}{2n} + \frac{4n \cos^3 \theta_o}{\pi^2 \sin \theta_o} \right]^{1/2} \quad (35)$$

Figures 11 and 12 are graphs of Equations (33) and (35), respectively, with the lower bound of the pattern range θ_o as a parameter. Again, the line edge deviation error shows that optimum choice of n can be made to minimize it, while the timing error motivates the use of a lower value of the optimums.

Colatitude Pattern

For the colatitude pattern, the expected phase-angle timing error is

$$\sigma_\tau(\Delta\lambda) = \omega\tau T \sin \theta \sqrt{2n} \quad (36)$$

The rms value of this error over the pattern range is

$$\frac{\bar{\sigma}_\tau}{\omega\tau} = \sqrt{T^2 n \left(1 + \frac{\sin 2 \theta_o}{\pi - 2 \theta_o} \right)} \quad (37)$$

The equation for the expected line edge dispersion is obtained from (14) and (19).

$$\sigma(\Delta\phi) = \frac{\epsilon}{r \sin \theta} \sqrt{1 + \frac{1}{4 n^2 T^2}}$$

Substitution into (15) yields

$$\sigma(\Delta\lambda) = \frac{\epsilon \sqrt{2}}{r} \sqrt{T^2 n + \frac{1}{4n}}$$

Since this expression is independent of the colatitude, it also represents the rms of the error. Therefore,

$$\bar{\sigma}_\epsilon \frac{r}{\epsilon} = \sqrt{2n T^2 + \frac{1}{2n}} \quad (38)$$

Figures 13 and 14 are graphs of the error Equations (37) and (38). They show the same characteristics as the corresponding graphs for the great circle and cosine patterns.

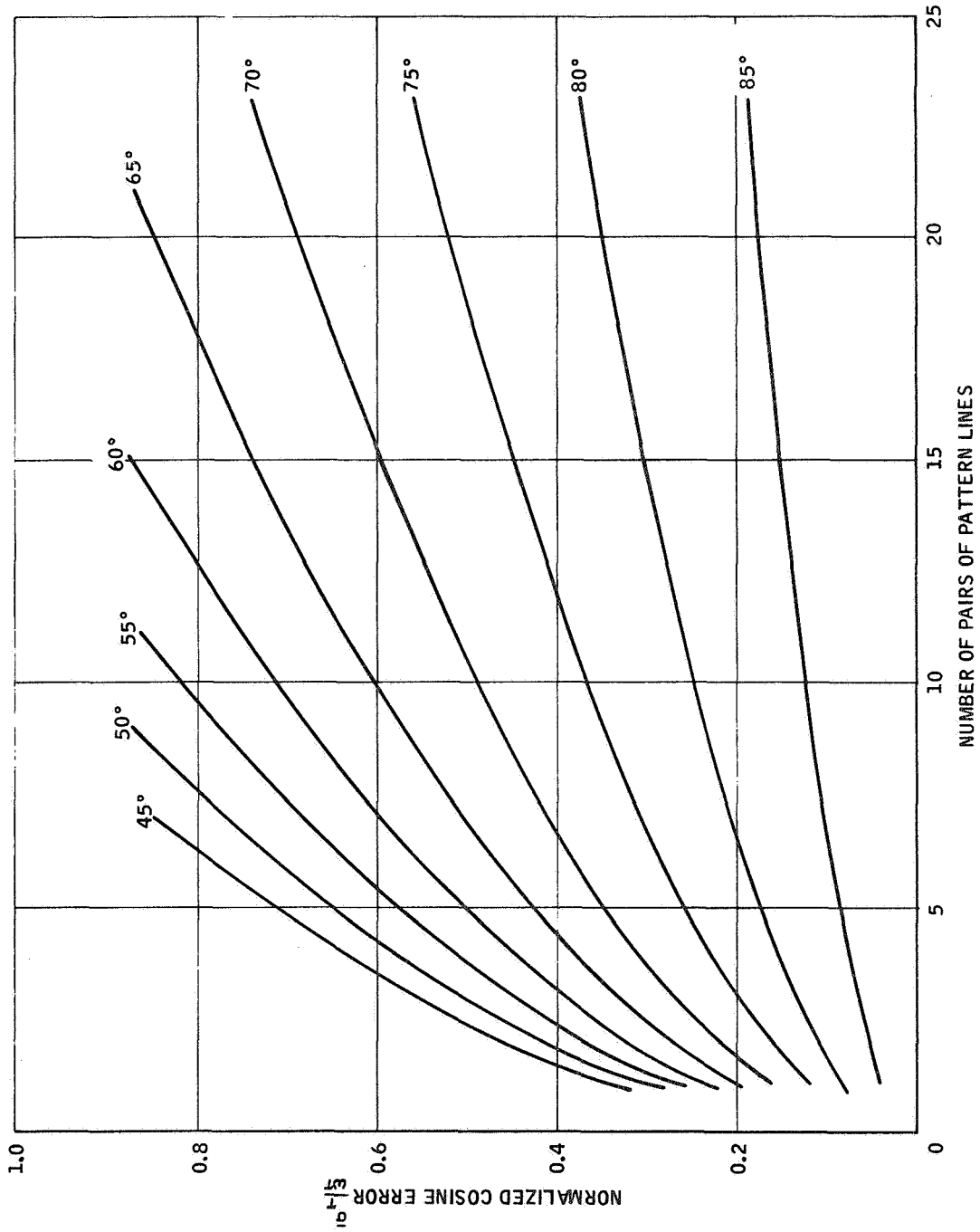


Figure 11. Normalized Expected rms Error from Phase Angle Timing Error, Cosine Patterns for Various Pattern Ranges

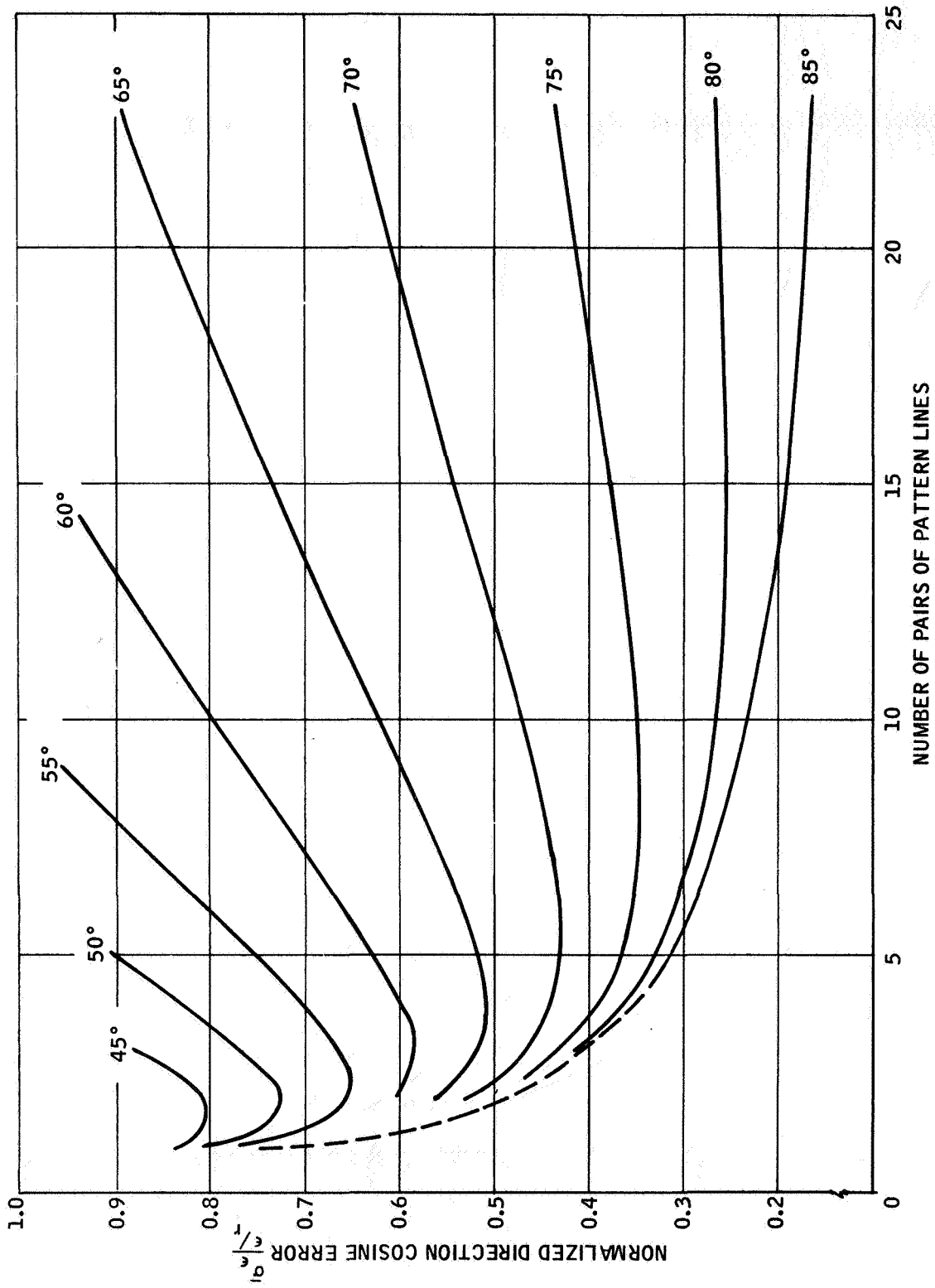


Figure 12. Normalized Expected rms Error from Line Edge Dispersion, Cosine Patterns for Various Pattern Ranges

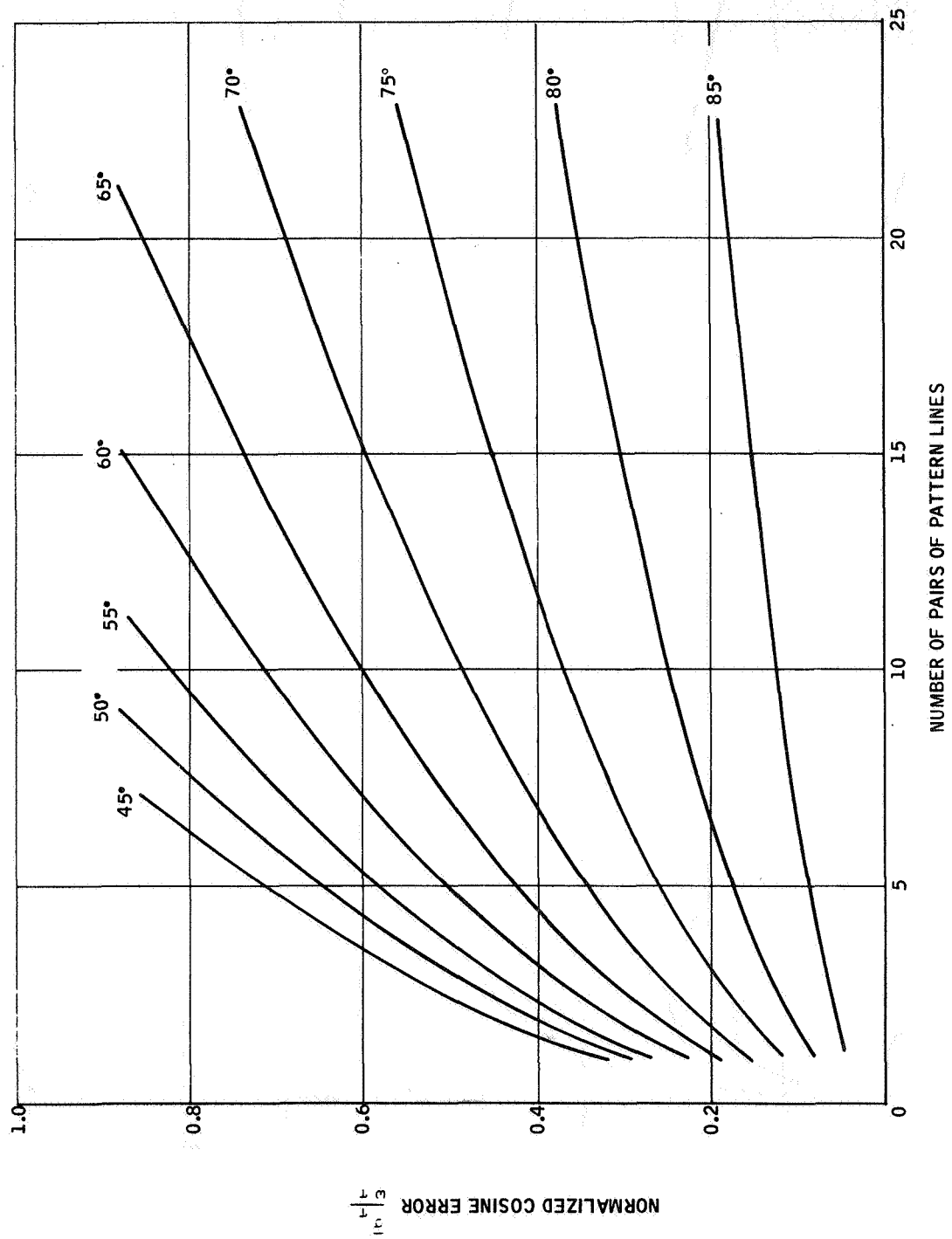


Figure 13. Normalized Expected rms Error from Phase Angle Timing Error, Colatitude Patterns for Various Pattern Ranges

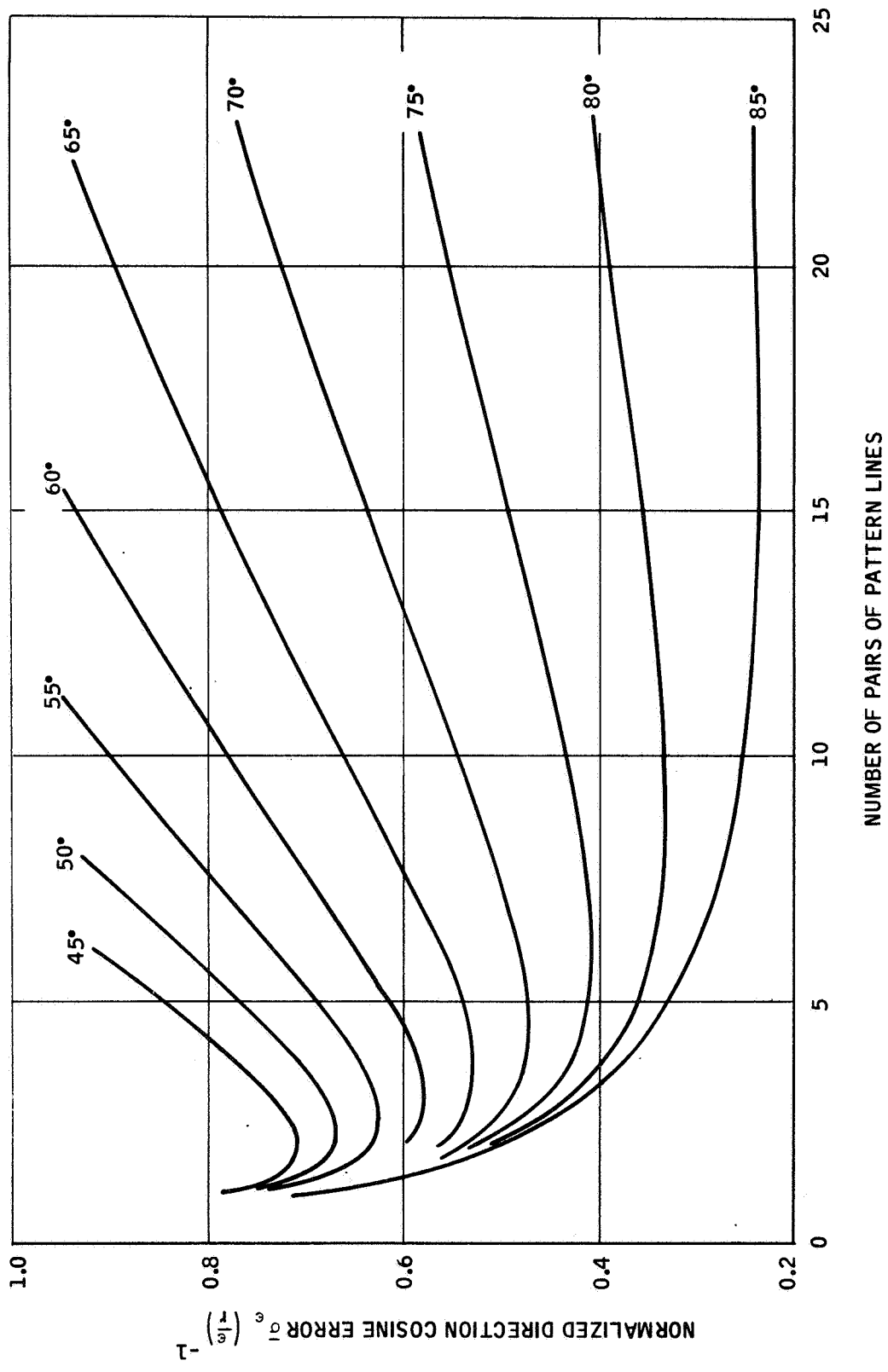


Figure 14. Normalized rms Expected Error from Line Edge Dispersion, Colatitude Patterns for Various Pattern Ranges

COMPARISON OF PATTERN TYPES

The three types of patterns which have been described can be compared to determine their relative utility in the ESVG. Of immediate interest are comparisons in three respects: amplification of timing and line edge dispersion errors, ease of applying the pattern to the rotor, and ease of mechanizing each pattern equation in a computer.

Comparison of Error Sensitivities

A comparison of the graphs shows that the readout error introduced by the timing uncertainties is not a strong function of the type of pattern used. Except for the larger-ranged patterns and for small numbers of pattern lines, the curves of Figures 9, 11, and 13 coincide. The colatitude and cosine patterns tend to result in smaller errors from timing uncertainties than the great circle; however, the difference is not very great.

The type of pattern has a greater influence on the expected error from line edge uncertainties, especially for larger-ranged patterns. The colatitude pattern produces the least expected rms error, while the cosine pattern produces the greatest. A better comparison of these differences is obtained by selecting a common pattern range and a common optimum value for n and examining the expected error from pattern edge dispersion as a function of the colatitude angle.

Since previous designs utilize a range of 90° ($\theta_0 = 45^\circ$), it seems advisable to examine this range as a basis of comparison. The optimum value of n for all three pattern types is two. The normalized expected direction cosine error from line edge dispersion given by Equations (31), (34), and (38) is compared in Figure 15 for $\theta_0 = 45^\circ$ and $n = 2$. The normalized expected third direction cosine errors from these patterns, which are calculated using Equation (30), are compared in Figure 16. That the error vanishes at $\theta = 90^\circ$ is not surprising when it is realized that under the assumptions leading to Equation (30) the magnitude of the third direction cosine is unity.

From Figure 15, it is observed that the cosine pattern produces the least sensitivity to edge dispersion in the central pattern region, whereas the great circle produces the least at the pattern extremities. The colatitude pattern provides uniform sensitivity. If third direction cosine errors were not sensitive to the direction cosines themselves, the colatitude pattern would be the optimum pattern with respect to edge dispersion.

With the presently used mode of obtaining three direction cosines from information given by two pickoffs, a pattern type that provides relatively small error amplification at the pattern extremities (the regions most likely read when the third direction cosine sensitivity is high) is the type which would likely provide the most uniform error amplification, if not the least amplification. However, other modes are considered in the next section; it will be

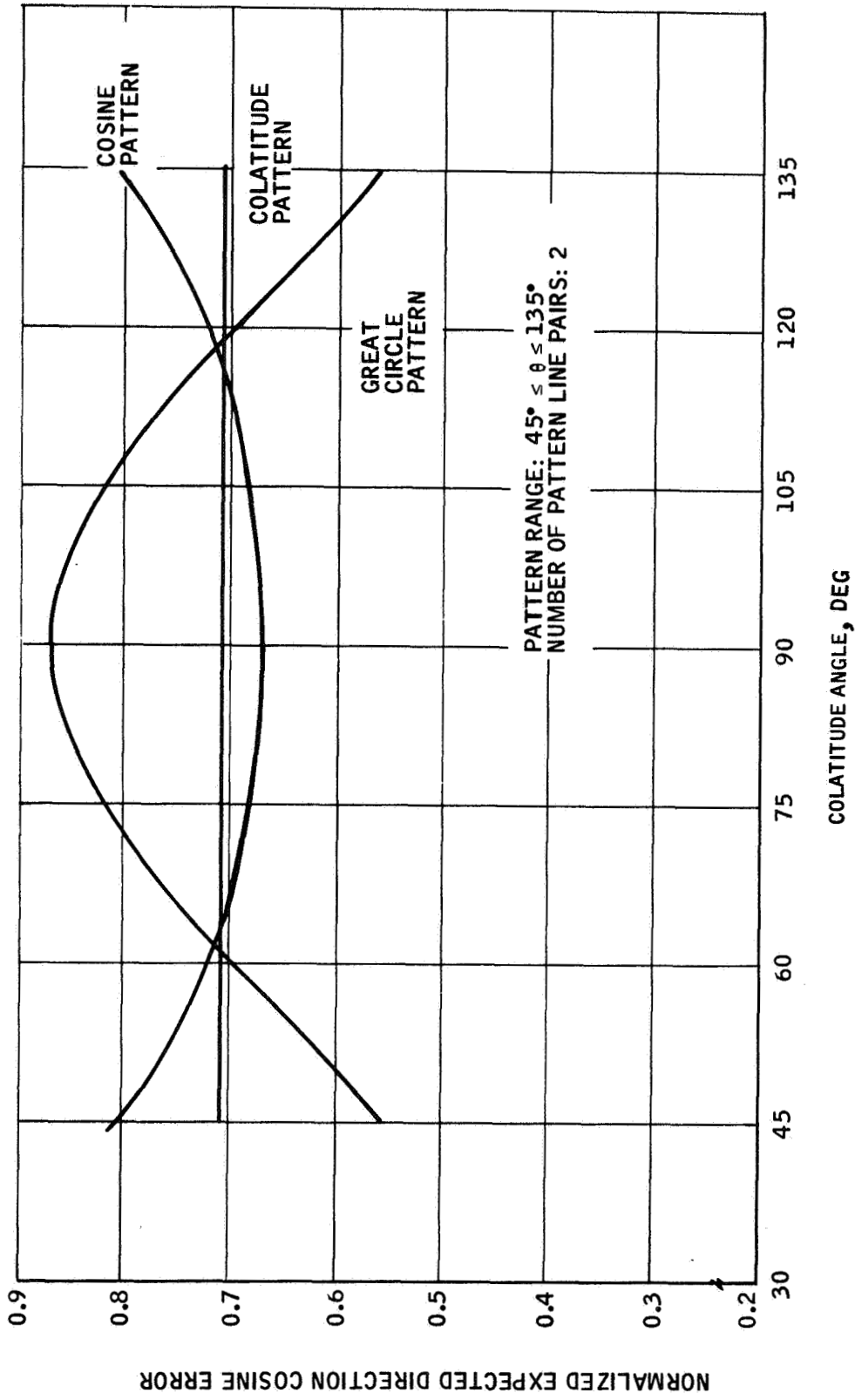


Figure 15. Comparison of Direction Cosine Errors from Pattern Edge Dispersion for Three Pattern Types

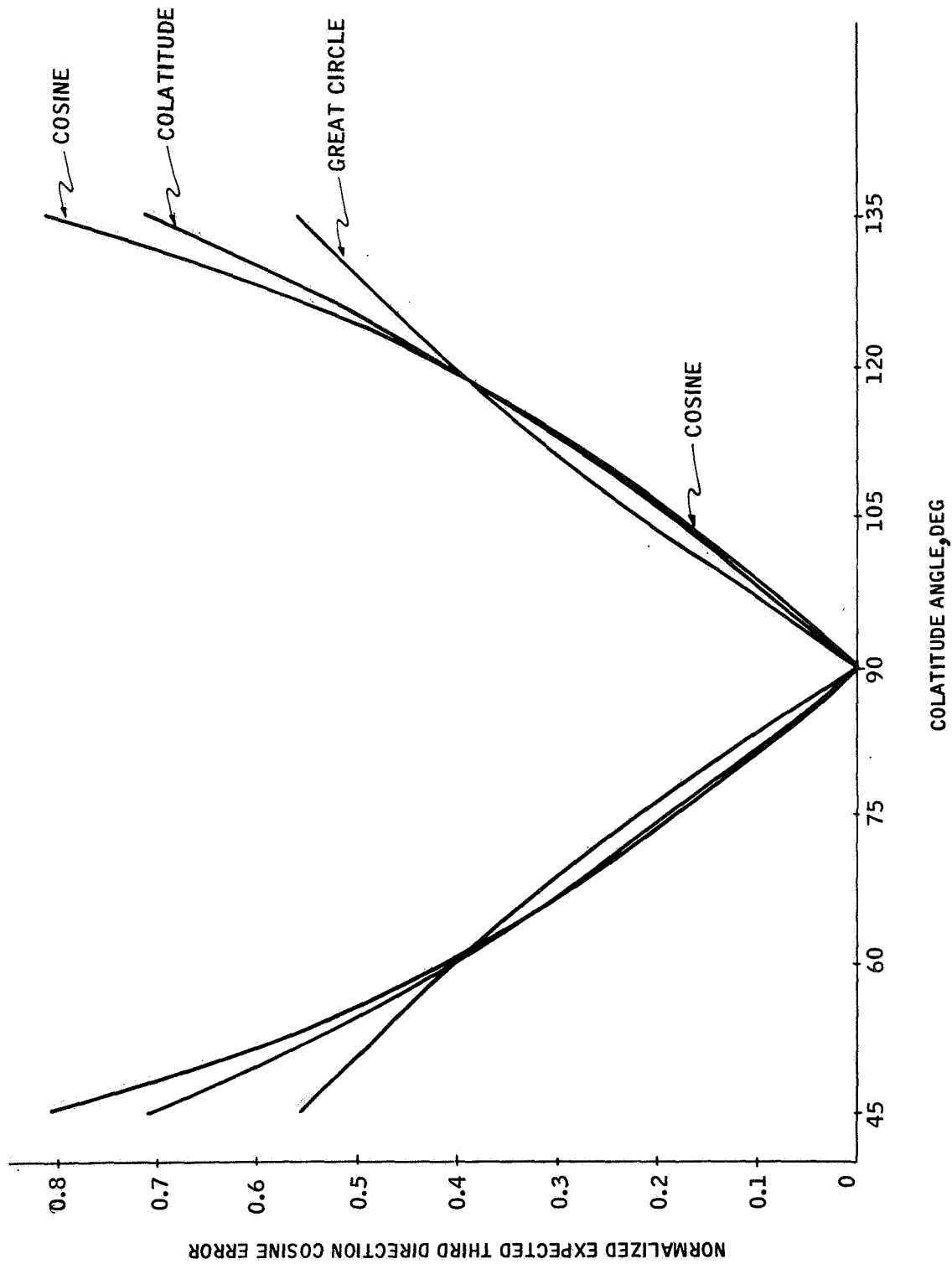


Figure 16. Third Direction Cosine Error from Pattern Edge Dispersion for Three Pattern Types

seen that the mode itself influences the amplification of edge errors. The optimum combination of pattern parameters and readout modes are better discussed there.

Comparison of Ease of Application

An important phase of the application process is that of defining the exact location of the line edge on the rotor. Since the great circle pattern is a planar pattern, its most distinct advantage is in the simplicity of defining its line edge. Figure 17 illustrates how a great circle line segment can be defined. The rotor is rotated about the axis normal to the plane defining the great circle. A reference point, normal to this axis which intersects the center of the rotor, defines the great circle of which the pattern segment is a part.

That this method of defining great circles is easily mechanized with hardware is the reason that great circle patterns were applied to the rotor when the concept of phase-angle measurement of pattern pulses was first utilized. The reference point is rigidly mounted on the apparatus; this rigid mounting eliminates error sources that occur in defining the other pattern types.

The definition of the other types of pattern lines is more difficult, since they are nonplanar. Figure 18 shows the apparatus presently used to apply a cosine pattern to the rotor. At the right is a double-size sphere on which a master pattern is scribed. The product rotor is mounted at the left. A pick-off views the master sphere; its mounting is servoed so that the pickoff is focused on the master pattern line. The angle of the mount is mechanically transferred to the grit nozzle mount at the left. The nozzle edge is the reference point that defines the cosine line. This arrangement can be used for any pattern which is scribed on the master sphere. Errors in addition to those obtained by the great circle arrangement are errors existing in the master line and nonlinearities of the transfer linkage.

A precise method of defining the pattern line on the master sphere is with a series of mathematically exact points. Errors in spindle scales can produce macroscopic deviations. Another problem is the quantization introduced with the use of points. The quantization is reduced by reducing the distance between points and averaging with a larger pickoff field of view.

Other methods of defining the colatitude and cosine patterns can be devised by considering the mathematical characteristics of each. A method for defining a colatitude line is shown in Figure 19. The reference point is mounted on an arm which is rotated about an axis that lies in the rotor equatorial plane. The rotor is rotated simultaneously, such that the ratio of the two rotation angles is constant. Figure 20 is a diagram of a cosine line defined on the rotor. The reference point is translated in the direction parallel to rotor spin axis. The reference point displacement (z), in this direction from the equatorial plane, is proportional to the cosine of the colatitude coordinate of the plane parallel to the equatorial plane containing the reference point. If the ratio of displacement change to change in rotor rotation about the spin axis is kept constant, the locus of points at which a line from the reference point intersecting the spin axis at right angles strikes the rotor surface defines a cosine line.

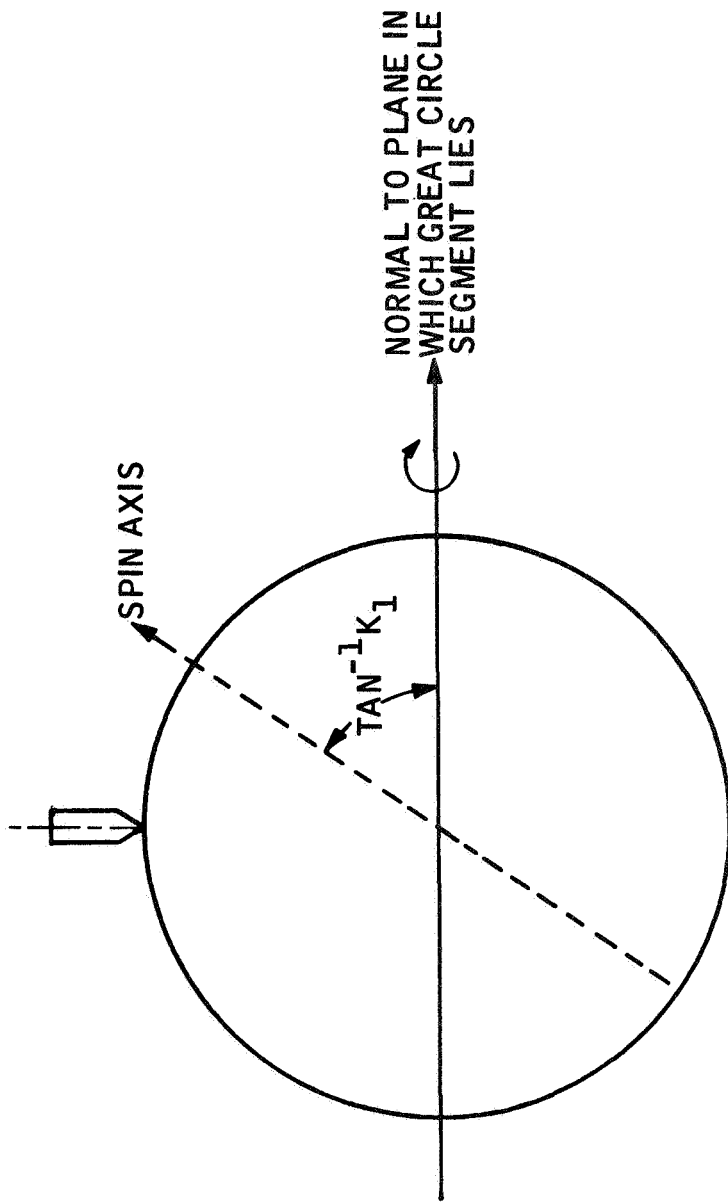


Figure 17. A Great Circle Pattern Applicator

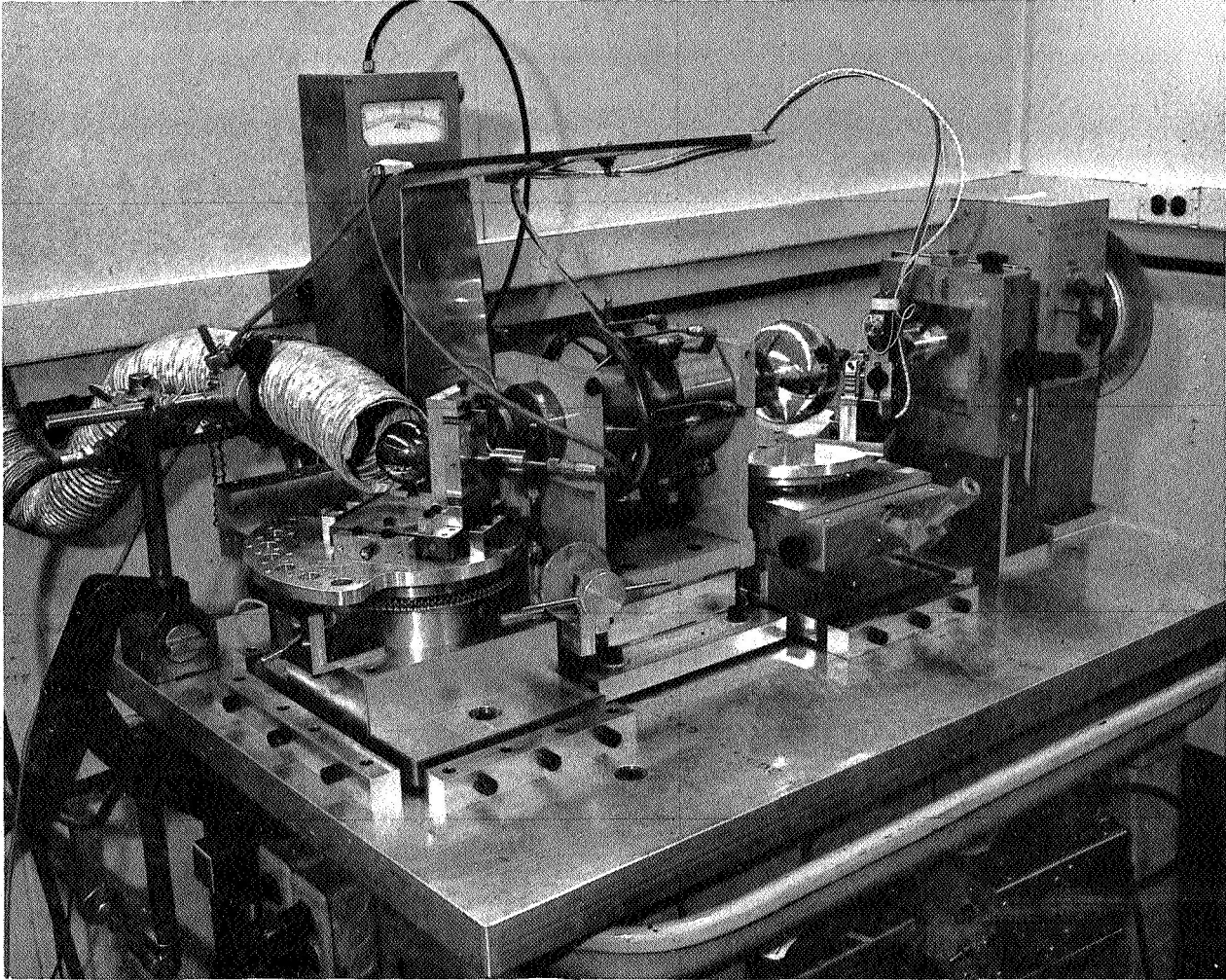


Figure 18. Pattering Jig

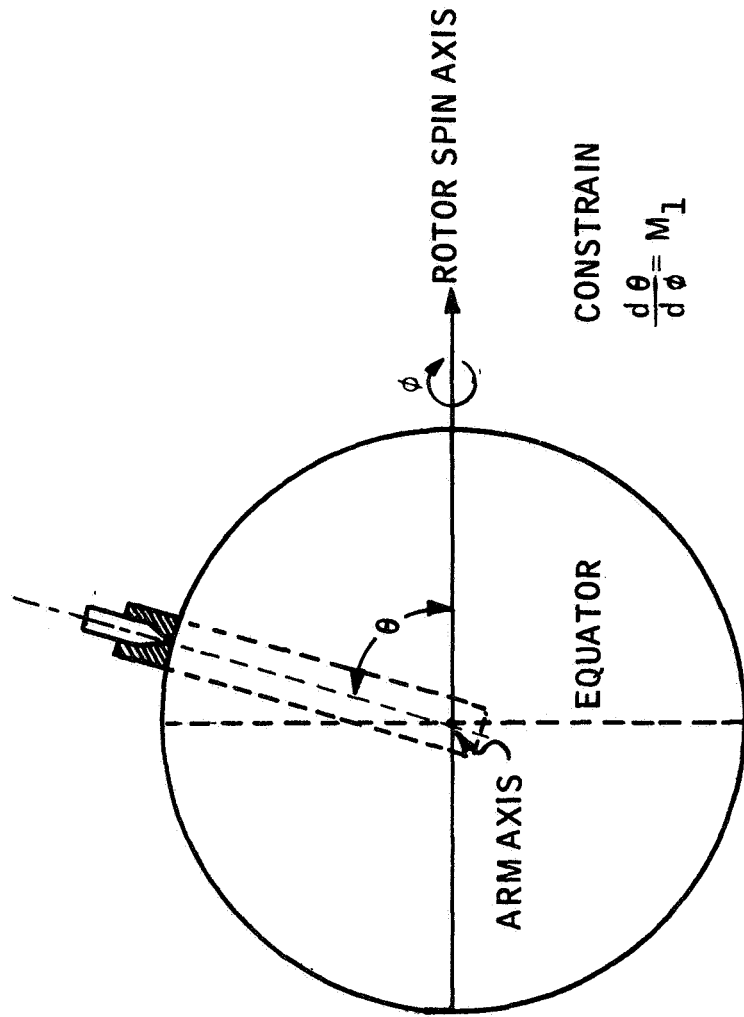
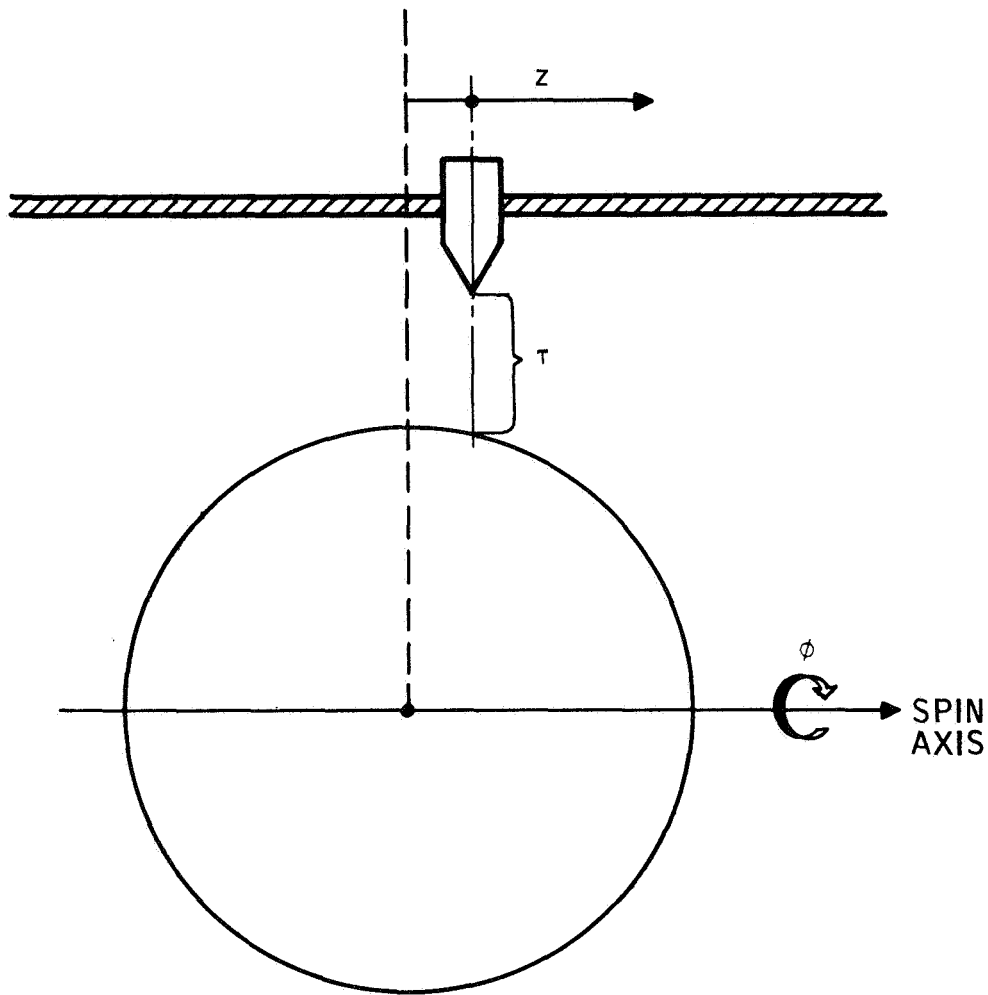


Figure 19. A Colatitude Pattern Applicator



$$\text{CONSTRAIN } \frac{dz}{d\phi} = A_1$$

Figure 20. A Cosine Pattern Applicator

These methods of defining pattern lines to the desired accuracy with hardware is not necessarily within the current state of art. The arrangement indicated for defining the colatitude line does not appear to be too difficult. It is more practical than the arrangement for the cosine line definition. For this line, it is difficult to make the required transfer from the reference point-through a changing distance, τ , to the surface whose normal to this line is also changing-with the required accuracy. This aspect renders this method very difficult to implement without first experimenting with new techniques.

For ease of application, the great circle pattern is definitely the easiest to pattern to the required accuracy. The colatitude line is more difficult to apply to the required accuracy, but appears to be within reach. The cosine line is the most difficult of the three. Some laboratory research into the engineering feasibility of defining the cosine and colatitude lines with the methods discussed here or with similar methods is warranted.

Comparison of Computer Mechanization Requirements

To determine the computer mechanization requirements, each of the mechanization equations must be broken down into the basic operations required for automatic computation. The basic mechanization equations are

$$\lambda = \frac{K_1 \sin \mu}{\sqrt{1 + K_1^2 \sin^2 \mu}} \quad (\text{great circle})$$

$$\lambda = A_1 \mu \quad (\text{cosine})$$

$$\lambda = -\sin M_1 \mu \quad (\text{colatitude})$$

where

$$\mu = \frac{1}{2n} \left(\pi - \sum_{k=1}^n v_k \right) = \frac{\pi}{2n} - \frac{\bar{v}}{2}$$

In addition to the equations, the accuracy requirements of the direction cosine and some estimate of the ranges of the variables and magnitudes of the constants are needed.

To provide an angular accuracy of one second at the pattern range extremities, the direction cosine should be known accurately to the sixth decimal place. A binary representation consisting of 24 bits provides adequate accuracy and safety margin for computational error buildup. For this comparison, it is assumed that temporary storage locations and numerical constants contain 24 binary bits.

The sequence of commands needed to complete the computation depends in part on how information is arranged on the accumulators and registers to carry out the arithmetic operations. It is convenient to choose a specific computer to provide these guidelines. The Packard-Bell 250 computer was chosen for this purpose.

The computation of μ is the first step and is independent of the pattern type. If one assumes that \bar{v} is furnished the computer by the phase-angle measurement electronics, μ is calculated by the steps shown in Table II. Although division by two is simpler by shifting the contents of the register one bit to the right, a division command was provided so that the input may be properly scaled. (This could be accomplished with a multiplication operation also.)

TABLE II. COMMAND SEQUENCE FOR CALCULATING μ

OP Code	Location*	Nature of Operation
CIB		Clear Input Buffer
TES		Waits for signal indicating Buffer is loaded with \bar{v}
LAI		Loads register A with \bar{v}
LDC	C_1	Loads register C with divisor
DIV		Quotient is formed in Register B
STB	X_1	Stores B temporarily in X_1
LDA	C_2	Loads A with constant $\frac{\pi}{2n}$
SUB	X_1	Subtracts contents of X_1 from A

* C_i denotes a constant in memory

X_i denotes a temporary storage location

It is convenient to consider the pattern mechanization equations in increasing order of complexity. The simplest one is the cosine mechanization. To complete the calculation for λ , the additional commands of Table III are needed.

The computer may then proceed to other computations necessary for vehicle navigation. With the cosine pattern, a total of 12 commands, three constants, and one temporary storage location are needed in the computer memory to calculate the direction cosine.

TABLE III. - COMMAND SEQUENCE FOR NOMINAL COSINE MECHANIZATION

OP Code	Location	Nature of Operation
IAC		Interchanges contents of A and C Registers
LDB	C ₃	Loads B with Multiplier A ₁
MUP		Product is formed in A
STA	λ	Stores direction cosine

To compensate for low-frequency deviations of the pattern line from the nominal location, the mechanization equation might take the form of a polynomial:

$$\lambda = P_0 + P_1\mu + P_2\mu^2 + \dots + P_m\mu^m$$

It is of passing interest to ascertain the memory required for such a mechanization. A sequence of commands for this equation is given in Table IV. The bracketed steps would be repeated for each term in the polynomial beyond the second (linear) term. The total memory required, as a function of m , may be written as follows:

Commands: $14 + 7(m - 2)$

Temporary Storage: 2

Constants: $m + 2$

The colatitude mechanization is considered next as it is less complex than the great circle mechanization. The series expansion of the sine function is used to calculate λ . To determine how many terms are needed to provide the desired accuracy, an estimate of the range of the product $M_1\mu$ is needed.

Since the cosine of the colatitude is equal to the sine of the latitude, it is easily seen that the term $(-M_1\mu)$ is equal to the latitude of the pickoff in radians. If 50° is a practical latitude limit on the pattern range, then

$$|M_1\mu| < 1$$

TABLE IV. - COMMAND SEQUENCE FOR POLYNOMIAL
MECHANIZATION DIRECTION COSINE

OP Code*	Location	Nature of Operation
IAC		Places μ in C
STC	X_1	Stores μ
LDB	C_4	Loads B with P_1
MUP		Product $P_1 \mu$ formed in A
ADD	C_3	P_0 added to $P_1 \mu$
STA	X_2	Partial sum stored
LDB	X_1	Loads B with μ
MUP		$\mu \cdot \mu^{k-1} = \mu^k$ formed in A
IAC		Replaces μ^{k-1} with μ^k in C
LDB	C_{k+3}	Loads B with P_k
MUP		Product $P_k \mu^k$ formed
ADD	X_2	Product added to partial sum
STA	λ	Stores direction cosine

*The bracketed terms are repeated for each additional term in the polynomial.

The term containing $\frac{1}{9!}$ is the last term needed in the expansion to give the desired accuracy; therefore, five terms are needed. A sequence of commands providing this calculation is given in Table V.

The bracketed terms are repeated four times to generate the sine function from the first five terms of the series. The memory required for the colatitude pattern mechanization (for $m = 5$) is

$$\text{Commands: } 16 + 7(m - 1) = 44$$

$$\text{Temporary Storage: } 2$$

$$\text{Constants: } m + 2 = 7$$

The great circle utilizes a sine function also; however, the possible range of the argument is different:

$$|\mu| \leq \frac{\pi}{2n}$$

To allow for the possibility that $n = 1$, a possible value of $\frac{\pi}{2}$ for μ is assumed. To obtain the desired accuracy, seven terms of the series for the sine function are required. The total number of commands required to form $\sin \mu$ can be determined by examining the command sequence for the colatitude mechanization. Since μ is not multiplied by a constant, the first three commands in Table V are not needed. The memory required to compute $\sin \mu$ (for $m = 7$) is:

$$\text{Commands: } 13 + 7(m - 1) = 55$$

$$\text{Temporary Storage: } 2$$

$$\text{Constants: } m + 1 = 8$$

To complete the calculation, a square root must be formed. Generally, an iterative method is used. If the first estimate of the root is sufficiently precise, Newton's process converges rapidly. To determine an equation for the first estimate and the number of iterations, an estimate of the magnitude of $(K_1 \sin \mu)$ is needed. An examination of Equations (16) and (20) leads to the conclusion that

$$|K_1 \sin \mu| \leq \cot \theta_0$$

If a practical range limit of 40° is assumed, the maximum value of this factor is 1.2. Thus,

$$1 \leq 1 + K_1^2 \sin^2 \mu < 2.5$$

TABLE V. - INSTRUCTION SEQUENCE FOR NOMINAL
COLATITUDE MECHANIZATION

OP Code*	Location	Nature of Operation
IAC		Places μ in Register C
LDB	C_3	Loads B with $(-M_1)$.
MUP		$x = (-M_1 \mu)$ formed in A
STA	X_2	Stores partial sum
IAC		Places x in C
LDB	X_2	Places x in B
MUP		x^2 formed in A
STA	X_1	Stores x^2
LDB	X_1	Enters x^2 in B
MUP		$x^2 - x^{2k-1}$ formed in A
IAC		Replaces x^{2k-3} with x^{2k-1} in C
LDB	C_{k+2}	Enters $\frac{(-1)^{k-1}}{(2k-1)!}$ in B
MUP		Term in series formed in A
ADD	X_2	Term added to partial sum
STA	X_2, λ	Stores partial sum or λ

*The bracketed terms are repeated for each term in the series.

If y is the desired square root, then

$$1 \leq \bar{y} < 1.582$$

A fairly good estimate of the square root can be obtained by

$$x_0 = 1 + \frac{K_1 \sin \mu}{2}$$

From Newton's process, the next estimate is obtained by forming

$$x_1 = \frac{1}{2} \left(x_0 + \frac{y^2}{x_0} \right)$$

Some experimentation shows that two iterations are needed to find y accurate to the sixth place. The sequence given in Table VI would then complete the calculation of λ with the great circle mechanization.

The first command in this sequence replaces the last command of Table V. The memory requirements for the great circle mechanization are, therefore,

Commands: 55 + 27 = 82

Temporary Storage: 3

Constants: 10

This sequence was formed under the assumption that the square-root command is not part of the computer command repertoire. If the square-root command is available, the bracketed terms in Table VI are deleted; two commands replace the iteration for a net reduction of 15 commands in the sequence.

The memory requirement is reduced to the following:

Instructions: 67

Temporary Storage: 2

Constants: 10

The word length of the commands depends on the number of different commands needed by the computer to conduct all of the computations. Since only one phase of the computer operations is considered here, one cannot judge command-word length on the basis of the instructions listed here. A fairly reasonable assumption on command-word length is 12 bits, or

TABLE VI. - COMMAND SEQUENCE OF GREAT CIRCLE MECHANIZATION GIVEN "SIN μ "

OP Code*	Location	Nature of Operation
IAC		Places $\sin \mu$ in C
LDB	C_9	Loads K_1 in B
MUP		Product formed in A
STA	X_1	Store $K_1 \sin \mu$
SRT		Divide by 2 by Rt. shift 1 bit
ADD	C_{10}	
STA	X_2	Store first estimate
LDC	X_1	Load $K_1 \sin \mu$ in C
LDB	X_1	Load $K_1 \sin \mu$ in B
MUP		Form $(K_1 \sin \mu)^2$ in A
ADD	C_{10}	Form Y^2 for Newton process
STA	X_3	Store Y^2 for second iteration
LDC	X_2	Loads first estimate in C
DIV		Quotient formed in B
SLT		Bring quotient across to A
ADD	X_2	Add first estimate to quotient
SRT		Divide by 2
STA	X_2	Replaces first estimate with second estimate
IAC		Load second estimate in C
LDA		Load Y^2
DIV		Quotient formed in B
SLT		Move quotient to A
ADD	X_2	Add second estimate to quotient
SRT		Divide by 2
IAC		Y sufficiently accurate enters C
LDA	X_1	Load $K_1 \sin \mu$ in A
DIV		λ formed in B
STB	λ	Stores direction cosine

*The bracketed terms are replaced by two other commands if a square root command is available.

one-half the length of a data word. All of the memory requirements can then be reduced to an equivalent number of 12-bit words; a summary of the requirements are compared in Table VII.

From this comparison, one can see that the great circle mechanization requires four to five times the memory required for the nominal cosine mechanization. If one makes a more realistic assumption (in terms of present-day patterning technology) that some form of polynomial mechanization is needed for the cosine pattern, the additional memory requirements for the great circle pattern are less. Current practices in microminiaturization of computer elements probably render the additional requirements for the great circle rather insignificant in terms of extra power and mass in the computer.

TABLE VII. - COMPARISON OF COMPUTER MEMORY REQUIREMENTS FOR THREE PATTERN MECHANIZATIONS

Type of Mechanization	Number of Commands	Temp. Storage		Constants		Total Memory	
		Req.	Eq. 12-bit word	Req.	Eq. 12-bit word	Eq. Comm. Words	Bits
Cosine							
Nominal	12	1	2	3	6	20	240
Polynomial (M=5)	35	2	4	7	14	53	636
Colatitude	44	2	4	7	14	62	744
Great circle							
(with square root)	67	2	4	10	20	91	1092
(without square root)	82	3	6	10	20	108	1296

SECTION IV

PICKOFF ARRANGEMENT STUDY

An important parameter in the ESVG readout system is the location of pickoffs. The pickoff axis is the fundamental frame of reference of the direction cosine calculated from phase-angle data. For this reason, the location of each pickoff axis should be precisely known or precisely adjusted to its desired point.

In this section, the role of pickoff arrangement to the overall contribution of readout error shall be studied. Two specific arrangements are selected for detailed study -- an orthogonal arrangement of three pickoffs and a nonorthogonal arrangement of four pickoffs. Since there is a desire to maintain uniform accuracy for all possible spin-vector directions, the pickoffs are located so that the distribution of axes is uniform in the three space dimensions.

Closely related to pickoff arrangement is the readout mode; i. e., the number of pickoffs employed to specify the spin-vector direction cosines with respect to a basic orthogonal frame of reference. When three pickoffs are employed, the direction cosines are completely specified; however, because the readout deals with a unit spin vector, the information from three pickoffs are redundant to that extent. This redundancy can then be utilized to provide partial compensation for any error present in the computations. When two pickoffs are employed, the unit vector property can be utilized to calculate the magnitude of the direction cosine normal to the plane of the two pickoff axes. (Throughout this report this cosine is called the third direction cosine.) The sign must be furnished from other information. The past history of that direction cosine has often been used in the past for determining its sign. Generally, no ambiguity develops with this technique, for when the direction cosine along that axis changes, another combination of two pickoffs is being used.

In this section, error sensitivities for each contemplated combination of pickoff arrangement and readout mode are developed. These sensitivity equations are then combined with the pattern sensitivity equations developed in Section III to search for the optimum combination of parameters that minimizes pattern line edge uncertainty.

SOLUTIONS TO THE THIRD DIRECTION COSINE SENSITIVITY PROBLEM

The calculation of the third direction cosine from data to two orthogonally placed pickoffs is sensitive to errors in the results of the calculations from pickoff signals. It has been observed that this sensitivity varies with the cosines themselves, and it has produced undesirable effects in drift data collected and analyzed from present gyros. In the overall effort to improve readout accuracy, a study of how the arrangement of pickoffs may be used to

reduce the third direction cosine sensitivity and control its variation to more tolerable levels was conducted.

There are several alternatives available to reduce the expected error of the third direction cosine.

- Use a more precise calibration of the pattern in those latitudes where the third direction cosine error sensitivity is large. Such a calibration will most likely lead to a larger number of terms in the mechanization equation.
- Implement a pattern wherein calculational sensitivity compensates the third direction cosine sensitivity, yielding a more uniform overall sensitivity.
- Extend the pattern range so that three cosines are calculated from pattern information for those conditions where third direction cosine calculational sensitivity is greater than desired.
- Add and arrange pickoffs in a manner such that the third direction cosine sensitivity is reduced and/or is more uniform.

Although the first alternative may not be the most desirable, it is the only one which can be employed for existing units. What experimentation that has been conducted has yielded improved results. It is hoped that such an alternative need not be further extended for future designs. The following study investigates the feasibility of the other alternatives and determines whether each or any combination will yield a system in which the readout sensitivity to pattern edge errors is significantly reduced.

GENERAL DIRECTION COSINE CALCULATIONS FROM PICKOFF COSINES

Let the axes of pickoffs P_1 and P_2 define a plane in the gyro stator assembly. Let axes X_1 and X_2 be two orthogonal axes in that plane, with axis X_1 located at angles σ_1 and σ_2 with respect to the pickoff axes as shown in Figure 21.

Let the direction cosines be known, as calculated from pickoff output information generated by the pattern, and be denoted as $\cos \theta_1$ for P_1 and $\cos \theta_2$ for P_2 . From knowledge of $\cos \theta_1$, $\cos \theta_2$, σ_1 , and σ_2 , it is desired to calculate the direction cosines of the spin vector with respect to X_1 and X_2 . The geometry of the calculation for the cosine with respect to X_1 is shown in Figure 22.

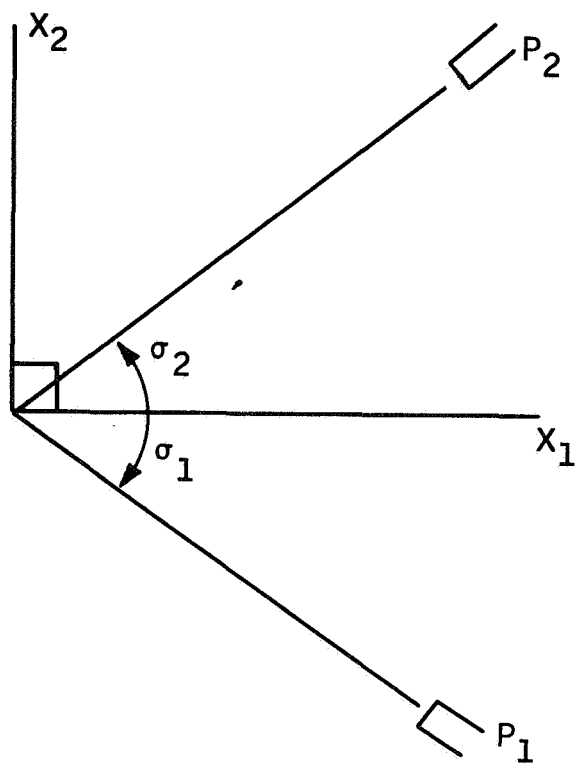


Figure 21. Plane of Two ESGV Pickoffs

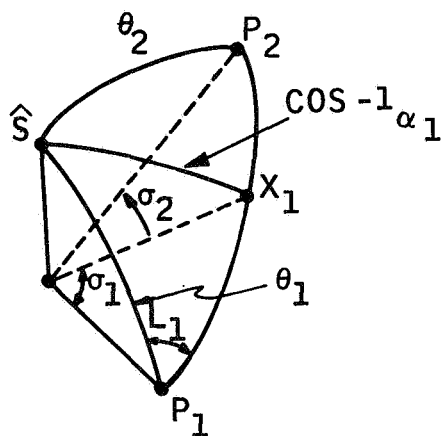


Figure 22. Geometry of Direction Cosine Calculation

With the aid of the relationships among the angles of spherical triangles, the equation for the cosine may be derived. From the law of cosines,

$$\cos \theta_2 = \cos \theta_1 \cos (\sigma_1 + \sigma_2) + \sin \theta_1 \sin (\sigma_1 + \sigma_2) \cos L_1$$

$$\alpha_1 = \cos \theta_1 \cos \sigma_1 + \sin \theta_1 \sin \sigma_1 \cos L_1$$

where α_1 is the direction cosine of the spin vector with respect to X_1 . The first equation may be substituted into the second to clear it of the unknown angle L_1 .

$$\alpha_1 = \cos \theta_2 \frac{\sin \sigma_1}{\sin (\sigma_1 + \sigma_2)} + \cos \theta_1 \left[\cos \sigma_1 - \frac{\sin \sigma_1 \cos (\sigma_1 + \sigma_2)}{\sin (\sigma_1 + \sigma_2)} \right]$$

Now

$$\sin (\sigma_1 + \sigma_2) \cos \sigma_1 - \cos (\sigma_1 + \sigma_2) \sin \sigma_1 = \sin (\sigma_1 + \sigma_2 - \sigma_1) = \sin \sigma_2$$

so that

$$\alpha_1 = \cos \theta_2 \frac{\sin \sigma_1}{\sin (\sigma_1 + \sigma_2)} + \cos \theta_1 \frac{\sin \sigma_2}{\sin (\sigma_1 + \sigma_2)} \quad (39)$$

The derivation for α_2 , the direction cosine with respect to X_2 , is similar:

$$\alpha_2 = \cos \lambda_2 \frac{\cos \sigma_1}{\sin (\sigma_1 + \sigma_2)} - \cos \lambda_1 \frac{\cos \sigma_2}{\sin (\sigma_1 + \sigma_2)} \quad (40)$$

The magnitude of the third direction cosine is calculated from the orthogonality identity [Equation (29)].

$$|\alpha_3| = \sqrt{1 - \alpha_1^2 - \alpha_2^2} \quad (41)$$

$$\alpha_3 = \pm \sqrt{1 - \frac{1}{\sin^2(\sigma_1 + \sigma_2)} \left[\cos^2 \theta_1 + \cos^2 \theta_2 - 2 \cos \theta_1 \cos \theta_2 \cos(\sigma_1 + \sigma_2) \right]} \quad (42)$$

The sensitivity of α_1 , α_2 , and α_3 to errors in the calculations of $\cos \theta_1$ and $\cos \theta_2$ is obtained by evaluating differentials of these equations. Let

$$\epsilon_1 = \Delta \cos \theta_1 = -\sin \theta_1 \Delta \theta_1$$

$$\epsilon_2 = \Delta \cos \theta_2 = -\sin \theta_2 \Delta \theta_2$$

Then,

$$\Delta \alpha_1 = \frac{\sin \sigma_1}{\sin(\sigma_1 + \sigma_2)} \epsilon_2 + \frac{\sin \sigma_2}{\sin(\sigma_1 + \sigma_2)} \epsilon_1 \quad (43)$$

$$\Delta \alpha_2 = \frac{\cos \sigma_1}{\sin(\sigma_1 + \sigma_2)} \epsilon_2 - \frac{\cos \sigma_2}{\sin(\sigma_1 + \sigma_2)} \epsilon_1 \quad (44)$$

$$\Delta \alpha_3 = \frac{1}{\alpha_3 \sin^2(\sigma_1 + \sigma_2)} \left\{ \left[\cos \theta_2 \cos(\sigma_1 + \sigma_2) - \cos \theta_1 \right] \epsilon_1 + \left[\cos \theta_1 \cos(\sigma_1 + \sigma_2) - \cos \theta_2 \right] \epsilon_2 \right\} \quad (45)$$

ARRANGEMENT OF THREE PICKOFFS

A uniform distribution of three axes in space is an orthogonal set of axes; the arrangement of three pickoffs which is considered is, therefore, an orthogonal arrangement. The basic reference for the direction cosines is also an orthogonal set. The study of the three-pickoff arrangement is simplified if it is assumed that these sets of coordinates coincide.

Two-Pickoff Readout Mode

The assumption of pickoff axis coincidence with the fundamental reference is implemented by setting

$$\sigma_1 = 0$$

$$\sigma_2 = \frac{\pi}{2}$$

The gyro axes direction cosines reduce to

$$\alpha_1 = \cos \theta_1 \tag{46a}$$

$$\alpha_2 = \cos \theta_2 \tag{46b}$$

$$\alpha_3 = \pm \sqrt{1 - (\cos^2 \theta_1 + \cos^2 \theta_2)} \tag{46c}$$

The error sensitivity equations are

$$\Delta \alpha_1 = \epsilon_1 \tag{47a}$$

$$\Delta \alpha_2 = \epsilon_2 \tag{47b}$$

$$\epsilon_3 = \Delta \alpha_3 = -\frac{1}{\alpha_3} [\epsilon_1 \cos \theta_1 + \epsilon_2 \cos \theta_2] = -\left(\epsilon_1 \frac{\alpha_1}{\alpha_3} + \epsilon_2 \frac{\alpha_2}{\alpha_3} \right) \tag{47c}$$

The equation for ϵ_3 shows how its sensitivity to ϵ_2 and ϵ_1 varies with spin vector direction. If a choice of pickoff combinations is available, the choice which minimizes error is the two pickoffs nearest the rotor equator, for then

$$\left| \frac{\alpha_1}{\alpha_3} \right| \leq 1 \tag{48a}$$

$$\left| \frac{\alpha_2}{\alpha_3} \right| \leq 1 \tag{48b}$$

If one of the two pickoffs nearest the equator is not used, one of these ratios is greater than the unity.

For the comparisons that are to be made later, it is convenient to assume a specific two-pickoff mode. Let the spin vector be defined to be

$$\hat{S} = \alpha \hat{i}_c + \beta \hat{j}_c + \gamma \hat{k}_c \quad (49)$$

where \hat{i}_c , \hat{j}_c , \hat{k}_c are the unit base vectors of the fundamental reference.

Let γ be the direction cosine whose magnitude is calculated from the orthogonality identity. Then

$$\alpha_1 = \alpha$$

$$\alpha_2 = \beta$$

$$\alpha_3 = \gamma$$

The error in the spin vector definition from readout errors is

$$\Delta \vec{S} = \Delta \alpha \hat{i}_c + \Delta \beta \hat{j}_c + \Delta \gamma \hat{k}_c$$

A convenient basis for comparing the error amplification is the magnitude of $\Delta \vec{S}$, which is easily calculated from its square

$$\Delta \vec{S}^2 = \Delta \alpha^2 + \Delta \beta^2 + \Delta \gamma^2 \quad (50)$$

For the specific mode assumed,

$$\epsilon_1 = \Delta \alpha$$

$$\epsilon_2 = \Delta \beta$$

$$\epsilon_3 = \Delta \gamma$$

Appropriate substitutions yield

$$\begin{aligned} \Delta \vec{S}^2 &= \Delta \alpha^2 \left(1 + \frac{\alpha^2}{\gamma^2} \right) + \Delta \beta^2 \left(1 + \frac{\beta^2}{\gamma^2} \right) \\ &= \frac{1}{1 - \alpha^2 - \beta^2} \left[\Delta \alpha^2 (1 - \beta^2) + \Delta \beta^2 (1 - \alpha^2) \right] \end{aligned}$$

The sources producing errors $\Delta\alpha$ and $\Delta\beta$ are such that their expected values are zero. Consequently, the variance of these error functions is equal to the expected value of their squares. If the variances of $\Delta\alpha$ and $\Delta\beta$ are known, the variance of $\Delta\vec{S}$ can then be calculated

$$\sigma^2 (\Delta\vec{S}) = \frac{1}{1 - \alpha^2 - \beta^2} \left[\sigma^2 (\Delta\alpha) (1 - \beta^2) + \sigma^2 (\Delta\beta) (1 - \alpha^2) \right] \quad (51)$$

Three-Pickoff Readout Mode

When the three-pickoff readout mode is used, all three direction cosines are determined from phase-angle information; the orthogonality identity is not used. In this case, the variance of $\Delta\vec{S}$ is

$$\sigma^2 (\Delta\vec{S}) = \sigma^2 (\Delta\alpha) + \sigma^2 (\Delta\beta) + \sigma^2 (\Delta\gamma) \quad (52)$$

When this mode is used, there is no assurance that the spin vector is a unit vector. If it is not a unit vector, it is produced by an error in the readout. In this case, the orthogonality identity can be used to correct the direction cosines so that the spin vector is a unit vector.

Other criteria may also be considered. For instance, the corrections may be weighted in proportion to the standard deviation of each of the direction cosines. However, such corrections are undesirable for two reasons:

- Weighting the corrections according to the standard deviation requires that the calculation of the standard deviation be programmed in the navigation computer. One only needs to refer to the equations developed in Section III to see how complex these equations could be. Since this is likely to be the only place where this calculation is needed, one should be assured that such weighting is soundly justified.
- Like the true spin vector, the error vector has three components. These components can be transformed into one component parallel to the spin vector and two components normal to it. The need for correction was sensed because the calculated spin vector is not of unit length. This information has significance only on that error component parallel to the spin vector.

The significance of the second reason is easily pointed out by an example. Suppose that corrections are weighted according to the standard deviation of the direction cosines in an ESVG readout system employing a great circle pattern on the rotor. Let the "initial" calculations from one read cycle show

that one of the three pickoffs is reading the pattern very close to the equator. From Figure 15 it is observed that the expected error from line edge dispersion is greatest for that pickoff nearest the equator. However, the primary contribution of error from this pickoff is in the plane normal to the spin axis; it has little bearing on spin vector length. The spin vector is more effectively normalized by correcting one or both of the other two cosines, which are of necessity reading the extreme pattern regions in order for a three-pickoff mode to exist. Since Figure 15 indicates that the expected error from line edge effects for the great circle pattern are almost minimum for these two cosines, the implementation of weighting according to standard deviation of line edge errors can lead to an inconsistency between the operation and its purpose.

Since the need for correction is based only on the length of the calculated spin vector, the most sensible correction on the spin vector is ordinary normalization:

$$\alpha' = \frac{\alpha}{\sqrt{\alpha^2 + \beta^2 + \gamma^2}} \quad (53a)$$

$$\beta' = \frac{\beta}{\sqrt{\alpha^2 + \beta^2 + \gamma^2}} \quad (53b)$$

$$\gamma' = \frac{\gamma}{\sqrt{\alpha^2 + \beta^2 + \gamma^2}} \quad (53c)$$

Such a normalization process will produce a reduction in the expected value of $\Delta \vec{S}^2$. Let the corrections based on the normalization of \vec{S} be

$$\Delta \alpha' = \alpha' - \alpha = \alpha \left(\frac{1}{1+\epsilon} - 1 \right) \cong -\epsilon \alpha \quad (54a)$$

$$\Delta \beta' = \beta' - \beta = \beta \left(\frac{1}{1+\epsilon} - 1 \right) \cong -\epsilon \beta \quad (54b)$$

$$\Delta \gamma' = \gamma' - \gamma = \gamma \left(\frac{1}{1+\epsilon} - 1 \right) \cong -\epsilon \gamma \quad (54c)$$

where

$$\alpha^2 + \beta^2 + \gamma^2 = (1 + \epsilon)^2 \quad (55)$$

Since $\Delta \alpha$, $\Delta \beta$ and $\Delta \gamma$ are the true errors,

$$(\alpha - \Delta \alpha)^2 + (\beta - \Delta \beta)^2 + (\gamma - \Delta \gamma)^2 \cong 1 \quad (56)$$

If Equations (55) and (56) are combined and second-degree error terms are dropped, one finds that

$$\alpha \Delta\alpha + \beta\Delta\beta + \gamma\Delta\gamma \cong \epsilon \quad (57)$$

The error in the corrected vector is

$$\begin{aligned} (\Delta\vec{S}')^2 &= (\Delta\alpha' + \Delta\alpha)^2 + (\Delta\beta + \Delta\beta)^2 + (\Delta\gamma' + \Delta\gamma)^2 \\ &= (\Delta\alpha - \epsilon\alpha)^2 + (\Delta\beta - \epsilon\beta)^2 + (\Delta\gamma - \epsilon\gamma)^2 \end{aligned}$$

from Equation (54). Expanding and substituting (50) and (57) into the expansion yields

$$(\Delta\vec{S}')^2 \cong \Delta S^2 - 2\epsilon^2 + \epsilon^2 = \Delta S^2 - \epsilon^2$$

Consequently, the variance in $\Delta\vec{S}'$ may be found by

$$\sigma^2(\Delta\vec{S}') = \sigma^2(\Delta\vec{S}) - \sigma^2(\epsilon) \quad (58)$$

All that remains is to evaluate the variance of $\sigma^2(\epsilon)$ which can be ascertained from the expected value of the square of Equation (57):

$$\begin{aligned} E(\epsilon^2) &\cong \alpha^2 E(\Delta\alpha^2) + \beta^2 E(\Delta\beta^2) + \gamma^2 E(\Delta\gamma^2) + 2\alpha\beta E(\Delta\alpha\Delta\beta) \\ &\quad + 2\alpha\gamma E(\Delta\alpha\Delta\gamma) + 2\beta\gamma E(\Delta\beta\Delta\gamma) \end{aligned}$$

The error variables $\Delta\alpha$, $\Delta\beta$, $\Delta\gamma$ are correlated only to the extent that they are likely to be identical functions of their parent parameters α , β , γ , respectively. Otherwise, they are independent. Since the probability that any two of the direction cosines will be equal is extremely small, one can confidently assume that

$$E(\Delta\alpha\Delta\beta) = E(\Delta\alpha\Delta\gamma) = E(\Delta\beta\Delta\gamma) = 0$$

Consequently,

$$\sigma^2(\epsilon) = E(\epsilon^2) = \alpha^2 \sigma^2(\Delta\alpha) + \beta^2 \sigma^2(\Delta\beta) + \gamma^2 \sigma^2(\Delta\gamma)$$

Therefore,

$$\sigma^2(\Delta\vec{S}') = \sigma^2(\Delta\alpha)(1-\alpha^2) + \sigma^2(\Delta\beta)(1-\beta^2) + \sigma^2(\Delta\gamma)(1-\gamma^2)$$

If there is relatively small variation of the variances of $\Delta\alpha$, $\Delta\beta$, $\Delta\gamma$ as a function of the parent parameters, a reasonable approximation to this equation is

$$\sigma^2(\Delta\vec{S}') = \frac{2}{3} [\sigma^2(\Delta\alpha) + \sigma^2(\Delta\beta) + \sigma^2(\Delta\gamma)] = \frac{2}{3} \sigma^2(\Delta\vec{S}) \quad (60)$$

ARRANGEMENT OF A FOUR-PICKOFF SYSTEM

It was noted earlier that the distribution of pickoff axes, in spatial coordinates to maintain accurate all-attitude readout, should be as uniform as possible. In the case of four pickoffs, the axes originating from the center of a regular tetrahedron that are normal to the faces of the tetrahedron would define the equal distribution of four axes in three-space. The same distribution is defined by lines which connect diametrically opposite corners of a cube. This fact provides the clue to the location of four pickoffs, which not only provides the desired distribution but also fits in well with the hexahedral electrode configuration - namely, at the Y-shaped intersections of the electrode boundaries. A pickoff could be located at either end of a diametrically opposite pair of intersections. To minimize alignment stabilities, it is desirable to mount all pickoffs on one housing piece. The arrangement which is considered here is that indicated in Figure 23.

It is worthwhile to ascertain the pattern limits required for complete attitude readout - one limit for which two pickoffs are the minimum number used and one for which three pickoffs are the minimum number used. Since the pattern is symmetrically located about the equator, the pattern limits will not depend on which end of the pickoff axis a pickoff is located. The limits can be defined with less chance of confusion by considering an equivalent arrangement in which a pickoff is located at each corner of one electrode.

To assure a minimum of two pickoffs viewing the pattern, the pattern should extend sufficiently far that four pickoffs can view the pattern when the spin axis is aligned with the center of the electrode. The direction angle between the spin axis and each pickoff is slightly less than 55° ; the pattern should then extend to 36° above and below the equator. The spin axis can traverse the path shown in Figure 24 (which lies in a plane defined by two electrode force axes) with two pickoffs always viewing the pattern.

To assure that a minimum of three pickoffs view the pattern, four pickoffs should view the pattern when the spin axis bisects the acute angle formed by two pickoff axes (Figure 24). An equivalent condition occurs when pickoffs at diagonally opposite electrode corners view the equator; the other two pickoffs should also view the pattern at the same time. Either condition yields the same result - that the pattern should extend a minimum of 55° on either side of the equator.

If pattern range has no effect on pattern accuracy and readout resolution, the single advantage of complete readout information (with the accompanying redundancy) from a three-pickoff readout mode would justify extending the range to 55° on either side of the equator. It is more likely that the pattern application accuracy and resolution can be increased as the pattern range is decreased. In this context, the treatment of pattern range as a variable in Section III is useful in the optimization study discussed later in this section.

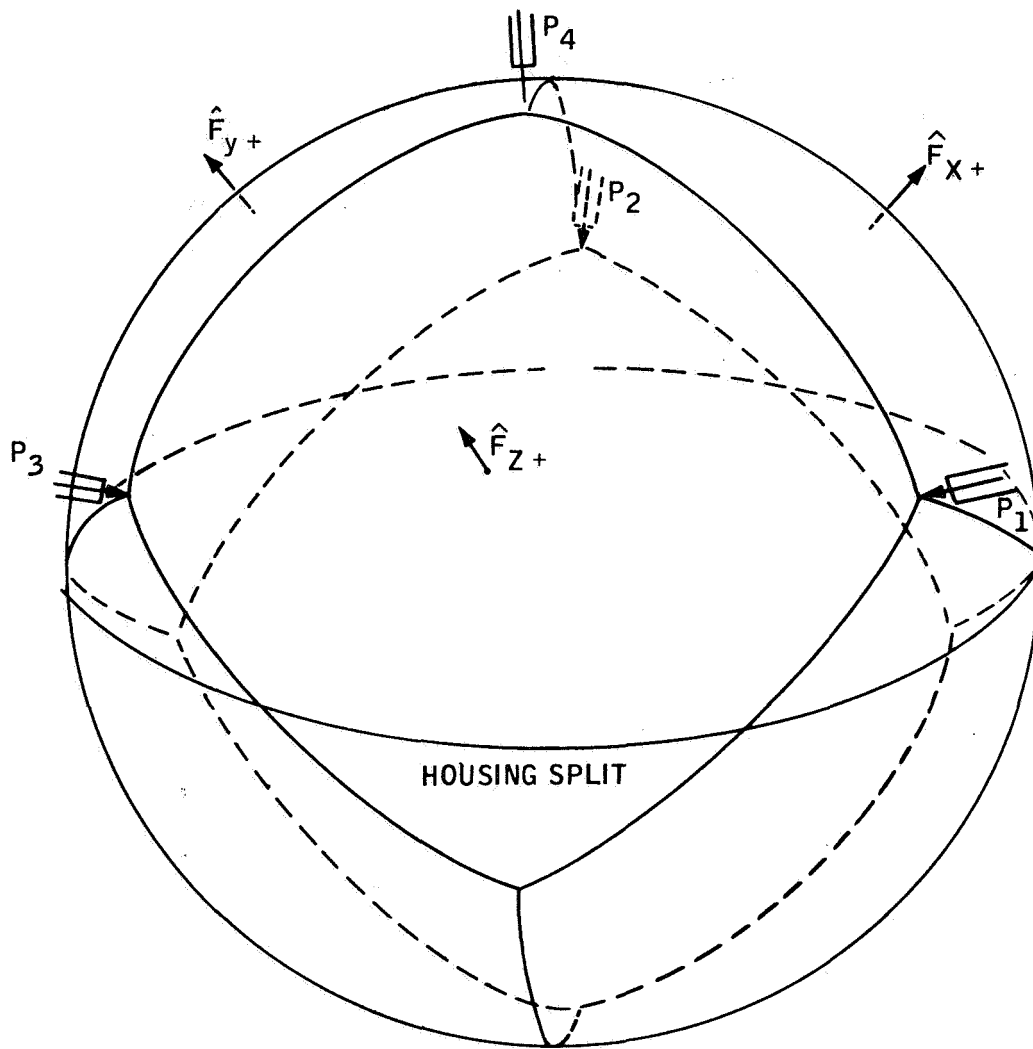
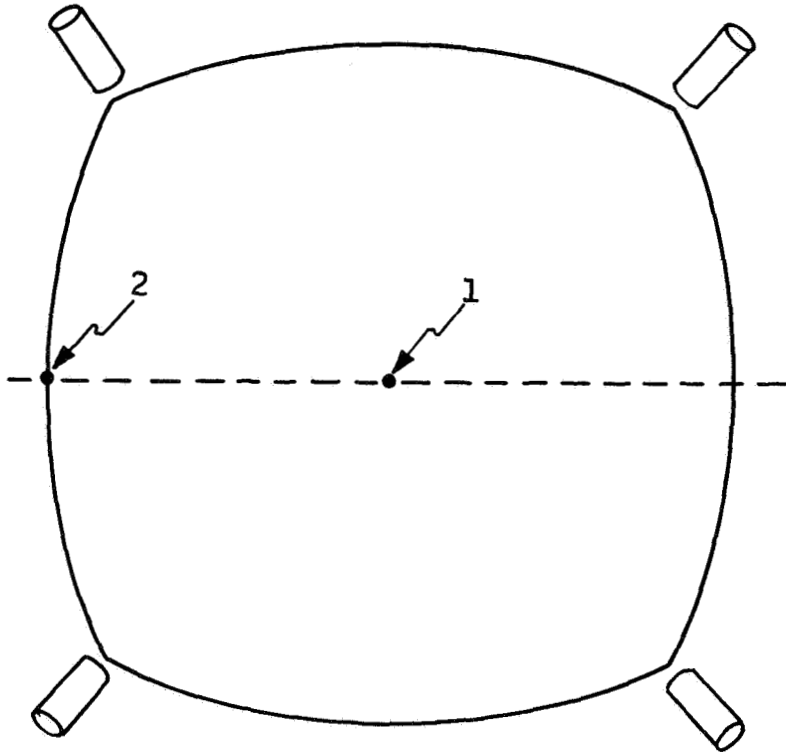


Figure 23. Arrangement of a System of Four Pickoffs



1. Four Pickoffs View Pattern When Spin Axis is Here to Assure at Least Two Pickoffs.
2. Four Pickoffs View Pattern When Spin Axis is Here to Assure at Least Three Pickoffs.

Figure 24. Determination of Minimum Pattern Ranges for Two- and Three-Pickoff Modes

Basic Direction Cosine Equations

The angles formed by the axes of pickoffs P_1 , P_2 , and P_3 are nominally $\cos^{-1} (-1/3)$, while the nominal angle between the axis of P_4 with each of the other three is $\cos^{-1} 1/3$. The desired axes of reference nominally bisect the angles formed by the axes of P_1 , P_2 , and P_3 . Each is coplanar with, but orthogonal to, the bisector of the axis of P_4 and another pickoff axis. The equations for force axis direction cosines should then assume a rather simple and symmetric character. Any computation not involving phase-angle data from the signals of pickoff P_4 takes the form of Equation (39) with

$$\sigma_1 = \sigma_2 = \cos^{-1} \sqrt{1/3}$$

Any computation involving data from pickoff P_4 takes the form of Equation (40) with

$$\sigma_1 = \sigma_2 = \cos^{-1} \sqrt{2/3}$$

Each of the six combinations of two pickoffs from the set of four can be used to ascertain one of the basic cosines directly and provides two equations for each direction cosine:

$$\alpha = \frac{\sqrt{3}}{2} (\cos \theta_1 + \cos \theta_2) = \frac{\sqrt{3}}{2} (\cos \theta_4 - \cos \theta_3) \quad (61a)$$

$$\beta = \frac{\sqrt{3}}{2} (\cos \theta_2 + \cos \theta_3) = \frac{\sqrt{3}}{2} (\cos \theta_4 - \cos \theta_1) \quad (61b)$$

$$\gamma = \frac{\sqrt{3}}{2} (\cos \theta_1 + \cos \theta_3) = \frac{\sqrt{3}}{2} (\cos \theta_4 - \cos \theta_2) \quad (61c)$$

Some relationships among the pickoff cosines are of interest and may be useful for checking the pickoff alignment. From each of these equations, one deduces that

$$\cos \theta_4 = \cos \theta_1 + \cos \theta_2 + \cos \theta_3 \quad (62)$$

The sum of the squares of the six distinct equations (two each for α , β , and γ) also yields an interesting result:

$$\begin{aligned}
2 (\alpha^2 + \beta^2 + \gamma^2) = 2 = 3/4 & \left[3 (\cos^2 \theta_1 + \cos^2 \theta_2 + \cos^2 \theta_3 + \cos^2 \theta_4) \right. \\
& + 2 (\cos \theta_1 \cos \theta_2 + \cos \theta_2 \cos \theta_3 + \cos \theta_1 \cos \theta_3) \\
& \left. - 2 \cos \theta_4 (\cos \theta_1 + \cos \theta_2 + \cos \theta_3) \right]
\end{aligned}$$

Using Equation (62), the following substitution can be made:

$$\begin{aligned}
2 \cos \theta_4 (\cos \theta_1 + \cos \theta_2 + \cos \theta_3) = (\cos \theta_1 + \cos \theta_2 + \cos \theta_3)^2 \\
+ \cos^2 \theta_4
\end{aligned} \tag{63}$$

so that Equation (63) can be reduced to

$$\cos^2 \theta_1 + \cos^2 \theta_2 + \cos \theta_3 + \cos^2 \theta_4 = 4/3 \tag{64}$$

Equations (62) and (64) would be useful in aligning and calibrating the pickoffs.

Two-Pickoff Readout Mode

To illustrate the calculations needed for complete specifications of α , β , and γ in the two-pickoff readout mode, assume that pickoffs P_1 and P_2 are the only pickoffs viewing the pattern. Only one of Equation (61) remains for a direct calculation of a basic direction cosine:

$$\alpha = \frac{3}{2} (\cos \theta_1 + \theta_2)$$

The direction cosine coplanar with these pickoffs and normal to \hat{F}_{x+} is not colinear with \hat{F}_{y+} nor \hat{F}_{z+} ; rather, it lies $\pi/4$ and $3\pi/4$ from them.

Defining

$$\hat{F}_{12} = \sqrt{1/2} (\hat{F}_{y+} - \hat{F}_{z+})$$

then

$$\hat{F}_{x+} \times \hat{F}_{12} = \sqrt{1/2} (\hat{F}_{z+} + \hat{F}_{y+}) = \hat{F}_{34} \quad (65)$$

The direction cosines with respect to these axes are

$$\hat{S} \cdot \hat{F}_{12} = \frac{\sqrt{6}}{4} (\cos \theta_2 - \cos \theta_1)$$

$$\left| \hat{S} \cdot \hat{F}_{34} \right| = \sqrt{1 - 9/8 (\cos^2 \theta_1 + \cos^2 \theta_2 + 2/3 \cos \theta_1 \cos \theta_2)}$$

The equations for β and γ are

$$\beta = \hat{S} \cdot \hat{F}_{y+} = \sqrt{1/2} \left[\hat{S} \cdot \hat{F}_{12} + \hat{S} \cdot \hat{F}_{34} \right]$$

$$\gamma = \hat{S} \cdot \hat{F}_{z+} = \sqrt{1/2} \left[\hat{S} \cdot \hat{F}_{34} - \hat{S} \cdot \hat{F}_{12} \right]$$

The sign of $\hat{S} \cdot \hat{F}_{34}$ is all that is needed for complete specification of β and γ . In a system where a pickoff provides information to the readout whenever it views the pattern, sign information can be provided by a memory element associated with a pickoff which is not one of the two pickoffs used for readout. In an orthogonally aligned three-pickoff system where the pickoffs are nominally coincident with the axes of reference, the application of such a memory element is direct. For a nonorthogonal system, its application is less direct, but nevertheless could be used.

An examination of Figure 23, in view of the definition of \hat{F}_{34} [Equation (65)], shows that this axis bisects the angle formed by the axes of pickoffs P_3 and P_4 . In the situation where pickoffs P_1 and P_2 are the pickoffs in use, a memory element which stores the sign of the last direction cosine reading of P_3 or P_4 (or both) would also define the sign of $\hat{S} \cdot \hat{F}_{34}$. That such a memory element can be utilized with reasonable dependability becomes apparent when it is observed that if the spin axis strays away from \hat{F}_{34} or $-\hat{F}_{34}$, either P_3 or P_4 begins to view the pattern, and a three-pickoff

readout mode or a different two-pickoff mode becomes possible.

An alternate method of determining the sign of $\hat{S} \cdot \hat{F}_{34}$ is to measure the phase angle of a pulse from P_2 generated by a meridional pattern line with respect to the pulse from P_1 generated by the same line. Figure 25 illustrates the geometry of this method. Let that phase angle be denoted by ϕ_{21} . The sign of $\sin \phi_{21}$ is positive if $\hat{S} \cdot \hat{F}_{34}$ is positive and negative if $\hat{S} \cdot \hat{F}_{34}$ is negative. When either one is nearly zero, P_3 or P_4 or both will be closer to the equator than P_1 or P_2 , and a three-pickoff mode or a different two-pickoff mode is available. Thus, a measurement is needed on ϕ_{21} only at times when it distinctly differs from zero or π .

To shorten the notation, let

$$\sigma_{21} = \left\{ \begin{array}{l} +1 \text{ if } \sin \phi_{21} > 0 \\ -1 \text{ if } \sin \phi_{21} < 0 \end{array} \right\}$$

then

$$\beta = \frac{\sqrt{3}}{4} \left[\cos \theta_2 - \cos \theta_1 + \sigma_{21} \sqrt{8/3 - 3(\cos^2 \theta_1 + \cos^2 \theta_2) - 2 \cos \theta_1 \cos \theta_2} \right] \quad (66a)$$

$$\gamma = -\frac{\sqrt{3}}{4} \left[\cos \theta_1 - \cos \theta_2 + \sigma_{21} \sqrt{8/3 - 3(\cos^2 \theta_1 + \cos^2 \theta_2) - 2 \cos \theta_1 \cos \theta_2} \right] \quad (66b)$$

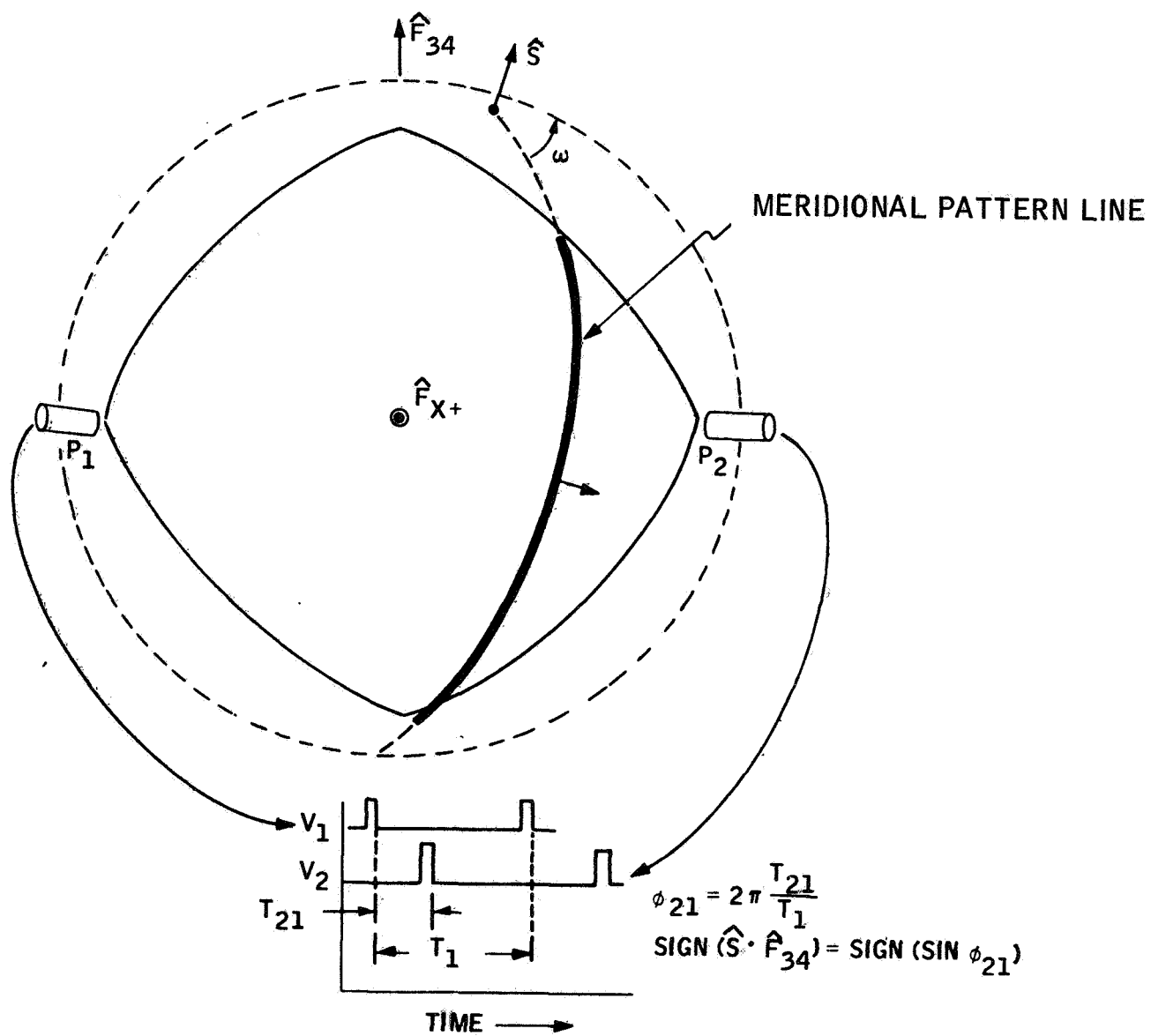


Figure 25. Measurement of a Phase Angle for the Sign of the Third Direction Cosine

It is readily apparent that another two-pickoff combination related to the combination of P_1 and P_2 is that of P_3 and P_4 . The same direction cosine computed directly from P_1 and P_2 is computed directly from P_3 and P_4 .

$$\alpha = \frac{\sqrt{3}}{2} (\cos \theta_4 - \cos \theta_3)$$

Also,

$$\hat{S} \cdot \hat{F}_{34} = \frac{\sqrt{6}}{4} (\cos \theta_4 + \cos \theta_3)$$

$$|\hat{S} \cdot \hat{F}_{12}| = \sqrt{1 - \frac{9}{8} (\cos^2 \theta_3 + \cos^2 \theta_4 - \frac{2}{3} \cos \theta_3 \cos \theta_4)}$$

The sign of $|\hat{S} \cdot \hat{F}_{12}|$ is determined by measuring the phase of a meridional line pulse from P_4 with respect to the same pulse from P_3 . Let

$$\sigma_{43} = \begin{cases} +1 & \text{if } \sin \phi_{43} > 0 \\ -1 & \text{if } \sin \phi_{43} < 0 \end{cases}$$

Then

$$\beta = \frac{\sqrt{3}}{4} \left[\cos \theta_4 + \cos \theta_3 + \sigma_{43} \sqrt{\frac{8}{3} - 3(\cos^2 \theta_3 + \cos^2 \theta_4) + 2 \cos \theta_3 \cos \theta_4} \right] \quad (67a)$$

$$\gamma = \frac{\sqrt{3}}{4} \left[\cos \theta_4 + \cos \theta_3 - \sigma_{43} \sqrt{\frac{8}{3} - 3(\cos^2 \theta_3 + \cos^2 \theta_4) + 2 \cos \theta_3 \cos \theta_4} \right] \quad (67b)$$

Equations (66) and (67) can be derived from one of the three-pickoff mode equations by solving Equations (62) and (64) simultaneously for one of the missing pickoff measurements, in terms of the two which are available and using the quadratic formula. A sign convention (i. e., σ_{21} and σ_{43}) still must be developed independently of this method for the sign of the square root of the discriminant.

The sensitivity of α , β , and γ to errors in the pickoff cosines can now be determined. Let

$$\epsilon_i = \Delta (\cos \theta_i)$$

The error sensitivity equation for a basic direction cosine can be expressed in general form:

$$\Delta \alpha_j = \sum_{i=1}^4 \frac{\partial \alpha_j}{\partial (\cos \theta_i)} \epsilon_i$$

Using this form for the combination of two pickoffs selected yields

$$\Delta \alpha = \frac{\sqrt{3}}{2} (\epsilon_1 + \epsilon_2)$$

$$\Delta \beta = \frac{\sqrt{3}}{4} \left\{ \epsilon_2 - \epsilon_1 - \frac{\sigma_{21}}{\sqrt{D_1}} \left[\epsilon_1 (3 \cos \theta_1 + \cos \theta_2) + \epsilon_2 (3 \cos \theta_2 + \cos \theta_1) \right] \right\}$$

$$\Delta \gamma = \frac{\sqrt{3}}{4} \left\{ \epsilon_1 - \epsilon_2 - \frac{\sigma_{21}}{\sqrt{D_1}} \left[\epsilon_1 (3 \cos \theta_1 + \cos \theta_2) + \epsilon_2 (3 \cos \theta_2 + \cos \theta_1) \right] \right\}$$

where

$$D_1 = \frac{8}{3} - 3(\cos^2 \theta_1 + \cos^2 \theta_2) - 2 \cos \theta_1 \cos \theta_2$$

Under the assumptions previously made about the expectation and correlation of the error variables ϵ_i , the variances of $\Delta\alpha$, $\Delta\beta$, and $\Delta\gamma$ become

$$\sigma^2(\Delta\alpha) = \frac{3}{4} \left[\sigma^2(\epsilon_1) + \sigma^2(\epsilon_2) \right]$$

$$\sigma^2(\Delta\beta) = \frac{3}{16} \left\{ \sigma^2(\epsilon_1) \left[1 + \frac{\sigma_{21}}{\sqrt{D_1}} \left(3 \cos\theta_1 + \cos\theta_2 \right) \right]^2 + \sigma^2(\epsilon_2) \left[1 - \frac{\sigma_{21}}{\sqrt{D_1}} \left(3 \cos\theta_2 + \cos\theta_1 \right) \right]^2 \right\}$$

$$\sigma^2(\Delta\gamma) = \frac{3}{16} \left\{ \sigma^2(\epsilon_1) \left[1 - \frac{\sigma_{21}}{\sqrt{D_1}} \left(3 \cos\theta_1 + \cos\theta_2 \right) \right]^2 + \sigma^2(\epsilon_2) \left[1 + \frac{\sigma_{21}}{\sqrt{D_1}} \left(3 \cos\theta_2 + \cos\theta_1 \right) \right]^2 \right\}$$

These variances are then summed to obtain the variance of the error vector $\bar{\Delta S}$.

$$\sigma^2(\bar{\Delta S}) = \frac{3}{8} \left\{ \sigma^2(\epsilon_1) \left[3 + \frac{(3 \cos\theta_1 + \cos\theta_2)^2}{D_1} \right] + \sigma^2(\epsilon_2) \left[3 + \frac{(3 \cos\theta_2 + \cos\theta_1)^2}{D_2} \right] \right\} \quad (68)$$

Three-Pickoff Readout Mode

When three pickoffs view the pattern, the basic direction cosines can be calculated from the three equations of (61), which do not involve the missing pickoff cosine. For example, if pickoffs P_1 , P_2 , and P_3 provide signals to the phase-angle electronics, the central terms of (61) are used. Accordingly, the error sensitivity equations for this combination of pickoffs are

$$\Delta\alpha = \frac{\sqrt{3}}{2} (\epsilon_1 + \epsilon_2)$$

$$\Delta\beta = \frac{\sqrt{3}}{2} (\epsilon_2 + \epsilon_3)$$

$$\Delta\gamma = \frac{\sqrt{3}}{2} (\epsilon_1 + \epsilon_3)$$

The variances of the direction cosines are

$$\sigma^2(\Delta\alpha) = \frac{3}{4} \left[\sigma^2(\epsilon_1) + \sigma^2(\epsilon_2) \right] \quad (69a)$$

$$\sigma^2(\Delta\beta) = \frac{3}{4} \left[\sigma^2(\epsilon_2) + \sigma^2(\epsilon_3) \right] \quad (69b)$$

$$\sigma^2(\Delta\gamma) = \frac{3}{4} \left[\sigma^2(\epsilon_1) + \sigma^2(\epsilon_3) \right] \quad (69c)$$

so that the variance in $\vec{\Delta S}$ is

$$\sigma^2(\vec{\Delta S}) = \frac{3}{2} \left[\sigma^2(\epsilon_1) + \sigma^2(\epsilon_2) + \sigma^2(\epsilon_3) \right] \quad (70)$$

It is interesting to note that, for the three-pickoff readout mode, $\vec{\Delta S}$ is more sensitive to a given error in a pickoff cosine in the four-pickoff arrangement than in the three-pickoff arrangement. The reason for this is easily noted in an expression for the sum of the squares of Equations (43) and (44):

$$\begin{aligned} \Delta\alpha_1^2 + \Delta\alpha_2^2 &= \frac{1}{\sin^2(\sigma_1 + \sigma_2)} \left[\epsilon_1^2 + \epsilon_2^2 + 2\epsilon_1\epsilon_2 \right. \\ &\quad \left. (\sin\sigma_1 \sin\sigma_2 - \cos\sigma_1 \cos\sigma_2) \right] \\ &= \frac{1}{\sin^2(\sigma_1 + \sigma_2)} \left[\epsilon_1^2 + \epsilon_2^2 - 2\epsilon_1\epsilon_2 \cos(\sigma_1 + \sigma_2) \right] \end{aligned}$$

When previously utilized assumptions about the nature of ϵ_1 and ϵ_2 are used, the expected value of this sum is

$$E \left(\Delta\alpha_1^2 + \Delta\alpha_2^2 \right) = \frac{1}{\sin^2(\sigma_1 + \sigma_2)} E \left(\epsilon_1^2 + \epsilon_2^2 \right) \quad (70)$$

This equation shows that the expected deviation of the direction cosines with respect to any two orthogonal axes in the plane defined by the pickoffs is minimized if the pickoff axes are orthogonal.

The spin vector may be normalized to reduce the expected value of $\overline{\Delta S}$. Substitution for the variances of $\Delta\alpha$, $\Delta\beta$, $\Delta\gamma$ from Equations (69) into (59) yields the desired variance for the normalized spin vector. If these variances are relatively constant over the range of θ_i , a fairly good approximation is given by Equation (60).

OPTIMUM PARAMETER STUDY

Computer Program Description

A search for the optimum combination of pattern parameters, pickoff arrangement, and readout mode that minimizes the pattern edge dispersion error amplification was conducted with the aid of a computer program. The parameters $(\cos^{-1} \alpha)$ and $(\cos^{-1} \beta)$ were serially incremented over the pattern range being investigated; the pickoff axis direction cosines for the three-pickoff arrangement are calculated for each combination of values. The pickoff axis direction cosines for the four-pickoff arrangement are calculated with the solutions of Equations (61) for $\cos \theta_i$. From the pattern parameters specified by the input, the expected error in the pickoff axis direction cosines are calculated using the equations derived in Section III. The expected error of the spin vector for each combination of pickoff arrangement and readout mode discussed in this section is calculated and printed out for easy comparison.

The calculation of error amplification from the pattern parameters was coded as a subroutine to the program. In addition to specifying pattern type, number of pairs of lines, and the pattern range, an additional parameter was furnished which allows space between the extremities of adjacent pattern lines. Allowance for this space is needed because pattern lines must have a width at least as great as the diameter of the pickoff field of view and because a finite time is required for the pulse output electronics (HIT) to be reinitialized in preparation for the signal produced by the next pattern line. The effect of the spacing margin angle was to reduce the parameter θ_0 in the error equations derived in Section III from the pattern range input to the program by that angle.

Since different pattern ranges are required for all-attitude readout for each pickoff arrangement, provision was made to input a separate range for each. Ranges which were specified were equal to or greater than the minimum required to provide a two-pickoff readout mode at all times; expected errors from a three-pickoff mode were calculated only if such a mode were possible.

Results of Study

It was noted on page 53 that pattern edge uncertainties produced by a colatitude pattern line are independent of the colatitude of the pickoff. This fact can be utilized to compare the amplification of error produced by the pickoff arrangement and readout mode. When the minimum pattern ranges for all-attitude readout in a two-pickoff mode are assumed for each arrangement, the combinations rank as follows in increasing order of average error amplification:

- Two-pickoff mode, four-pickoff arrangement
- Three-pickoff mode, three-pickoff arrangement
- Three-pickoff mode, four-pickoff arrangement
- Two-pickoff mode, three-pickoff arrangement

Some observations and conditions are worthy of note:

- When three pickoffs in a four-pickoff arrangement view the pattern, four choices of readout modes are available: the three-pickoff mode and three combinations of two pickoffs. Of the three combinations of two, the two nearest the rotor equator yield the smallest error amplification.
- When a three-pickoff mode is available, the error amplification in the normal spin vector from this mode, in most cases, is smaller than that obtained from any two-pickoff mode. This is generally true for the four-pickoff arrangement and invariably true for the three-pickoff arrangement.
- Large variations in the error amplification occur in the two-pickoff modes, especially for the three-pickoff arrangement. This is attributed directly to the sensitivity of the third direction cosine error to the other cosines. The amplification is greatest when a three-pickoff mode is available.
- Even when taking into account the reduced pattern range necessary for the four-pickoff arrangement, the error amplification from three-pickoff readout modes is smaller for the three-pickoff arrangement than for the four-pickoff arrangement. This finding is attributed directly to the fact that the pickoff axes of the three-pickoff arrangement are mutually orthogonal.

Comparisons of pattern type, with all other parameters equal, showed that the average error amplification, in increasing order, ranked as follows:

- Cosine Pattern
- Colatitude Pattern
- Great Circle Pattern

With other parameters equal, the differences in average error between the cosine pattern and the colatitude pattern range from one to six percent, whereas those between the great circle pattern and the colatitude pattern range from five to 20 percent. The reason for the significantly larger error amplification from the great circle pattern is not apparent. Therefore, the great circle pattern would be preferred only if its edge uncertainty were significantly smaller than that of the other pattern types.

Attention was focused on the comparison of the two-pickoff mode to the three-pickoff mode for the three-pickoff arrangement as a function of pattern range. It was assumed that two pairs of cosine pattern lines were used with a colatitude spacing margin of two degrees. The comparisons are illustrated in Figure 26.

The top curve is that rms of all two-pickoff modes that were calculated; included were many cases for which the magnitude of either or both direction cosines exceeded the magnitude of the third direction cosine. The large variation observed in this mode is dramatized by comparing it with the bottom curve, which depicts the error amplification when the two pickoffs used for readout both view the equator. It is also dramatized by comparing it with the "restricted" two-pickoff rms curve, which includes only those cases for which $|\alpha| \leq |\gamma|$ and $|\beta| \leq |\gamma|$ [or when Equations (48) are satisfied]. Approximately 70 percent of the cases included in the top curve are retained in the "restricted" rms. The rms of the three-pickoff modes includes only the cases for which such a mode is available. As the pattern range is increased, the number of available three-pickoff cases becomes more numerous.

The "mixed mode rms" curve is the rms of error amplification when one adopts a strategy of using the three-pickoff mode when it is available and the two-pickoff mode only when one of the pickoffs does not view the pattern. Note that this curve is not as sensitive to the pattern range as the others over the range under consideration. For the three-pickoff arrangement, such a strategy appears to offer the smallest overall error amplification. A pattern extending from a colatitude of 40° to 140° will provide a three-pickoff mode in all situations where a two-pickoff mode would otherwise yield excessive error amplification. A comparison of this strategy with the readout strategy employed with the present ESGV indicates a potential overall readout improvement of 20 percent.

The use of two pattern lines yields minimum error amplification for all pattern types over the ranges which were investigated. The improvement it provided over one pair of pattern lines is approximately two percent for the colatitude line and ranges from three to five percent for the cosine line. If multiple pairs of pattern lines cannot be employed without significantly increasing the logic of the readout electronics, a single pair of pattern lines may well be the better choice.

The choice of a 10° spacing margin may not be practical for all cases. However, since this is the angle needed to provide a usable pattern for the present system, it is a reasonable choice for this study.

It was noted earlier that, with the colatitude pattern, a three-pickoff mode was preferred more often than the optimum two-pickoff mode in a four-pickoff arrangement when the three-pickoff mode was available. A "mixed-mode" strategy similar to that outlined for the three-pickoff arrangement would then lead to the least average error amplification for this combination. However, if the minimum range cosine pattern is used instead, the

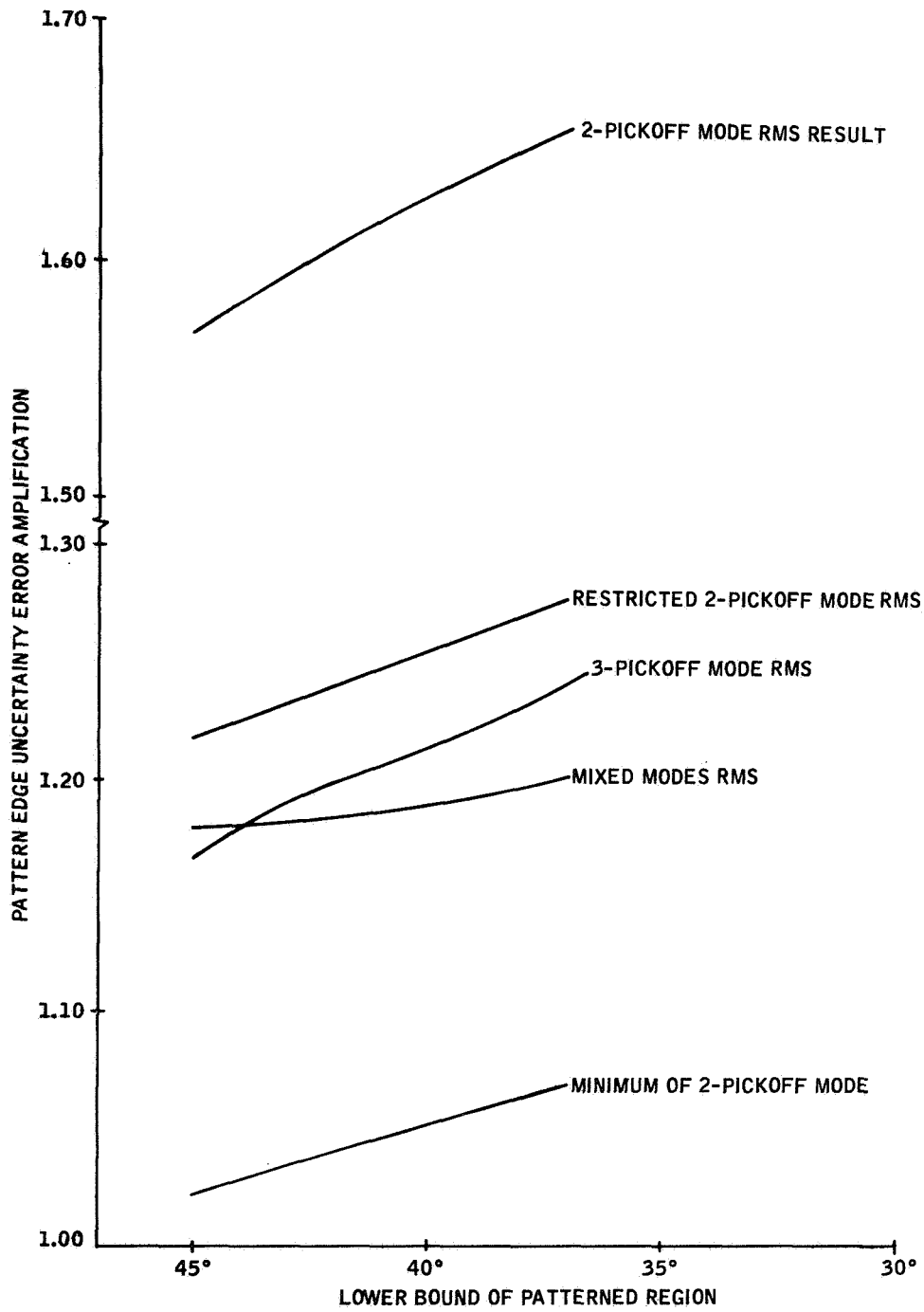


Figure 26.

optimum two-pickoff mode is found to provide less error amplification more often than does the three-pickoff mode. The best strategy for this combination would therefore be one in which a two-pickoff mode is employed at all times; when a choice exists, the two pickoffs nearest the rotor equator must be determined first. Such a strategy increases the complexity of the logic and leads to an average error amplification approximately two percent less than the mixed-mode strategy for a three-pickoff arrangement using a minimum range cosine pattern. The likely reason for such a small gain is the nonorthogonal arrangement employed for four pickoffs.

It is therefore concluded that the optimum combination of parameters that minimizes pattern edge error amplification and retains a relatively simple logic in the readout electronics is:

- An orthogonal arrangement of three pickoffs
- One pair of cosine pattern lines
- Pattern range extending from 40° to 140° of colatitude
- Mixed-mode strategy of reading three pickoffs when available and reading two pickoffs only when necessary

SECTION V

PATTERN EDGE IMPROVEMENT

In the previous section we have seen how the pattern parameters and location of pickoffs affect the magnitude of the expected readout error from pattern edge uncertainties. It was shown that the realizable reduction of error when utilizing the pattern application technology employed in previously built gyros, but altering the pattern parameters, is approximately 25 percent. Such a reduction is insufficient to realize the potential mission requirements of the ESG. Therefore, it is necessary to investigate methods of improving the pattern edge itself.

SOURCES OF PATTERN EDGE UNCERTAINTIES

A major source of edge uncertainty is provided by the pattern application process. The optical system detects the pattern line by the change in the intensity of light reflected back to the pickoff by the rotor surface. The surface on one side of the readout line must be highly reflective and the surface on the other side must diffuse and/or absorb the light. Pattern application experiments (which will be described in detail later in this section) have shown that greater accuracy in readout line definition results if the line is simple to mechanize and if the number of steps in the line application is kept to a minimum. A grit-blast method of the great circle line would, therefore, produce the least error.

Another contributing source of error is the quality of the rotor surface finish. The polishing process tends to gouge the sintered beryllium material; consequently, satisfactory results have not been consistently obtained. Some experiments have been conducted in plating rotors with chromium before polishing. The plated rotors polished well; however, the plated surface was found to be unstable under large temperature variations. There is also some question on the stability of the plate at high rotor speeds. Nevertheless, further experimentation with plated rotors may provide a way to overcome these difficulties.

The electric fields which support the rotor also produce stresses within the rotor and electrode material. If the fields become sufficiently great, clumps of material can break off the electrode and be deposited on the rotor. These deposits, commonly called arc marks, produce diffuse spots on the surface. These spots alter the reflectance of the surface and cause noise pulses in the optical signal received by the pickoff. Two aspects of arc marks are of concern in regard to readout accuracy: large marks that produce signals as large as that produced by a nonreflective portion of the rotor and cause false triggering of the signal processing electronics, and marks adjacent to the readout line that distort the true pulse and cause an error in the timing of the trigger.

The effects of these errors, and the methods of compensation, fall into three categories:

- False triggering
- Nonrandom (low frequency) edge deviation
- Random (high frequency) edge deviation

False triggering can be produced by large arc marks and pock marks that are capable of generating relatively large noise pulses in the pickoff signal. Often these pulses are narrower than the signal pulses and can be filtered by pulse width discrimination techniques.

Errors in the pattern line mechanization process produce deviations from the desired readout line. The portion that is nonrandom, or of low frequency, can be compensated by adding terms or adjusting the coefficients of the mechanization line. It is desirable to keep these additions and adjustments to a minimum, as sophisticated calibration techniques would be needed to quantitatively determine these additions and adjustments.

In the grit-blast method of defining pattern lines, dispersion of the grit reduces the sharpness of the line edge. The slope of the pickoff output signal is reduced by this "fuzziness"; the triggering point as a function of colatitude becomes randomized at high frequency. A similar randomization is produced by the presence of arc marks and polishing imperfections on the rotor surfaces. The nature of this error is such that mathematical compensation is very difficult. Attempts at compensating for this error have indicated that a table look-up method is the most practical alternative.

RESULTS OF PREVIOUS IMPROVEMENT STUDIES

A major area of laboratory studies for improved pattern application is that of vacuum or vapor depositing an optically contrasting material onto the rotor surface. To control precisely the region on which the material is deposited, a mask is needed. A deposition technique generally requires the following steps:

- Apply masking material to surface
- Remove mask from areas to be deposited
- Clean substrate surfaces
- Deposit material onto substrate
- Remove mask from rotor

The material to be deposited, in addition to being an optically contrasting substance, must adhere to the surface sufficiently to withstand the forces from the electric fields and rapid rotation. Titanium and cerium oxide have been deposited on rotors and have been found to resist scuffing; whether such resistance indicates that the deposit can withstand centrifugal and electric forces is not definitely known. A method for precision-balancing an ESGV rotor was developed by vapor-depositing gold on the rotor. The deposit passed a "tape test", but was not subjected to a scuffing test; it was later found that this deposit was removed by the electric fields.

The masking material should be one that adheres to the rotor surface, is easy to cut away from areas to be deposited, and can easily be removed from the surface after deposition. For a vacuum deposition process, the mask should not outgas; for vapor deposition, it should not be damaged or vaporized by the heat. Copper has been found to be better suited for a mask material than other materials tested. However, it is quite fragile and can chip away from the pattern edge. Extreme care must be exercised at the time that the copper is removed from the areas to be deposited.

The adhesive quality of the deposit has been found to depend highly on the cleanliness of the rotor surface and deposition system. Sufficient cleanliness was not achieved without mechanically cleaning the substrate; such cleaning often damaged the delicate mask.

The overall success of this deposition technique rests on the workability and durability of the mask. Copper is one of the few materials which is easily deposited and removed from the beryllium surface; however, it appears to be too fragile for use as a mask. When compared with the grit-blast technique, the number of steps required for this technique becomes a distinct disadvantage.

Another general area of laboratory investigation has been photo-optical film techniques, similar to those used in microcircuitry. However, the primary limitation is obtaining an adequate light source. Such a problem could perhaps be solved today with the use of lasers as a light source. Both the high output and the small divergence characteristics of gas laser beams could be put to good use in precisely defining a cosine line on a photo-sensitive film covering the rotor. Some further evaluation of these techniques would presently be warranted.

The presently used grit-blast technique has undergone laboratory study to determine how pattern line sharpness and contrast can be maximized with minimum disturbance of the surface. These factors depend on the size of the grit and the exposure to the blast.

The size of the grit has a surprisingly great influence on the effectiveness of the grit-blast technique. A 10-micron grit produces the greatest contrast, but not a very sharp edge. A 0.3-micron grit produces a sharp edge; the contrast is not very great. A 0.7-micron grit has virtually no effect on the surface. An investigation of the effects showed that the 10-micron grit abraded the surface, providing the diffuse surface that was desired. The 0.3-micron grit was deposited on the surface, forming a single layer. Since such a layer could produce undesirable effects (such as a catastrophic arc) in an operating gyro, the use of this size grit was not considered further. A possible reason that the 0.7-micron grit was ineffective is that this size is one that collides elastically with the pressed crystals that comprise the beryllium material.

The optimum exposure time is that long enough to produce microscopic rearrangement of the surface into peaks and pits. Further exposure reduces the contrast; this may be attributed to surface peaks being broken off by the excess grit. The pattern line that results becomes a depression in the surface, which can be responsible for spurious electric torques.

There is some speculation that nozzle geometry has some influence on line edge sharpness. The desired distribution of grit would indicate that a rectangular nozzle with a side parallel to the line edge would provide better edge sharpness than a circular nozzle. To pattern a curvilinear line such as the cosine line with a rectangular nozzle would require that the angle of the nozzle as well as its position would have to be controlled in the patterning process. This additional constraint was not considered to be within the scope of the improvement program at the time; hence, a circular nozzle is used for the cosine line. However, a rectangular nozzle can be utilized without great difficulty for a great circle pattern.

In general, dispersion of the grit does not produce a line edge as sharp as could be obtained with the deposition technique. However, the grit-blast method does involve fewer steps and provides more consistent results than other techniques discussed so far. Another distinct advantage is that it causes the least change in rotor balance (whereas the material added in the deposition technique must be considered a factor of rotor balance). Consequently, it is the method adopted for patterning rotors at present.

Other studies have been conducted to determine how the occurrence and the effects of arc marks can be reduced. This is an important consideration in the design of the suspension circuits and the electrodes; significant progress has been made in the long-term development of the ESVG. During normal operation, arcing is now likely to occur only when the gyro is subjected to severe acceleration environments. Little attention has been paid to the prevention of arcing when the rotor is lifted; experience has indicated that it deserves further study.

In an early development program, some rotors were plated with chromium as a means to improve the reflectivity of the surface. The chromium did not gouge during the polishing process, nor did arcing damage the chrome surface as it does the beryllium surface. Chromium plated rotors offer significant readout improvement potential over the unplated rotors. However, the plating was found to be unstable over large thermal changes because of the difference in the expansion coefficients between chromium and beryllium. Greater shape stability may be achieved with thinner coats of chromium; for the potential gain it offers in readout accuracy, coated rotors should be further studied in the future.

ARC MARKS AND TRIGGERING ERRORS

The pattern line in the present system is a diffuse area on an otherwise reflective rotor. The height-insensitive trigger is designed to produce a pulse at the instant when the signal is a fixed proportion of the amplitude of the input pulse. The signal from the reflective area serves as a baseline for measuring the pulse amplitude.

The presence of arc marks affects the triggering point of the height-insensitive trigger in two ways. Marks adjacent to the pattern line distort the critical signal on which the triggering point is defined. Marks elsewhere cause a change in the baseline reference, producing an error in the

measurement of the amplitude on which the triggering point is determined. If arc marks must be tolerated in the readout signal, the signal baseline should be less sensitive to arc marks.

The baseline can be made insensitive to arcs if the baseline signal comes from a diffuse area of the rotor surface. The pulse signal must then come from a reflective portion of the surface. Such a system would require a reflective pattern line in a diffuse background.

The diffuse background does not have to cover the entire rotor surface (this would not be desirable, since such a surface could encourage arcing). If the reflective pattern line can be rendered less vulnerable to arcs (such as by a chromium coat), the vulnerability of the readout accuracy to arcs and polishing imperfections can be reduced considerably.

RECOMMENDATIONS FOR FUTURE STUDY

Polishing imperfections and arc marks produce significant readout errors in the present system. Their occurrence or their effects must be reduced before accuracy improvements can be made. Some laboratory investigations would therefore be justified in

- Chromium plating techniques and durability of these plates
- Polishing techniques to improve the final rotor finish
- Suspension modifications to avoid arcing during lift

Some investigation of an infrared readout system would be worthwhile on the chance that infrared wavelengths are not diffused as much as visible wavelengths by arc marks.

Film could be deposited on the rotor and the laser could be used to define the line by photochemical means with a setup as shown in Figure 27. This would be followed by other suitable processes to complete the pattern application.

The use of a laser as shown in Figure 27 could also be a direct means of pattern application if the laser has sufficient power. The beam is focussed so that the beams converge on the spin axis. The meridional angle intercepted by the beam remains constant as the laser traverses along z . The variation of beam intensity also compensates in part for the variation of the angle between the beam axis and the rotor surface normal. This method of referencing a cosine pattern has enough attractive features to warrant concerted laboratory experimentation.

Electron beams have potentially more powerful intensities. However, the aberrations encountered with electron lenses and space charge effects pose some complex problems in the control of these beams. If laser beams are found to be unsuitable for use in the pattern application process, electron beams should then be further explored as a possible alternative.

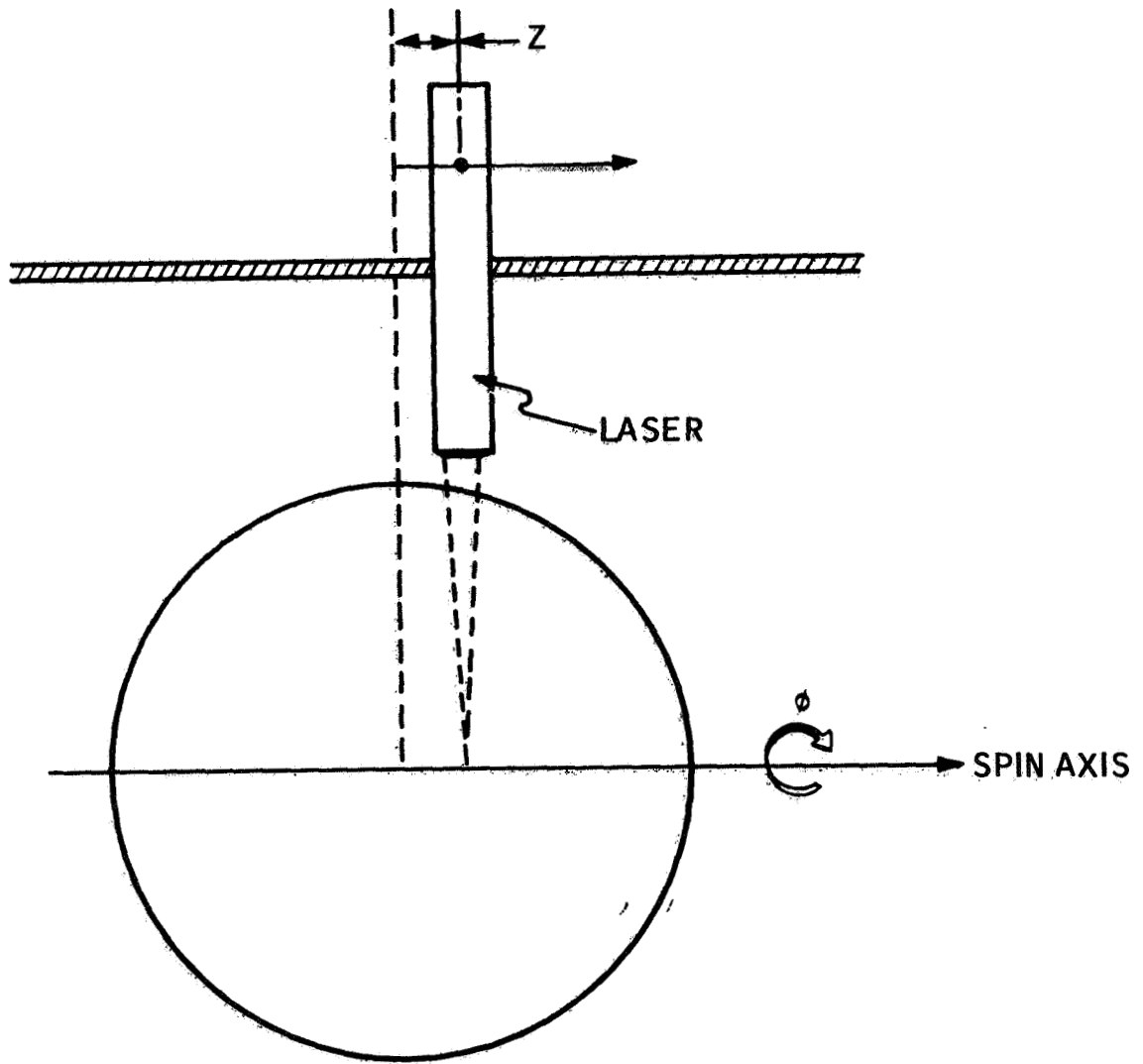


Figure 27. A possible Setup for Defining Cosine Pattern with Laser

SECTION VI

PHASE-ANGLE MEASUREMENT TECHNIQUES

With the introduction of a tilted great circle line scribed on the ESVG rotor to provide spin-vector readout, the measurement of the meridional angle between two points of great circle segments located at the same colatitude has been used to determine the location of the spin axis. To ensure adequate accuracy in the meridional angle measurement during the gyro test phase, an elaborate system has been devised for directly measuring the time interval between the passage of pattern lines by counting pulses of a high-frequency precision oscillator. Pulses generated by the pattern in the pickoff signals are used to start and stop the counting process. This system, in its present size, is not amenable for use in a vehicle navigation system.

There is little doubt that a phase-angle measurement system based on the presently used scheme can be built much more compactly for use on a vehicle. How this can be accomplished is described briefly in this section. However, this high-speed, all-digital system contains a higher degree of sophistication than is actually needed at the system level. Consequently, a hybrid phase-lock system is considered and discussed. No comparisons in physical size were made between the two systems in this study. The accuracy of the hybrid system depends on the null sensitivity of the phase discriminator; some improvement is needed over the sensitivities claimed in the literature to be adequate for ESVG needs. Available in the hybrid system, however, is an analog signal that could provide rate information to the navigation system.

ALL-DIGITAL CLOCK SYSTEM

The phase-angle measurement system presently used in the ESVG test facility is one in which high-frequency precision pulses are counted; hence, the name "clock system". A block diagram of the system is shown in Figure 28.

The pickoff output pulses are separated into logic pulse train P_0 and phased trains P_1 and P_2 . The phased trains are used to gate one counter which provides a measurement of the time interval between P_1 and P_2 . This time interval is proportional to the accumulated count, C_1 , which is then submitted to the computer. The logic pulse starts and stops the second counter; the counts accumulated on this counter, $(C_1 + C_2)$, are proportional to the rotor period. The ratio of C_1 to $(C_1 + C_2)$ is equal to the phase angle (the dimension of the ratio, always less than unity, is in revolutions).

The pulse trains which gate the counters must themselves be gated by the readout initiation signal. The counters are first reset. Then counts are accumulated until M rotor revolutions are completed; the count accumulation is stopped, and the results sent to the computer. In this way, M revolutions are averaged.

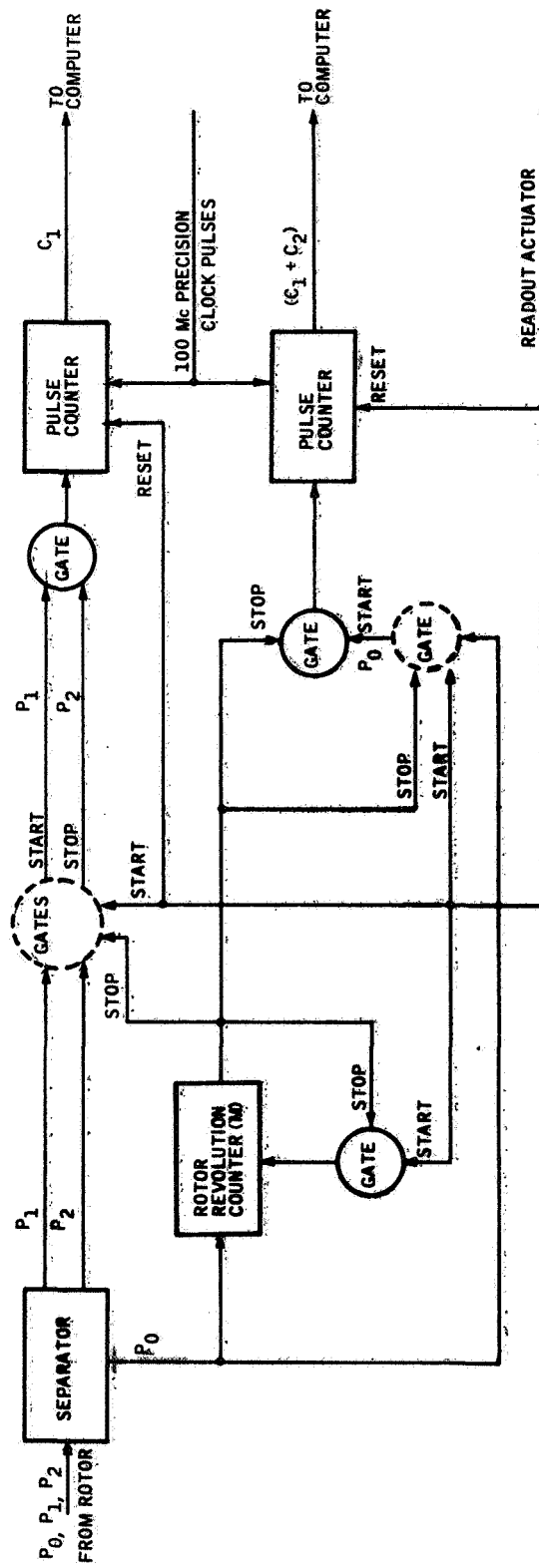


Figure 28. Block Diagram of Present Phase-Angle Measurement System

To project the physical size of a vehicle-mounted version of this system, three factors are considered:

- Microminiaturization of the electronic components in terms of up-to-date technology
- Instrumentation and display capability needed at the test phase but not in the navigation system
- Prospect of utilizing one subsystem to provide a common function at several needed points in the system

The test facility system was designed to utilize components and instruments available in 1962. If it were necessary to build a compact version of the same system for test facility use today, it is probable that a significant size reduction could be effected with components and instruments now available.

The test facility system has instrumentation and versatility not needed for a vehicle-mounted navigation system. Time-keeping units, display panels for the counters, and the circuits which adapt the unit to be used at any of a wide range of ESVM rotor speeds can be eliminated. Since the vehicle-mounted unit must be completely automated, the manual controls for readout mode and sampling rate would be bypassed.

The sampling of data is initiated by a clock at precise intervals in the test facility system. Since the time of each sample is important in the gyro drift analysis phase, it is part of the data recorded with each sample. Driving the clock is a precision, high-frequency oscillator; the clock is essentially a properly scaled pulse counter and accumulator. The oscillator is needed to actuate the sampling for the navigation system and to provide the pulses needed to measure the phase angle. However, other units such as the navigation computer itself require a precision oscillator. Conceptually, it is possible that one precision oscillator can provide precision timing pulses, with proper frequency scaling for each, at all points where needed in the navigation system.

When such factors are taken into consideration, a functional all-digital, phase-angle measurement system for a vehicle is likely at a considerable reduction in physical size and power from that of the test facility unit. Without taking into account an oscillator for the time-keeping and time-measurement functions, the size of such a system is expected to compare with the size of the gyro and its suspension electronics.

HYBRID PHASELOCK SYSTEM

The all-digital clock system provides phase-angle information suitable for immediate processing in a computer. However, the method used to provide this convenient form also enables a complete data sample to be taken (assuming no averaging) in less time than that required for the rotor to make two full revolutions. The sampling rates made possible by this method far

exceed the system requirements, even when one averages over several consecutive revolutions. Consideration of a method where comparable accuracy requirements may be achieved with lower-speed equipment at a sacrifice in the sampling rate capability has led to the suggestion of a phaselocking system in which the analog output of a phase discriminator is nulled with a digitally delayed feedback signal. A block diagram of such a system is shown in Figure 29.

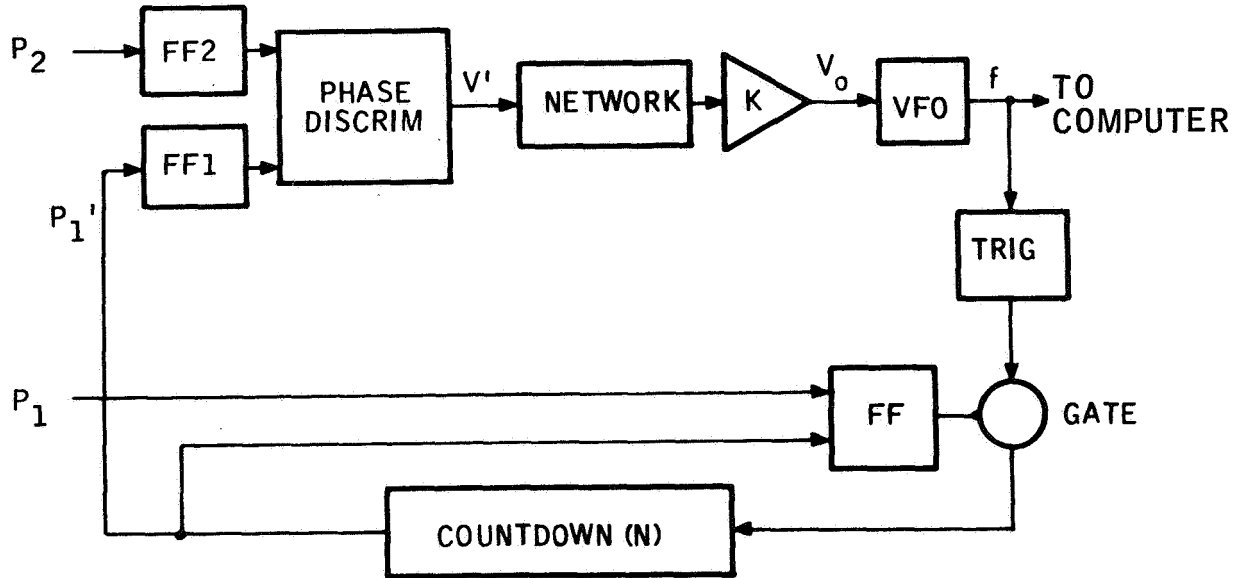


Figure 29. Diagram of Basic Phaselock Loop

Pulse train P_1' is delayed from P_1 by time T and compared with pulse train P_2 . The phase angle between these trains generates a voltage V' which through a network produces a control voltage V_o which drives a variable frequency oscillator (VFO). The error signal changes the frequency of the VFO in such a way that the delay time T is adjusted so that the phase discriminator produces a null signal. At null, the frequency generated by the VFO is a representation of the time interval between the pulse trains P_1 and P_2 .

The delay is produced by counting pulses from the VFO. P_1 starts the counting process. After N pulses are generated, an overflow pulse is produced which stops the count. The series of overflow pulses is P_1' which has been delayed by

$$T = \frac{N}{f} \quad (71)$$

Under steady-state conditions, the time delay between P_1 and P_2 remains fixed. Pulse trains P_1' and P_2 are simultaneous, V' is null, and T represents the time delay of P_2 with respect to P_1 . When the phase between P_1

and P_2 changes, P_1' and P_2 are not simultaneous, and an error signal ($V' \neq 0$) is developed in the phase discriminator. The network functions as an integrator; a nonzero input changes V_0 in the direction required to render P_1' simultaneous with P_2 . If the loop has a relatively constant response time, the error signal V' is a measure of the rate of change of the phase angle between P_1 and P_2 .

There are two aspects of this system which require further study:

- The accuracy to which P_1' can be adjusted for null output
- The dependence of the output to a change in rotor speed

The feasibility of using this system for readout depends on the null sensitivity capability to which a phase discriminator can be built. A literature search has been conducted to determine this capability.

Results of the Literature Search

Null sensitivity accuracy can be expected to depend on the input wave forms and the frequency range of the input signals. Literature which deals with phase discrimination of pulse trains at audio frequencies is considered most pertinent to the ESGV readout problem; however, much of the literature deals with sinusoidal wave forms and with sonar, radio, and microwave frequencies. The number of articles which provided useful information is small.

A serious limitation encountered in the precise measurement of phase angles is the stability of the instrument supply voltages, which limits the precision of ordinary phase meters to 0.1° . Kalmus and Hedrich (Ref. 2) devised a circuit which on alternate cycles delayed a pulse in Train A, then a pulse in Train B, by approximately 180° . A switching arrangement causes the undelayed pulse to turn on a flip-flop and the delayed pulse to turn it off. The integrated output is a square wave superimposed on a d-c bias, with the amplitude of the square wave proportional to the phase angle between the pulse trains. In this manner, d-c shifts are eliminated from measurement errors. A full scale deflection sensitivity of 0.01° is claimed. The frequencies over which the authors work ranged was not mentioned.

Of incidental interest is a circuit described by King (Ref. 3) that provides a polarity sensitive ternary signal for use with a phasemeter where only phase-angle magnitude is measured. Phase-angle magnitude is proportional to the pulse width of the output; the polarity of the pulse tells which pulse train occurs first. This information is of course vital in any phase-angle readout based on a null-seeking technique.

2. Kalmus, H.P.; Hedrich, A.L.: IRE Proc. 47, 90 (1959).

3. King, R.E.: Electronic Eng. 36, 615 (1964).

Accuracy claims in the literature cannot be compared directly with the ESVG readout requirements without taking into consideration possible errors of the signal-shaping circuits employed by the authors which are not within the scope of this measurement study. The resolution of the present ESVG pulse-shaping electronics is of the order of nine seconds in the meridional angle, or one-fourth the angle represented in the sensitivity claimed by Kalmus and Hedrich for their phase meter circuit. If their sensitivity includes the uncertainty contributed by their signal-shaping electronics, one could believe that their circuit may show better sensitivity when the ESVG pickoff signals are input.

If no significant improvement beyond 0.01° can be expected in the phase-angle measurement, one could explore methods of phase-angle multiplication which would render an effective phase meter sensitivity commensurate with the resolution of the input signal. A possible method is suggested by the block diagram of Figure 30.

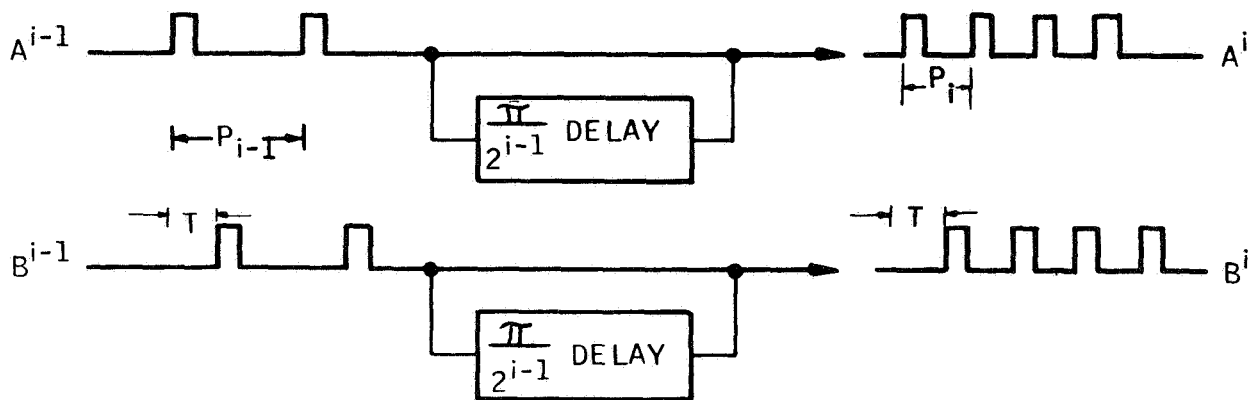


Figure 30. Phase-Angle Amplification by Doubling the Frequency

The input signals are delayed 180° and superimposed onto the original signal, which doubles the pulse frequency. On the output, the pulse period P_i is one-half that of the input period P_{i-1} while the delay time T is maintained. The phase angle, proportional to T/P_k , is doubled. Delays of this nature could be applied successively as long as $T > P_k$. A "coarse-fine" measurement can be obtained by using the phase meter output from A^k and B^k as the fine measurement and the pulse count in A^k before a pulse occurs in B^0 (or pulse count from B^k before a pulse in A^0) as the coarse measurement. The phase nulling process by the feedback circuit would be a two-step process, a nulling of the coarse measurement followed by a nulling of the phase meter output.

Compensation for Rotor Speed Changes

The phase angle is related to the delay time at null as follows:

$$\phi = 2\pi f_r T$$

where f_r is the rotor frequency. Substituting this relation into (71) yields

$$\nu = \frac{2\pi f_r N}{f} \quad (72)$$

To mechanize a measurement for ν , a provision to evaluate the ratio f_r/f is needed. A pulse counter similar to the units used in the clock system could be used. Pulses which are a multiple of rotor frequency may be accumulated in a counter which is gated and reset by pulses from the variable frequency oscillator. For the required resolution, the multiple of f_r to be counted should be of the order of 5×10^5 times the range of f . An alternative would be to divide down f with a countdown similar to that in the feedback loop in Figure 29.

An alternative is to allow N to be a rotor speed dependent variable.

If

$$N = \frac{K}{f_r} \quad (73)$$

then

$$\nu = \frac{2\pi K}{f}$$

and f is a measurement of the reciprocal of ν . The reciprocal result, in the case of a cosine pattern, is not the most desirable, but this can be rectified in the mechanization equation for the direction cosine. For a great circle pattern, the cosine mechanization from the reciprocal of phase is not likely to be any more complicated than that from the phase angle itself. An unattractive feature of this alternative is the calculation of N from f_r with (73); this would require a division process in the computer, or counting pulses from a reference oscillator with gating provided by reference pulses from the rotor.

The most practical method of calculating ν with (72) is to mechanize that equation in the computer. Low-speed counters can be used to measure f_r and f , or parameters that enable their quick calculation.

A Phaselock System for ESVM Readout

A block diagram of a potentially feasible phaselock system with compensation for rotor speed is shown in Figure 31. Signals containing logic pulse P_0 and phased pulses P_1 and P_2 are separated; the logic pulse is used as the basis of separation and for providing rotor speed information. The same logic pulse can be used with the logic pulse from another pickoff to determine the sign of the third direction cosine, in the manner discussed on page 87 with the King polarity sensitive circuit.

To provide adequate feedback resolution, the VFO output frequencies are likely to be quite high. It may be found convenient to heterodyne this output f down to a lower frequency f' . This output and the logic pulse frequency multiplier output would trigger pulses which are counted and input to the computer for calculation of the phase angle by Equation (72). The precision clock pulses can be input under computer control and be used to start the readout cycle.

In addition to driving a network that adjusts the VFO output, V' is fed into a second network which outputs a signal proportional to the phase-angle rate of change. The nominal purpose of this network is to compensate for any feedback loop nonlinearities.

The successful implementation of a phaselock system depends primarily on the null sensitivity of the phase discriminator. With the implementation of the circuit reported by Kalmus and Hedrich, there is a reasonable chance that a system compatible with accuracy requirements and/or other sources of error can be built. If it is insufficiently accurate, a phase amplification circuit (by stepping up the pulse frequency as shown in Figure 30) can be considered. To be sufficiently accurate, high-frequency pulses must be counted in the countdown delays; frequencies of the same order as the VFO output would be needed. The phase-angle nulling process would consist of a two-step "coarse-fine" sequence. The phaselock-loop block diagram would be similar to that shown in Figure 32.

CONCLUSIONS

Before an experimental phaselock system can be built and tested, further study is needed to determine the loop and network parameters. If the simpler loop of Figure 31 can be implemented with sufficient accuracy, chances are that the physical size of a phaselock system can be significantly smaller than the all-digital clock system. If it is important to obtain rate information from the ESVM, and a phaselock system indeed provides this information, such a system is certainly an attractive one.

The additional hardware shown in Figure 32 would increase the physical size, how much depends on the size requirements of the frequency multipliers. Under these circumstances, other criteria than physical size may determine the better choice between the clock and the phaselock systems.

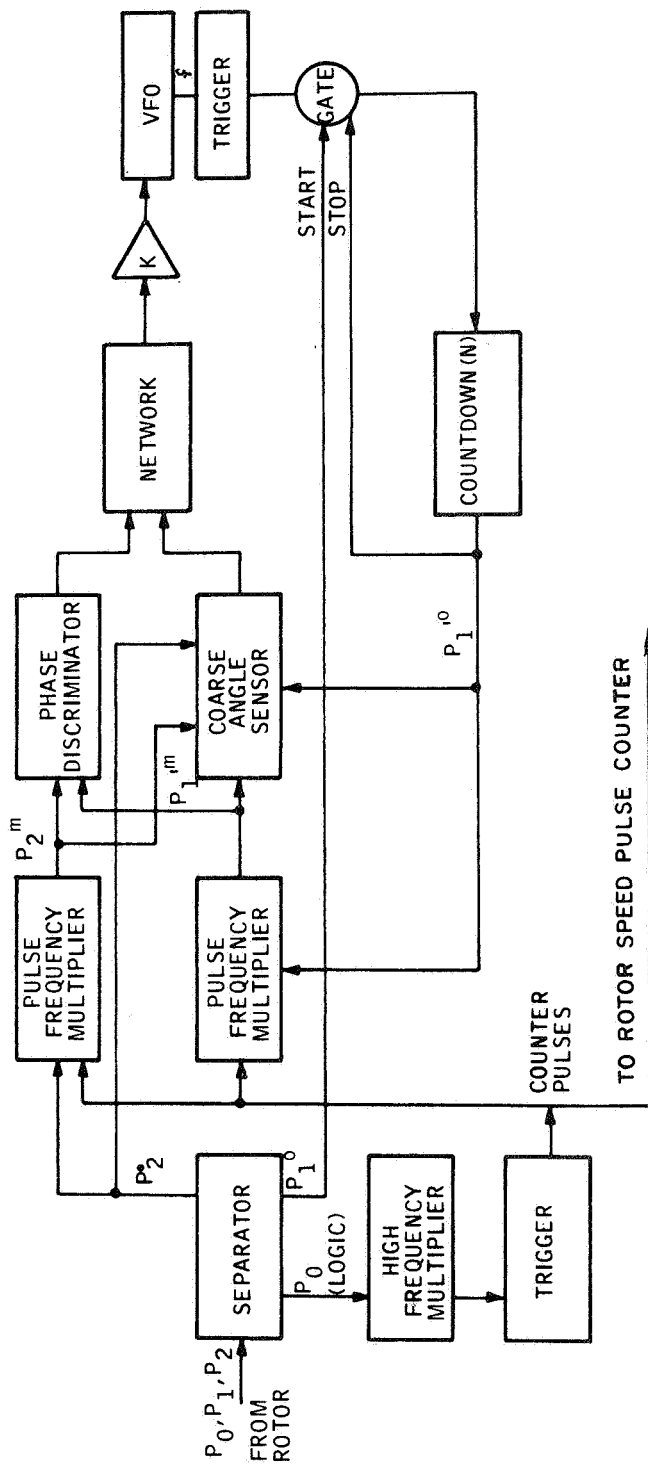


Figure 32. A Phaselock System with Phase Amplification

SECTION VII DYNAMIC ENVIRONMENTS

Maximum readout precision is possible only if the ESG rotor maintains the position in the electrode cavity that it assumes during the readout alignment calibrations and adjustments, and if the pickoff colatitude does not change during the readout cycle. In this section, the effects of environments which produce rotor displacements and changing colatitudes are evaluated - static acceleration, vibration, and angular rotation. These effects are minimized if readily mechanizable computer compensation for translation is implemented if several rotor revolutions are averaged per data cycle, and if all pickoffs are read out simultaneously.

STATIC ACCELERATION

The ESG rotor translates with respect to the cavity center in response to vehicular acceleration. This translation will cause a change in the colatitude which some pickoffs of the readout system view.

Geometrical Considerations

A rotor whose center, O' , is displaced from its nominal location O in response to an acceleration vector \vec{A} is diagrammed in Figure 33. With respect to a spin axis-oriented cartesian coordinate system center at O' , the direction of pickoff P_1 has changed. On the other hand, the direction of pickoff P_2 , which is in the direction of \vec{A} , has not changed. Where P_1 may be viewing a different rotor colatitude, the only change occurring to P_2 is in the distance between the pickoff and the rotor surface. While this has caused a change of focus, the change is small enough (a few microinches compared to a distance of 0.1 inch from the pickoff lens to the rotor surface) that its effect is not noticed. Therefore, the component of displacement in the direction of the pickoff axis causes no error in the colatitude reading. Only the projection of displacement in the plane normal to the pickoff axis needs to be considered. An equation for this projection is

$$\vec{T}_i = (\hat{P}_i \times \vec{T}) \times \hat{P}_i \quad (74)$$

where \vec{T} is the translation vector and \hat{P}_i is the unit pickoff axis vector. Since it depends on the pickoff axis in question, the projection is indexed accordingly.

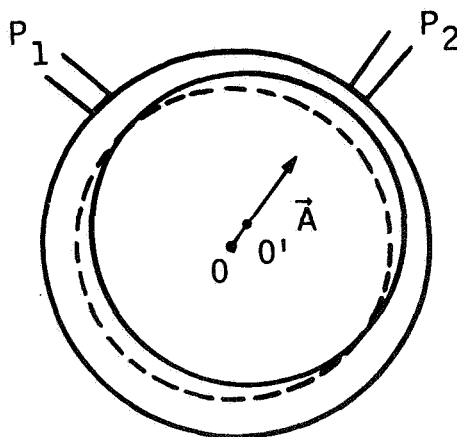


Figure 33. Geometry of Rotor Response to Acceleration

The change in colatitude observed by the pickoff depends also on the orientation of the projected translation with respect to the spin vector. For example, if the spin vector is normal to the plane of Figure 33, no change in colatitude would be sensed by pickoff P_1 . It is convenient to consider components of \vec{T}_i with respect to coordinates defined from the spin vector; for this purpose the projection of the spin vector in the plane normal to \hat{P}_i is also defined:

$$\vec{S}_i = (\hat{P}_i \times \hat{S}) \times \hat{P}_i \quad (75)$$

As shown in Figure 34, \vec{T}_i can be resolved into components parallel to and normal to \vec{S}_i . Before considering each of these components separately, it is worth mentioning that when \hat{S} is parallel to \hat{P}_i , \vec{S}_i is zero. This case need not be separately considered because pickoff P_i is not being used, since it is not viewing the pattern. Consequently, \vec{S}_i will never be zero for realizable readout conditions.

Readout Translation-Sensitive Error Equations

The parallel component of \vec{T}_i to \vec{S}_i (denoted by p) changes the observed colatitude by the magnitude of p , as measured on the surface of the rotor, and is independent of the magnitude of \vec{S}_i . Consequently, this component can be evaluated by computing the inner product of \vec{T}_i and \hat{S}_i , where \hat{S}_i is the unit vector parallel to \vec{S}_i . From Equations (74) and (75),

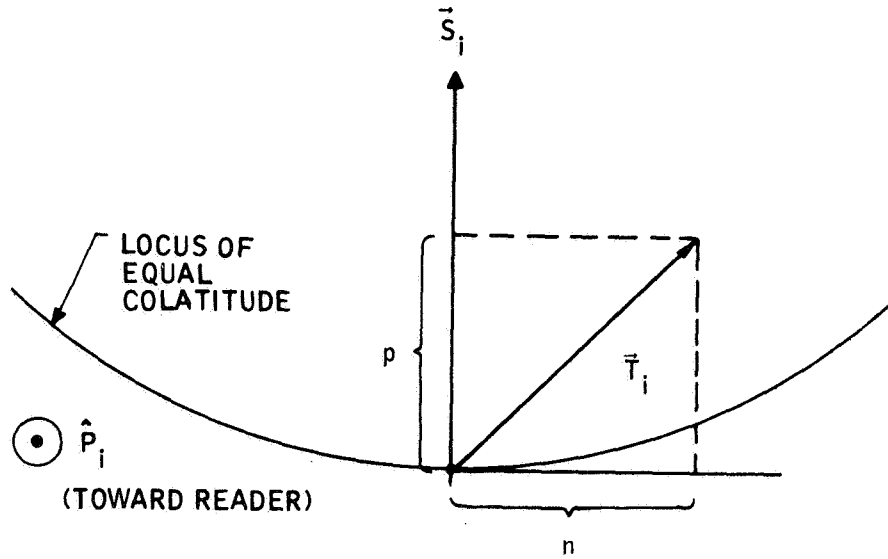


Figure 34. Observed Colatitude Sensitivity to Rotor Translation

$$p = \frac{1}{|\hat{P}_i \times \hat{S}|} [(\hat{P}_i \times \vec{T}) \times \hat{P}_i] \cdot [(\hat{P}_i \times \hat{S}) \times \hat{P}_i] = r \Delta\theta;$$

Let θ_i denote the colatitude read by P_i if the rotor were centered, or at zero displacement. Then

$$|\hat{P}_i \times \hat{S}| = \sin \theta_i$$

Using some vector product identities,

$$\begin{aligned} [(\hat{P}_i \times \vec{T}) \times \hat{P}_i] \cdot [(\hat{P}_i \times \hat{S}) \times \hat{P}_i] &= [\hat{P}_i \times (\vec{T} \times \hat{P}_i)] \cdot [\hat{P}_i \times (\hat{S} \times \hat{P}_i)] \\ &= [(\vec{T} \cdot \hat{P}_i) \hat{P}_i - \vec{T}] \cdot [(\hat{S} \cdot \hat{P}_i) \hat{P}_i - \hat{S}] = \vec{T} \cdot \hat{S} - (\vec{T} \cdot \hat{P}_i) (\hat{S} \cdot \hat{P}_i) \\ &= \vec{T} \cdot \hat{S} - \cos \theta_i (\vec{T} \cdot \hat{P}_i) \end{aligned}$$

where $\hat{S} \cdot \hat{P}_i = \cos \theta_i$.

If the direction cosines are the basic spin vector variables rather than the colatitude angles, the change in direction cosine is a more desirable entity:

$$\Delta(\cos \theta_i) = \sin \theta_i \Delta\theta_i = \frac{1}{r} \vec{T} \cdot (\hat{P}_i \cos \theta_i - \hat{S}) \quad (76)$$

Note that this change is expressed in terms of known or measurable parameters. The translation vector T can be determined from capacitance bridge measurements in the suspension, or it can be evaluated from the equation

$$\vec{T} = G \vec{A}$$

where G is the suspension gain matrix and \vec{A} is the acceleration of the gyro. For an isotropic support system, G reduces to a scalar. The acceleration vector can be measured with accelerometers. As a result, mathematical compensation for direction cosine error from rotor translation produced by steady-state acceleration can be implemented.

A potential difficulty with using Equation (76) for compensation is that it is written in terms of the spin vector coordinates with the rotor centered, instead of the observed coordinates. However, if the change is small enough, the observed coordinates can be substituted for the centered spin vector coordinates without incurring intolerable error. From Figure 33 it is seen that the magnitude of the change does not exceed the ratio of $|\vec{T}|$ to r . In Volume III, the maximum displacement of the rotor is assumed to be 10 percent of the rotor-electrode gap; in Volume II it was observed that the ratio of gap to radius on existing gyros ranged from 1:167 to 1:500. If one makes the rather pessimistic assumption that the ratio of $|\vec{T}|$ to r does not exceed 10^{-3} , the error of the compensation would be equal to the square of that ratio, or not greater than 10^{-6} . This is equivalent to an uncertainty of a fraction of an arc second and can, therefore, be neglected.

The normal component of \vec{T}_i to \vec{S}_i (denoted by n) produces a change in pickoff colatitude resulting from the curvilinear nature of colatitude parallels on the rotor surface. Referring to Figure 35, the change in direction cosine can be expressed as

$$\Delta (\cos \theta_i) = \cos b - \cos \theta_i$$

From the law of cosines of a right spherical triangle,

$$\cos b = \cos \theta_i \cos \frac{n}{r}$$

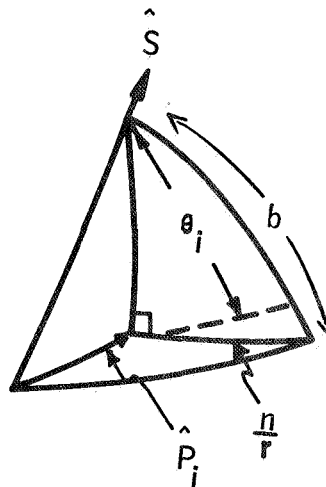


Figure 35. Curvilinear Shift Geometry

Therefore,

$$\Delta (\cos \theta_i) = \cos \theta_i (\cos \frac{n}{r} - 1) \approx - \frac{n^2}{2r^2} \cos \theta_i$$

Similar to the parallel component p , the normal component n never exceeds $|\vec{T}|$. Under the same assumptions about the relative magnitude of $|\vec{T}|$ to r , one concludes that compensation for the curvilinear effect, while it is possible, is not needed since the error is small enough to be tolerated.

VIBRATION

In a vibration environment, the acceleration is a bounded function of time. The translation function determined by the suspension servo transfer characteristics is also a bounded function of time. The equation for the direction cosine change from translation (76) can then be considered with \vec{T} as an independent variable in time. In inertial space, the spin vector S remains invariant except for its drift from torque. Over the interval of time required to read the gyro, the drift can be neglected. The direction of \vec{P}_i will change only if rotation or rotational vibration is present. Hence, if translational vibration is the only form of vibration present, \vec{P}_i and the true colatitude angle θ_i are invariant, and the apparent change in direction cosine is the inner product of a constant vector and \vec{T} . Since the direction cosine variation is a scalar, it can be boiled down to a scalar function of the vibration:

$$\Delta(\cos \theta_i) = f(t)$$

Since no products of vibration-induced variables occur, the characteristic frequencies of the direction cosine variation are the same as the vibration-induced translation.

The observed colatitude angle, however, will change with vibration; for that reason, it is worthwhile to evaluate the effect of using observables in the compensation scheme for vibration inputs. Such effects depend on the vibration frequency. Three different ranges are considered:

- Frequencies that are low compared to the frequency represented by the data cycle
- Frequencies above the response frequency of the translation measurement apparatus
- Intermediate frequencies

In this discussion, it is assumed that the response frequency of the translation measurement apparatus is higher than that represented by the data cycle (equal to the reciprocal of the data period).

At the low frequencies, the translation and colatitude change is small during the data period. The steady-state component of both parameters is expected to be of greater significance in the correction. As such, the compensation error is of the order of that of steady-state acceleration, which was previously shown to be less than 10^{-6} .

At the high frequencies, the translation measurement apparatus doesn't follow the vibration; high frequencies are then not expected to be sensed by the output. Consequently, no correction for high-frequency vibration is possible, and one must depend on the spin vector observables to assume an average value of its instantaneous function. Except at frequencies resonant with rotor frequency and its harmonics, some averaging can be expected. The standard deviation from the mean of a sample of data points taken during high-frequency vibration will likely be greater than that of a similar sample taken during no vibration.

At intermediate frequencies, the compensation effects are not as predictable as for the other regions. Errors larger than steady-state errors can occur; for instance, if the spin vector observables are some average values of the instantaneous values and if the translation measurement yields an (instantaneous) extreme value during a data sample. If such is indeed a possibility, it may be desirable to reduce the response frequency of the translation measurement apparatus to one approximately equal to the data cycle or to bypass the computer compensation for vibrations above a specified frequency.

When rotational vibration occurs, \hat{P}_i and $\cos \theta_i$ are functions of the vibration, and their product contains rectified terms that are second degree in the vibration amplitude. Since rectification occurs, the average value of the product is not zero, but deviates from zero in proportion to the square of the vibration amplitude. If the amplitude is small, such products can be disregarded.

If rotational vibration occurs without translation vibration or steady-state vibration, the translation vector \vec{T} is zero and no correction is available. An increase in the standard deviation of a sample taken during this vibration can be expected. If either translational vibration or steady acceleration occurs with rotational vibration, a rectification occurs which is at least second degree in the acceleration and vibration parameters. The specific vibration parameters must be known before the rectification can be realistically assessed. Generally, these effects are small enough to be tolerated without compensation.

ANGULAR ROTATION

When the gyro case is rotating, a pickoff direction cosine is constantly changing. When the direction cosines are read out, resolution is lost, with the calculated cosine being some value which occurs during the readout interval. An upper bound of the change of colatitude observed by a pickoff during a readout interval is

$$\Delta\theta_{\max} = \Omega \tau$$

where Ω is the vehicular rate and τ is readout interval. Generally, it is small enough that over the change in colatitude the change in phase angle is linear with time; the measured colatitude from the pickoff data, therefore, is expected to be the colatitude at the midpoint of the data cycle. If the data cycle mid points for all pickoffs can be made to occur simultaneously, maximum precision in specifying the spin vector direction during rotation is assured.

Equations of Motion

Consider a rotating set of coordinates in inertial space. By the coriolis law,

$$\frac{d}{dt} \hat{S} = \frac{d'}{dt} \hat{S} + \vec{\Omega} \times \hat{S}$$

where

$$\frac{d}{dt} = \text{time derivative with respect to the inertial frame}$$

$$\frac{d'}{dt} = \text{time derivative with respect to the rotating frame}$$

$$\vec{\Omega} = \text{angular velocity of the case frame with respect to the inertial frame}$$

It is assumed that the unit spin vector is space stabilized.

Thus,

$$\frac{d}{dt} (\hat{S}) = 0,$$

and the observed rotation of the spin vector in the rotating frame is described by

$$\frac{d'}{dt} \hat{S} = \hat{S} \times \vec{\Omega} \tag{77}$$

Let

$$\begin{aligned}\hat{S} &= \alpha \hat{i}_c + \beta \hat{j}_c + \gamma \hat{k}_c \\ \vec{\Omega} &= \Omega_1 \hat{i}_c + \Omega_2 \hat{j}_c + \Omega_3 \hat{k}_c\end{aligned}$$

where α , β , γ are the direction cosines of the spin vector in the (rotating) case coordinates.

Then

$$\frac{d'}{dt}(\alpha \hat{i}_c + \beta \hat{j}_c + \gamma \hat{k}_c) = (\alpha \hat{i}_c + \beta \hat{j}_c + \gamma \hat{k}_c) \times (\Omega_1 \hat{i}_c + \Omega_2 \hat{j}_c + \Omega_3 \hat{k}_c)$$

Now

$$\frac{d'}{dt} \hat{S} = \frac{d'\alpha}{dt} \hat{i}_c + \frac{d'\beta}{dt} \hat{j}_c + \frac{d'\gamma}{dt} \hat{k}_c$$

because

$$\frac{d'}{dt} \hat{i}_c = \frac{d'}{dt} \hat{j}_c = \frac{d'}{dt} \hat{k}_c = 0$$

which is another way of saying that the rotating coordinate unit vectors are not moving in the rotating system.

The vector equation reduced to three scalars:

$$\frac{d'\alpha}{dt} = \beta\Omega_3 - \gamma\Omega_2 = \dot{\alpha} \quad (78a)$$

$$\frac{d'\beta}{dt} = \gamma\Omega_1 - \alpha\Omega_3 = \dot{\beta} \quad (78b)$$

$$\frac{d'\gamma}{dt} = \alpha\Omega_2 - \beta\Omega_1 = \dot{\gamma} \quad (78c)$$

Now, information on the spin vector components can be provided by the read-out system and the applicable mechanization equation. If the phase-angle measurement electronics utilize a phaselocking technique like that described in Section VI, information on the rate of change of α , β , and γ may be obtained rather simply. The network driving the variable frequency oscillator is basically an integrator of V' with respect to time; consequently, V' is a function of the rate of change of the phase angle. If the relationship between V' and phase-angle rate is linear, and a cosine pattern is used, V' only needs to be properly scaled to provide a direct output for α , β , or γ . Consequently, information can readily be made available for the solution of Equations (78) for the angular rotation.

Gyro Information Limitations

Complete specification of $\vec{\Omega}$ from the solution of these equations is, however, impossible. Although α , β , and γ may be independently determined with a three-pickoff mode, they are not independent because they satisfy the identity

$$\alpha^2 + \beta^2 + \gamma^2 = 1$$

The derivative of this identity with respect to time is

$$\alpha\dot{\alpha} + \beta\dot{\beta} + \gamma\dot{\gamma} = \hat{S} \cdot \frac{d'}{dt} \hat{S} \equiv 0$$

This is merely an equational statement of the fact that no information regarding changes in rotation angle parallel to \hat{S} is available from the gyro; a second gyro whose spin vector is nominally orthogonal to \hat{S} is needed to provide that information.

That complete information about $\vec{\Omega}$ is not possible from a solution to Equations (78) is readily apparent because Equation (77), from which the scalar system is derived, deals with the cross product $\hat{S} \times \vec{\Omega}$. Information about $\hat{S} \cdot \vec{\Omega}$ is immediately lost in this operation. If complete information about $\hat{S} \times \vec{\Omega}$ is obtained from a solution of (78), the projection of $\vec{\Omega}$ in the plane normal to \hat{S} can be obtained from the triple product

$$(\hat{S} \times \vec{\Omega}) \times \hat{S}$$

When similar information from a second gyro (whose spin vector is nominally orthogonal to \hat{S}) is added, a complete solution for $\vec{\Omega}$ is, in principle, obtainable.

A solution of the system (78) will not be attempted here; some characteristics of α , β , and γ with the time will be derived if $\vec{\Omega}$ is constant.

Constant Angular Rotation

Assuming that $\vec{\Omega}$ is constant, Equations (78b) and (78c) can be substituted into the derivative of (78a) with respect to time to give

$$\ddot{\alpha} + \alpha(\Omega_3^2 + \Omega_2^2) = \Omega_1(\gamma\Omega_3 + \beta\Omega_2) \quad (79)$$

Now, if

$$\vec{\Omega} \cdot \hat{S} = 0 \quad (80)$$

then

$$\gamma\Omega_3 + \beta\Omega_2 = -\alpha\Omega_1$$

and a differential equation in α only is obtained:

$$\ddot{\alpha} + \alpha(\Omega_3^2 + \Omega_2^2 + \Omega_1^2) = 0 \quad (81)$$

The same manipulations give similar differential equations for β and γ . Thus, the direction cosines are simple harmonic in time if the angular rotation is constant and normal to \hat{S} . Equation (79) can now be differentiated with respect to time and (78b), (78c), and (78a) in sequence substituted into that derivative to obtain the same differential equation in $\dot{\alpha}$:

$$\ddot{\dot{\alpha}} + \dot{\alpha}(\Omega_3^2 + \Omega_2^2 + \Omega_1^2) = 0 \quad (82)$$

Consequently, the first derivative of the direction cosines satisfies the equation for simple harmonic motion. The general solution to α is, therefore,

$$\alpha = \bar{\alpha} + A_0 \cos(\Omega t - \psi)$$

where

$$\Omega = |\vec{\Omega}| = \sqrt{\Omega_1^2 + \Omega_2^2 + \Omega_3^2}$$

It is interesting to note that Ω can be determined by measuring the period of the direction cosine function. From this calculation and a solution for $(\hat{S} \times \vec{\Omega})$, the magnitude, but not the sign, of $\hat{S} \cdot \vec{\Omega}$ can be determined. If the apparent change of rotor speed due to the angular rotation can be sensed, the sign of the change would determine the sign of $\hat{S} \cdot \vec{\Omega}$. Neither of these determinations would be precise, except in the case that $|\hat{S} \cdot \vec{\Omega}|$ is large compared to $|\hat{S} \times \vec{\Omega}|$.

In examining the general solution (82) in view of (79), (80), and (81), it is apparent that $\bar{\alpha}$ is non zero only if $\vec{\Omega} \cdot \hat{S}$ is non zero. From the geometry of conditions imposed by constant $\vec{\Omega}$, one intuitively arrives at the following equation for $\bar{\alpha}$:

$$\bar{\alpha} = \frac{1}{\Omega^2} (\hat{S} \cdot \vec{\Omega}) (\hat{i}_c \cdot \vec{\Omega})$$

similar equations for $\bar{\beta}$ and $\bar{\gamma}$ can also be written.

CONCLUSIONS

From this study of dynamic environments, some general conclusions can be stated:

- Static acceleration produces a rotor displacement which produces an error in readout. However, by utilizing the

parameters ordinarily measured in a navigation system, adequate mathematical compensation can be implemented with a computer.

- Vibration causes a rotor displacement that varies with time within bounded limits. This causes a variation in phase-angle measurement that can be reduced by averaging over several revolutions and/or over several samples. Even so, the dispersion of readout samples from their means is likely to increase with vibration.
- Angular rotation produces a constantly changing direction cosine. When the rotation is constant, the direction cosines are sinusoidal function of time. To produce reasonably precise readout of the spin axis, the pickoffs must be read out simultaneously. If direction cosine rates are measured, information ordinarily provided by a rate gyro can be calculated from ESGV readout parameters.